# DEVELOPMENT OF MULTIFUNCTIONAL MICROGELS FOR NOVEL BIOMEDICAL APPLICATIONS

A Dissertation
Presented to
The Academic Faculty

by

Purva Ganesh Kodlekere

In Partial Fulfillment
of the Requirements for the Degree
Doctor of Philosophy in the
School of Chemistry and Biochemistry

Georgia Institute of Technology
December 2015

# DEVELOPMENT OF MULTIFUNCTIONAL MICROGELS FOR NOVEL BIOMEDICAL APPLICATIONS

Approved by:

Dr. L. Andrew Lyon, Advisor
Schmid College of Science and Technology
*Chapman University*

Dr. M.G. Finn
School of Chemistry and Biochemistry
*Georgia Institute of Technology*

Dr. Robert Dickson
School of Chemistry and Biochemistry
*Georgia Institute of Technology*

Dr. Philip Santangelo
Department of Biomedical Engineering
*Georgia Institute of Technology*

Dr. Facundo Fernandez
School of Chemistry and Biochemistry
*Georgia Institute of Technology*

Dr. Julie Champion
School of Chemical and Biomolecular Engineering
*Georgia Institute of Technology*

Date Approved: November 3, 2015

To my parents Suneeti (aai) and Ganesh (baba), my sister Madhura, my husband Kaushik
and
my grandmother, Shailaja (aji) (November 4, 1934 – September 23, 2015)

# ACKNOWLEDGEMENTS

I owe everything I have ever achieved, to my parents. I am extremely grateful to them for always encouraging me to follow my dreams. They have constantly supported me in all my decisions and have been there for me with unconditional love, support and confidence, regardless of what they have had going on. There aren't enough words for me to express my appreciation and gratitude towards them, for everything they have done, so suffice to say that I would not be where I am without them. I would also like to thank my sister, for all her love and support, timely humor and for her confidence in me. She has played a pivotal role in pushing me to always do my best, and encouraging me to keep pursuing my passions, irrespective of the difficulty of the situation.

Next, I would like to thank my husband. While a Ph.D. is extremely rewarding, at times it can be very stressful and more so, when both spouses are graduate students. My husband has been amazingly supportive, understanding and a constant source of encouragement. He has always helped me believe that I am capable of anything, and not only has he shared my happiness when I have been successful, but he has always been even happier than me, for me, at such times. For all that and more, I am very thankful. I am also extremely grateful to my parents-in-law and my sister-in-law, for all their support and love.

I have to thank my grandparents, aji and ajoba, for being so amazing and always teaching us, through example, to be kind to everyone and to always have confidence in oneself. Aji was the epitome of strength and independence for everyone in our family. Through her constant willingness to learn new things and embrace new technology, while

still knowing how to stay grounded in reality, she has gifted us with an example we will always follow. Her teachings and love will always remain with us.

Next, I definitely need to thank my amazing friends. My best friend Aswathy, for all the love and compassion, and all the friends I made at Georgia Tech. Classes and literature exams were a lot more fun to prepare for, in the company of such amazing people.

I would also like to express my gratitude for all the members of the Lyon group. In particular, I'd like to thank Nicole Welsch for being such an amazing friend and mentor. I would also like to thank Mike Smith, who taught me my first microgel synthesis when I joined the lab and patiently answered all my questions. I am also thankful to Anabel Cartelle, for being an amazing undergraduate student. I am very grateful to my collaborators Dr. Erin Dickerson, Dr. John McDonald, Aida Demissie and Dr. Robert Dickson, and all other members of the Lyon research group as well, for all their advice, support and help.

Last but not the least, I would like to thank Dr. Andrew Lyon for being such a great advisor. His advice and motivation have been very helpful to me through the course of my Ph.D. I have always admired his teaching abilities and his multidimensional approach to research and I am really grateful for his continued support and encouragement.

# TABLE OF CONTENTS

# LIST OF TABLES

# LIST OF FIGURES

# LIST OF SCHEMES

Page

# LIST OF SYMBOLS AND ABBREVIATIONS

| | |
|---|---|
| Anti-EGFR | Anti-epidermal growth factor receptor |
| PEG | Poly(ethyleneglycol) |
| MRI | Magnetic Resonance Imaging |
| LCST | Lower critical solution temperature |
| NIPAm | N-isopropylacrylamide |
| BIS | N,N′-methylenebis(acrylamide) |
| VPTT | Volume phase transition temperature |
| NIPMAm | N-isopropylmethacrylamide |
| DHEA | N,N′-(1,2-dihydroxyethylene)bisacrylamide |
| DMHA | N,O-dimethacryloyl(hydroxylamine) |
| ULCs | Ultralow crosslinked particles |
| AFM | Atomic force microscopy |
| SDS | Sodium dodecyl sulfate |
| PS | Polystyrene |
| FRET | Fluorescence energy resonance transfer |
| EPR | Enhanced permeability and retention |
| Dox | Doxorubicin |
| siRNA | Small interfering RNA |

| | |
|---|---|
| APMA | N-(3-aminopropyl)methacrylamide hydrochloride |
| AEMA | 2-aminoethylmethacrylate hydrochloride |
| V50 | 2,2'-azobis(2-methylpropionamidine)dihydrochloride |
| APS | Ammonium persulfate |
| HEPES | N-(2-hydroxyethyl)piperazine-N′-(2-ethanesulfonic acid) |
| CAPS | 3-(cyclohexylamino)-1-propanesulfonic acid |
| APTMS | 3-aminopropyltrimethoxysilane |
| PSS | poly(4-styrenesulfonic acid) sodium salt |
| $R_H$ | Hydrodynamic radius |
| DLS | Dynamic light scattering |
| CBQCA | (3-(4-carboxybenzoyl)quinoline-2-carboxaldehyde) |
| PEG-DA | Poly(ethyleneglycol) (200) diacrylate |
| CHES | 2-(cyclohexylamino)ethanesulfonic acid |
| MES | 4-Morpholineethanesulfonic acid |
| MGITC | Malachite green isothiocyanate |
| RB | Rose bengal |
| EDC | N-(3-dimethylaminopropyl)-N′-ethylcarbodiimide hydrochloride |
| NHSS | N-hydroxysulfosuccinimide sodium salt |
| PBS | Phosphate buffered saline |
| DMSO | Dimethyl sulfoxide |
| EthD-1 | Ethidium homodimer-1 |
| $D_H$ | Hydrodynamic diameter |
| CLSM | Confocal laser scanning microscopy |
| MG | Malachite green |

| | |
|---|---|
| tPA | Tissue-type plasminogen activator |
| GPRP | GPRPFPAC |
| GPSP | GPSPFPAC |
| AHRP | AHRPYAAC |
| AAc | Acrylic acid |
| AEM | 2-Maleimidoethylamine trifluoroacetate salt |
| mRhoB | Methacryloxyethyl thiocarbamoyl rhodamine B |
| GFP | Green fluorescent protein |
| C/S | Core/shell |
| AFA | Acrylamidofluorescein |
| EMCA | 6-maleimidohexanoic acid |

# SUMMARY

This dissertation describes the development of multifunctional microgels for utilization in novel biomedical applications. The functionality of microgels has been utilized for a number of fundamental studies in the past. It has also been exploited to facilitate the conjugation of biologically relevant molecules to microgels through a variety of routes. This dissertation explores microgel functionality and focuses on fundamental characterization and potential applications of microgel conjugates in two major biological applications. It also delves into the use of core/shell microgels and explores the merits of the utilization of this particular microgel architecture.

Microgels are solvent swollen, polymer based, hydrogel microparticles that demonstrate tremendous versatility in their synthesis. They can thus be synthesized to have diverse properties, functionalities and architectures, and to have sizes in the nano- or micro- range. Their dimensions make them particularly useful for biological applications, because they can be utilized to visualize and/or manipulate cell processes that occur at the same length scale. **Chapter 1** gives an insight into the history of microgels, along with a description of the multitude of biological applications in which they have been demonstrated to be useful.

A number of applications, such as bioimaging, specific targeting and sensing, require microgels to be conjugated to different moieties. This can usually be achieved through incorporation of functional groups in microgel matrices either during or post-synthesis. Two such functional groups, that provide opportunities for a range of conjugations, are primary amines and carboxylic acids.

Although primary amine functionalities have remarkable potential to be utilized in conjugation reactions, the synthesis of stable microgels with high densities of amine groups has been challenging due to a variety of reasons. Therefore, we have developed a range of functional cationic microgel constructs containing primary amines, in different size ranges. Cationic microgels with distinct properties could be obtained through subtle changes in reaction conditions and **Chapter 2** provides a detailed description of the characterization of these microgels. A major focus of this chapter was the quantification of amine functionalities present in microgels. This knowledge can be leveraged to executing well controlled conjugation reactions.

**Chapter 3** focuses on a model cationic microgel construct and utilization of its primary amine functionalities for the conjugation of two dyes with properties that make them attractive for use as photoacoustic contrast agents. Through its multivalency, a single microgel has the capability to 'concentrate' the contrast agent within its small volume and this high local concentration of contrast agents was quantified in this chapter. Such high concentrations are particularly useful for an application like photoacoustics, where irradiation of a single particle can potentially generate very high intensity signals.

In addition to bioimaging, microgel conjugates also have potential applicability in site-specific targeting, through attachment of the relevant moieties to their functionalities. **Chapter 4** describes the development of such carboxylic acid functionalized microgels, targeted to fibrin clots though the conjugation of fibrin-specific peptides. The particles developed in this chapter have a core/shell architecture, with the functionalities localized primarily to the outer shell. Microgels in three different size ranges were developed, in order to investigate their size-based differential localization in porous fibrin clots. These

experiments provided information about microgel interactions with the clot and the interplay between microgel dimensions and clot porosity. The conjugation of one fibrin-specific peptide to microgels, in essence, converted microgels themselves into fibrinolytic agents and **Chapter 4** describes experiments demonstrating this phenomenon. We hypothesize that the multivalency of microgels plays an important role in this function, resulting in rapid dissolution of the fibrin clot, at a rate that has not been observed before.

Finally, **Chapter 5** describes some future directions and additional studies that need to be performed in order to understand the systems investigated in the previous chapters better, and exploit them to the best of their capabilities. Due to the endless avenues microgel systems present, their applications are manifold, especially when considering biological systems. Obtaining a fundamental understanding of their functioning is thus extremely important and will be extremely beneficial for the generation of highly effective constructs.

# CHAPTER 1

# INTRODUCTION

## 1.1 Polymer-based biomaterials

A number of essential components of the human body are comprised of molecules made from repeating units. Polysaccharides, proteins and DNA consisting of repeating units of sugar molecules, amino acids and nucleic acids respectively are polymers that play very important roles in regulating and maintaining normal bodily function. Additionally, biopolymers like collagen and fibrin are responsible for specific functions like maintaining the integrity of the extracellular matrix and augmenting hemostasis by facilitating clotting of blood, respectively. Thus, a number of materials responsible for maintaining regulatory function within the body are polymeric in nature. Chitosan and alginate are examples of bio-derived polymers obtained from other sources.

In addition to the naturally existing biopolymers, a number of synthetic polymers have been investigated for their utility as biomaterials. The applications of these polymers range from the development of three-dimensional porous scaffolds for tissue engineering[1-3] to the development of separation membranes,[4] construction of prostheses[5] and the generation of vehicles for the delivery of therapeutics.[6,7] The primary requirements for the properties of these materials depend on the application under consideration and thus, most often, on the tissue type with which the material will be in contact.[8] Therefore, when compatibility with soft tissue like cardiovascular tissue is essential, materials like elastomers are beneficial.[9,10] For constructs that need to lend themselves to circulation in the blood stream, long term survival in the body with least

detrimental effects is the requirement that takes priority.[11-13] While in these applications, biodegradability is a desirable quality, for others like those used in some prostheses, the ability of the construct to withstand large magnitudes of mechanical stress is a prerequisite.[14] There exists a vast array of available choices with regards to the identity of the constituent polymers and the ability to tune properties of these constructs in a controlled fashion. Depending on the specific requirements, various approaches dealing with different polymer synthesis conditions or post-synthesis modifications can be employed. One of the most significant advances in the field came in the form of a drug depot formulation composed of N-vinylpyrrolidine conjugates of glycyl-L-leucine-mescaline, in 1955.[15] Thus, the utilization of polymers as biomaterials has gained increasing interest in the past six decades. A number of methods have since evolved in order to fully exploit the versatility that these systems offer.

### 1.2 Polymeric particles in bioapplications

Nanotechnology has been a booming subject of research, with applications in several areas such as biomedical technology,[16-20] energy storage[21,22] and catalysis.[23,24] Particularly in the biological field, the dimensions of nano and microparticles make them attractive candidates for visualization, manipulation and analysis of cellular processes and components. For instance, Gao et al. developed semiconductor quantum dots modified with block copolymers attached to tumor-targeting ligands in order to facilitate *in vivo* imaging[25] and Muhlen et al. generated solid lipid nanoparticles, or SLNs with the aim of achieving controlled release of drugs.[26] Similarly, Huang et al. synthesized gold nanorods and conjugated them to malignant cell-specific anti-epidermal growth factor

receptor (anti-EGFR) monoclonal antibodies, thus generating constructs that could serve the dual purpose of molecular imaging and photothermal therapy.[27]

When considering biomedical applications, polymers form an important class of materials, as mentioned in the previous section. Polymers like poly(ethylene glycol) (PEG) have been used extensively to coat nanoparticles in order to improve their circulation time in the body through reduction of uptake by the reticuloendothelial system (RES).[28,29] PEGylation of bovine adenosine deaminase as a method of replacement therapy for severe combined immunodeficiency (SCID)[30] and that of interferons for treatment of viral infections like Hepatitis C[31] are two such examples. Microparticles entirely based on PEG have also been generated for added biocompatibility.[32-34] In a similar manner, other polymers have been synthesized to generate nano and micro sized composites for applications like the delivery of therapeutics.[35,36] A number of these composites are multicomponent and thus multifunctional.[37,38] A polymer by itself can act as a drug or sequestrant. One example is poly(allylamines), which work by lowering serum phosphorus and parathyroid hormone, or controlling cholesterol absorption, by binding phosphates or bile acids respectively.[39,40] Alternatively, they may be utilized as delivery vehicles for therapeutic agents either in the form of polymer-drug conjugates[41,42] or as polymeric assemblies such as micelles,[43,44] which can be loaded with the relevant therapeutic agent.[45,46] In addition to their efficacy as delivery agents, polymeric constructs have also been researched for their utility in several imaging modalities, either by themselves or in conjunction with contrast agents that have known imaging capabilities. Thus, conjugated polymers have been developed as detection agents of specific nucleic acids and proteins.[47] On the other hand, contrast agents have been

conjugated to polymers to form constructs with potential applicability in magnetic resonance imaging (MRI)[48,49] and fluorescence imaging.[50-52] One class of polymeric particles in the nano- to micro- scale, that have been demonstrated to be promising in a wide range of biomedical applications, are microgels.

### 1.3 Microgels: an introduction

Microgels are polymer-based, colloidally stable nano or microparticles. Similar to their bulk hydrogels counterparts, they are solvent swollen. Due to the flexibility available in their synthesis conditions and components, microgels can be synthesized to have dimensions in the nano or micro range. They can also have different mechanical properties,[53,54] optical properties[55,56] and functionalities. Some examples of nonionic vinyl monomers that have been utilized to prepare microgels are acrylamide, N-vinyl caprolactam,[57] N-ethylacrylamide[58] and N-vinylformamide.[59] Above a characteristic temperature known as the lower critical solution temperature (LCST), polymer chains of these molecules collapse upon themselves. This entropically driven coil to globule transition takes place through expulsion of water into the surrounding environment, due to polymer-polymer interactions being favored over polymer-solvent interactions. Microgels synthesized from these monomers also possess this thermoresponsivity. N-isopropylacrylamide (NIPAm) is a well explored monomer for microgel synthesis. Its polymer pNIPAm has an LCST of 31 $^{0}$C and hence, pNIPAM based microgels demonstrate thermoresponsivity around this temperature. Since this transition is reversible through a change in temperature, microgels have several potential applications in drug delivery, such as the pulsatile delivery of insulin as demonstrated by Nolan et

al.[60] and in sensing devices.[61] The responsivity of microgels extends to other stimuli as well[62] and this responsivity along with numerous other application dependent desirable properties like biodegradability[63-66] and extreme deformability[54] can be engineered into constructs through modifications in their syntheses.

### 1.3.1 Microgel synthesis

One of the earliest examples of microgel synthesis was reported by Pelton et al. in 1986.[67] In a typical synthesis (Scheme 1.1), an aqueous solution of NIPAm and a crosslinker such as N,N'-methylenebisacrylamide (BIS) is heated and polymerization is initiated at a temperature above the LCST of pNIPAm. The thermoresponsivity of pNIPAm based microgels translates into their synthesis and thus, initiation triggers the formation of pNIPAm chains that undergo the coil to globule transition described above. A number of these globules combine and eventually form a colloidally stable microgel.

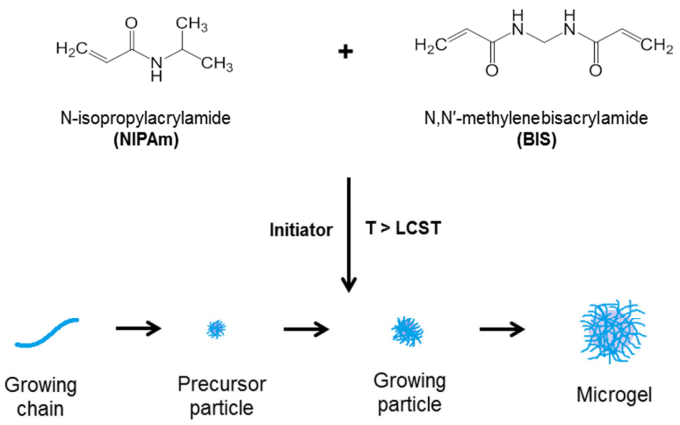


**Scheme 1.1.** Typical microgel synthesis leading to the formation of pNIPAm based, BIS crosslinked microgels

The microgels thus formed also possess thermoresponsivity and display it in the form of a volume transition, i.e. at a temperature above 31 $^{0}$C, these spherical particles collapse and expel water, causing a dramatic change in their volume. Thus, in reference to microgels, this temperature is referred to as a volume phase transition temperature (VPTT).

While pNIPAm has been used extensively in order to study the kinetics of microgel syntheses,[64] mechanical properties of microgel assemblies[68] and various architectures of the constructs, when considering utilization in conjunction with biological systems, its utility specifically spans those areas warranting collapsed particles at the physiological temperature of 37 $^{0}$C.[60] Some applications, however, may require solvent swollen microgels at this temperature. One example involves time controlled delivery of loaded therapeutics,[69] which may not be accomplished since microgel density and hence interactions between the polymer chains and loaded therapeutics change drastically following collapse. A second example relates to the utilization of microgels in imaging, where collapse may lead to a reduction in the signal due to interference because of increased scattering or self-quenching of dyes present within or conjugated to the microgel matrix. For such applications, a methyl substituted relative of NIPAm is promising. N-isopropylmethacrylamide (NIPMAm) when polymerized, forms pNIPMAm with an LCST that is elevated when compared to that of NIPAm, due to the methyl substitution on the α carbon of the backbone. When microgels composed of primarily pNIPMAm are synthesized, their VPTT is therefore also elevated, at 44 $^{0}$C, thus causing them to remain swollen at the temperature of the human body.

In addition to the primary monomers, various additional synthesis components and conditions can be altered in order to generate particles with desirable properties. For instance, different comonomers may be used in order to impart differential functionality to the microgels. These will be discussed in more detail in section 1.3.2. Furthermore, polymerizable fluorescent comonomers may be introduced during the synthesis in order to facilitate the incorporation of the fluorescent entity throughout the polymer matrix. This is useful for investigations on optical properties or for the purpose of visualization of particles in future investigations.[70,71] A range of bifunctional crosslinkers can also be utilized in place of BIS. Examples of these include 1,3-divinylimidazolid-2-one (BVU),[59] 1,4-butanediol diacrylate[72] and polyethylene glycol dimethacrylate.[73] Some crosslinkers like N,N′-(1,2-dihydroxyethylene)bisacrylamide (DHEA)[74] and N,O-dimethacryloyl(hydroxylamine) (DMHA)[65] have been utilized in order to introduce biodegradability as described earlier. Variation in crosslinker identity and crosslinking density can also aid manipulation of reaction kinetics, leading to changes in mechanical properties of the microgels.[75,76] pNIPAm based microgels can also be synthesized without a crosslinker, as shown by Gao et al. in 2003.[77,78] Recently, we synthesized ultralow crosslinked particles or ULCs (refer to **Appendix A**) in a range of sizes (diameters of ~ 400 nm to ~ 4 μm) and characterized their deformability through studies on surface spreading, pore translocation, and Atomic Force Microscopy (AFM) nanoindentation.[54]

Microgel size can be partially controlled through the introduction of a specific concentration of initiator. In general, utilization of a high concentration of initiator creates a bias towards the formation of nucleation sites vs. the propagation of polymer chains, thus leading to the development of a large number of smaller particles. The use of

a lower temperature of initiation also influences microgel size, generally leading to the formation of larger particles due to a smaller number of initiation sites being generated and chain propagation being favored. Additionally, microgel size and stability may also be altered through the use of a surfactant like sodium dodecyl sulfate (SDS).[79] Higher concentrations ordinarily cause early stabilization and hence smaller sizes of formed particles.

Almost all properties described above have the ability to be influenced by the presence and identity of comonomers used. However, the chief reason for utilizing comonomers is more often the introduction of functionalities within microgel matrices, the presence of which can be leveraged to a wide range of post-synthesis modifications.

### 1.3.2 Microgel functionality and responsivity to pH

The introduction of functional groups in microgel matrices can either be done during particle formation or as an additional step following synthesis. This may be done for the purpose of enabling conjugations of pertinent moieties to the matrices, for imparting responsivity to additional stimuli such as pH to the particles, or for performing fundamental investigations on polymerization kinetics and the effects of the presence of charged species.[80] The presence of a large number of polymerizable functional group containing monomers provides a range of options for appropriate selection depending on the application. Some of the functionalities most commonly incorporated into microgels are carboxylic acids,[81] amines[82] and alkynes.[83] Depending on the similarities or differences in polymerization kinetics of the primary and comonomers and their reactivity ratios, diverse combinations of these entities can be utilized.

If functionalities with pKa values in the relevant range are introduced, pH responsivity can be introduced into microgels, which manifests itself in form of microgel volume phase transitions, when the functional groups are uncharged. Examples of some anionic comonomers that have been introduced in microgel matrices during syntheses are acrylic acid, fumaric acid, vinyl acetic acid[84] and 4-vinylphenylboronic acid.[85] Similarly, cationic comonomers such as allylamine,[86] N-3-dimethylaminopropylmethacrylamide[87] and poly(2-(diethylamino)ethyl) methacrylate (PDEAEMA)[88] have also been incorporated into microgel matrices. It is worth noting that not all these functionalities lend themselves to the conjugation reactions mentioned before, since opportunities for substitutions are not available in all the above examples. When such ionic functionalities are distributed throughout the interior of microgel particles, depending on the pKa of the comonomer, at a pH when the functional groups are charged, the presence of counterions and accompanying water causes the microgels to be swollen. A change of pH to a value on the other side of the pKa spectrum causes the functionalities to be uncharged, thus making the microgels deswell through expulsion of the water associated with the counterions. This pH responsivity of microgels is thus useful to gauge the incorporation of functional groups and in applications relating to delivery of therapeutics through expulsion of loaded cargo.[89]

### 1.3.3 Conjugations to microgels

The introduction of functional groups in microgel matrices either during or post synthesis is vital for permitting covalent conjugations of a vast number of species. The conjugates generated have been demonstrated to be useful in a wide array of applications.

For example, microgels conjugated to aptamer probes have been synthesized for the detection of proteins by Srinivas et al.[90] Other microgel based detection systems include microgel-DNA oligonucleotide conjugates immobilized on paper strips for DNA detection[91] and glucose sensing devices. The latter have primarily exploited the interaction between glucose and 3-aminophenylboronic acid (APBA) leading to swelling responses[92] or the use of etalons to observe shifts in reflectance peaks.[93] Another interesting utilization of bioconjugation was in the generation of hemoglobin loaded microgels, developed by Chen et al., for utilization as oxygen carriers, or artificial red blood cells.[94] Similarly, the generation of artificial platelets has utilized bioconjugation of a fibrin-specific species onto microgels.[95] A number of constructs have been developed for specific targeting to cancer cells for imaging or the delivery of therapeutics. Therefore, conjugations of a variety of species to microgels can be carried out and tailored to particular applications to yield highly effective systems.

### 1.3.4 Microgel core/shell architectures

In addition to the versatility they provide in terms of size and functionality, microgels also can be synthesized to possess different architectures such as core/shell, core/double shell, hollow and yolk/shell particles.[38] All of these can be considered as derivatives of the primitive core/shell structure, which is relatively straightforward to synthesize and is extremely valuable in applications that require dual or multiple functionality.

The synthesis of core/shell microgels with multifunctionality has been reported by a number of research groups.[96-99] The core may be hard sphere based, composed of a material such as polystyrene,[100-103] silica[104] or metal nanoparticles[105] or it could constitute

a porous network of polymers such as pNIPAm or pNIPMAm.[106,107] Core/shell microgel constructs have thus been developed from a number of different constituents, by utilizing a range of techniques, leading to the generation of particles with varying properties and suited to diverse applications such as catalysis,[108] delivery of therapeutics[71] and imaging.[109] The development of core/shell microgel architectures with degradable components has been particularly useful for studying the relationship between the two components.[107,110] Incorporation of a degradable crosslinker such as N,N′-(1,2-dihydroxyethylene)bisacrylamide (DHEA) can generate hollow particles, such as those reported by Nayak et al.[74] Recently, Tripathi et al. demonstrated the utility of such thermoresponsive constructs in separation and catalysis.[111] Geest et al. developed dextran based self-exploding microgels with the shell in the form of a semipermeable membrane that would rupture upon core degradation, thus releasing the encapsulated cargo.[112,113] The core/shell architecture was developed further using a three step synthesis and a second shell was added onto the first, degradable shell, by Hu et al. Degradation of the first shell generated multicompartment particles, and is useful for enhanced isolation of the microgel components.[114]

### 1.4 Microgels in bioapplications

As is evident from the previous section, microgels have tremendous potential for utilization in conjunction with biological systems. From bioimaging to drug delivery and diagnostics, the versatility of microgel constructs makes them amenable to utilization in an array of such applications. In addition to their biologically relevant dimensions, the possibilities of suitable bioconjugations and opportunities to tune their biocompatibility make them particularly valuable for use in biological systems.

### 1.4.1 Microgels in bioimaging

While a few of the aforementioned biological applications require the microgels to lend themselves to be imaged while serving their primary purpose, some microgels have been developed with the sole purpose of generating imaging agents. When considering optical probes, these constructs can broadly be divided into three different classes. The first of these includes particles with analyte recognition ligands, which can be used as sensors for DNA, proteins or other biomolecules, as discussed earlier (refer to section 1.3.3). The second category comprises of contrast agents like dyes either incorporated into microgels during polymerization or conjugated to them following synthesis, thus generating constructs with a high local concentration of the contrast agent in the microgel volume. This is beneficial for generating high intensity output signals. The last category combines optical properties of contrast agents with the ability of microgels to deswell on receiving an external stimulus. On undergoing a volume phase transition, microgels cause a change in the physicochemical environment of the contrast agent, which can be detected through a change in the optical signal. Some groups have utilized a combination or modified versions of these techniques. For example, Zhou et al. developed a ratiometric imaging/sensing system for antigen presenting cells (APCs) in the form of core/shell microgels with oxygen and pH sensitive probes in the core and shell respectively. These particles with a polystyrene (PS) core and pNIPAm shell were found to be biocompatible and have potential applications in disease diagnosis and the investigation of cellular metabolic processes using a multi-sensor platform.[109] Similarly, pNIPAm microgel based ratiometric probes for glucose and temperatures were generated by Wang et al., by incorporating glucose recognizing APBA residues and fluorescence

resonance energy transfer (FRET) donor and acceptor dyes within microgel matrices.[115] Furthermore, microgel-quantum dot hybrids have also been developed using numerous strategies and have been demonstrated to be useful in high quality photoluminescence imaging[116] and detection of biomolecules.[117] In addition to optical imaging, microgel systems have also been modified to lend themselves to magnetic resonance imaging (MRI). In one technique, microgels themselves were developed as the contrast agents by reacting manganese tetra(3-vinylphenyl) porphyrin with NIPAm or NIPMAm using free radical emulsion polymerization. This system can be utilized to monitor small changes in temperature using MRI, due to thermoresponsivity of the polymers.[118] Another recent demonstration of microgels for MRI involved the encapsulation of dye (as a drug mimic) loaded temperature sensitive and non-temperature sensitive liposomes within alginate microgels, following loading of a $T_1$ MRI contrast agent into the liposomes. The microgels were crosslinked with a $T_2$ MRI contrast agent and this arrangement thus facilitated simultaneous visualization of drug release and the microgels.[119] Thus, microgel constructs have been built for compatibility with some imaging modalities. However, this is a continuously evolving field and new developments related to newer imaging platforms continue to develop due to the abundance of opportunities that are being realized.

### 1.4.2 Microgels for targeted delivery of drugs and small molecule therapeutics

The porous nature of microgels and the ability to incorporate functionalities within their network (refer to section 1.3.2) have led to the generation of dually functional microgels, for specific targeting and delivery of therapeutics. Although some

systems of this nature have been discussed briefly in the preceding sections, this segment aims at discussing in detail, the range of systems developed specifically for this purpose with intricacies related to a few examples.

The delivery of chemotherapeutic agents specifically to cancer cells has been a prominent area of research, predominantly in order to mitigate off-target effects of cancer drugs like doxorubicin, such as myelosuppression and cardiotoxicity.[120] Targeted delivery systems are thus an important field of research and microgels form an important class of such materials. While passive targeting methodologies rely on the enhanced permeability and retention (EPR) effect due to abnormal vasculature at tumor sites,[121] active targeting is achieved by taking advantage of differential expression of certain moieties on cancer cells and their specific interactions with molecules that can be conjugated onto microgels. The types of interactions utilized for this targeting have been multifarious. While Nayak et al. targeted the folate receptor, utilizing the excessive folic acid demand specific to cancer cells,[122] Lu et al. utilized methotrexate (MTX), an analog of folic acid for simultaneous targeting and anti-cancer activity through interference in the folate metabolic pathway. The nanogels used by this group were gold nanoparticle loaded, polyacrylamide based particles.[123] Das et al. conjugated microgels to transferrin, with the goal of targeting the transferrin receptor that is upregulated in cancer cells and loaded the particles with doxorubicin (Dox), an anti-cancer drug.[124] Zhang et al. utilized the same interaction, but with chitosan microgels.[125] Thiol functionalized microgels were developed by Cook et al. as delivery systems for chemotherapeutic agents to the urinary bladder.[126] In addition to the delivery of anti-cancer drugs, RNA interference[127] has been explored in order to combat multidrug resistance developed by cancer cells through gene

silencing. Small RNAs like small interfering RNA (siRNA) and microRNA (miRNA)[128] have been demonstrated to be useful for this purpose, but reliable methods for their delivery still remain elusive. Dickerson et al. developed a nanogel based siRNA delivery vehicle, by conjugating functional groups on microgel shells to peptide mimics of the ephrin-A1 ligand, which specifically targets the EphA2 receptor that is overexpressed in cancer cells.[71,129] The difference in internal temperatures of healthy cells (~ 37 $^{0}$C) and tumor cells (~ 42 $^{0}$C) has also been exploited as a possible method of targeting by Rubio-Retama et al.[130] and Teng et al.[131] Additionally, core/shell poly(vinyl alcohol)-hyaluronic acid microgels were synthesized *via* click chemistry by Kupal et al. The specific targeting of these cells to adenocarcinoma colon cells was achieved through hyaluronic acid-CD44 interactions.[132]

In addition to the delivery of anti-cancer agents, microgel based systems have also been developed for delivery of other therapeutics to specific cells or organs. For example, oxidized starch microgels were demonstrated to be effective in protection of encapsulated anthocyanins from degradation in the upper gastric tract, for efficient delivery to the intestine by Wang et al.[133] Similarly, carboxymethyl starch/β-cyclodextrin microgels were developed for prevention of release of ascorbic acid before it reached the intestine. In this case, the therapeutic was incorporated into the delivery vehicle in the form of a microgel-ascorbic acid inclusion complex.[134] With the goal of generating an anti-osteoporotic effect and reducing uptake of particles by the liver, Heller et al. developed dextran based nanogels with click-able functional groups for biphosphonate ligand attachment.[83] These modular microgels are promising for delivery of therapeutics specifically to bone tissue, which is an arena that has remained relatively unexplored.[135]

The field of targeted delivery using microgels has thus grown tremendously over the past few years. The utilization of microgels in a number of biological applications is also gaining interest as the potential of different microgel constructs is being realized. The following chapters will focus on the detailed characterization of functional cationic microgel constructs (Chapter 2) and conjugations to these particles for generating imaging agents (Chapter 3). The utilization of core/shell microgel constructs in novel biomedical applications will also be discussed in the following chapters.

## 1.5 References


(1) Lutolf, M. P.; Hubbell, J. A.: Synthetic biomaterials as instructive extracellular microenvironments for morphogenesis in tissue engineering. *Nat. Biotechnol.* **2005**, *23*, 47-55.

(2) Chung, S.; Gamcsik, M. P.; King, M. W.: Novel scaffold design with multi-grooved PLA fibers. *Biomedical Materials* **2011**, *6*.

(3) Nair, L. S.; Laurencin, C. T.: Biodegradable polymers as biomaterials. *Prog. Polym. Sci.* **2007**, *32*, 762-798.

(4) Ulbricht, M.: Advanced functional polymer membranes. *Polymer* **2006**, *47*, 2217-2262.

(5) Morrison, C.; Macnair, R.; MacDonald, C.; Wykman, A.; Goldie, I.; Grant, M.: In vitro biocompatibility testing of polymers for orthopaedic implants using cultured fibroblasts and osteoblasts. *Biomaterials* **1995**, *16*, 987-992.

(6) Duncan, R.: The dawning era of polymer therapeutics. *Nat. Rev. Drug Discov.* **2003**, *2*, 347-360.

(7) Haag, R.; Kratz, F.: Polymer therapeutics: Concepts and applications. *Angew. Chem.-Int. Edit.* **2006**, *45*, 1198-1215.

(8) Peppas, N. A.; Langer, R.: New challenges in biomaterials. *Science* **1994**, *263*, 1715-1720.

(9) Silver, J. H.; Hart, A. P.; Williams, E. C.; Cooper, S. L.; Charef, S.; Labarre, D.; Jozefowicz, M.: Anticoagulant effects of sulfonated polyurethanes. *Biomaterials* **1992**, *13*, 339-344.

(10) Wang, Y. D.; Ameer, G. A.; Sheppard, B. J.; Langer, R.: A tough biodegradable elastomer. *Nat. Biotechnol.* **2002**, *20*, 602-606.

(11) Sigal, G. B.; Mammen, M.; Dahmann, G.; Whitesides, G. M.: Polyacrylamides bearing pendant alpha-sialoside groups strongly inhibit agglutination of erythrocytes by influenza virus: The strong inhibition reflects enhanced binding through cooperative polyvalent interactions. *J. Am. Chem. Soc.* **1996**, *118*, 3789-3800.

(12) Gregoriadis, G.; McCormack, B.; Wang, Z.; Lifely, R.: Polysialic acids - potential in drug delivery. *FEBS Lett.* **1993**, *315*, 271-276.

(13) Roy, R.; Zanini, D.; Meunier, S. J.; Romanowska, A.: Synthesis and antigenic properties of sialic-acid based dendrimers. In *Synthetic Oligosaccharides: Indispensable Probes for the Life Sciences*; Kovac, P., Ed.; Amer Chemical Soc: Washington, 1994; Vol. 560; pp 104-119.

(14) Tormala, P.; Vasenius, J.; Vainionpaa, S.; Laiho, J.; Pohjonen, T.; Rokkanen, P.: Ultra-high-strength absorbable self-reinforced polyglycolide (sr-pga) composite rods for internal-fixation of bone-fractures - invitro and invivo study. *J. Biomed. Mater. Res.* **1991**, *25*, 1-22.

(15) Jatzkewitz, H.: An ein kolloidales blutplasma-ersatzmittel (polyvinylpyrrolidon) gebundenes peptamin (glycyl-l-leucyl-mezcalin) als neuartige depotform fur biologisch aktive primare amine (mezcalin). *Zeitschrift Fur Naturforschung Part B-Chemie Biochemie Biophysik Biologie Und Verwandten Gebiete* **1955**, *10*, 27-31.

(16) Agarwal, A.; Huang, S. W.; O'Donnell, M.; Day, K. C.; Day, M.; Kotov, N.; Ashkenazi, S.: Targeted gold nanorod contrast agent for prostate cancer detection by photoacoustic imaging. *J. Appl. Phys.* **2007**, *102*.

(17) Bardhan, R.; Chen, W. X.; Perez-Torres, C.; Bartels, M.; Huschka, R. M.; Zhao, L. L.; Morosan, E.; Pautler, R. G.; Joshi, A.; Halas, N. J.: Nanoshells with Targeted Simultaneous Enhancement of Magnetic and Optical Imaging and Photothermal Therapeutic Response. *Advanced Functional Materials* **2009**, *19*, 3901-3909.

(18) Chen, M.; Tang, S. H.; Guo, Z. D.; Wang, X. Y.; Mo, S. G.; Huang, X. Q.; Liu, G.; Zheng, N. F.: Core-Shell Pd@Au Nanoplates as Theranostic Agents for In-Vivo Photoacoustic Imaging, CT Imaging, and Photothermal Therapy. *Adv. Mater.* **2014**, *26*, 8210-8216.

(19) Cheng, L.; Gong, H.; Zhu, W. W.; Liu, J. J.; Wang, X. Y.; Liu, G.; Liu, Z.: PEGylated Prussian blue nanocubes as a theranostic agent for simultaneous cancer imaging and photothermal therapy. *Biomaterials* **2014**, *35*, 9844-9852.

(20) Erathodiyil, N.; Ying, J. Y.: Functionalization of Inorganic Nanoparticles for Bioimaging Applications. *Accounts of Chemical Research* **2011**, *44*, 925-935.

(21) Frey, N. A.; Peng, S.; Cheng, K.; Sun, S. H.: Magnetic nanoparticles: synthesis, functionalization, and applications in bioimaging and magnetic energy storage. *Chem. Soc. Rev.* **2009**, *38*, 2532-2542.

(22) Wang, J.; Polleux, J.; Lim, J.; Dunn, B.: Pseudocapacitive Contributions to Electrochemical Energy Storage in TiO2 (Anatase) Nanoparticles. *J. Phys. Chem. C* **2007**, *111*, 14925-14931.

(23) Stevens, P. D.; Fan, J. D.; Gardimalla, H. M. R.; Yen, M.; Gao, Y.: Superparamagnetic nanoparticle-supported catalysis of Suzuki cross-coupling reactions. *Org. Lett.* **2005**, *7*, 2085-2088.

(24) Daniel, M. C.; Astruc, D.: Gold nanoparticles: Assembly, supramolecular chemistry, quantum-size-related properties, and applications toward biology, catalysis, and nanotechnology. *Chemical Reviews* **2004**, *104*, 293-346.

(25) Gao, X. H.; Cui, Y. Y.; Levenson, R. M.; Chung, L. W. K.; Nie, S. M.: In vivo cancer targeting and imaging with semiconductor quantum dots. *Nat. Biotechnol.* **2004**, *22*, 969-976.

(26) zur Muhlen, A.; Schwarz, C.; Mehnert, W.: Solid lipid nanoparticles (SLN) for controlled drug delivery - Drug release and release mechanism. *Eur. J. Pharm. Biopharm.* **1998**, *45*, 149-155.

(27) Huang, X. H.; El-Sayed, I. H.; Qian, W.; El-Sayed, M. A.: Cancer cell imaging and photothermal therapy in the near-infrared region by using gold nanorods. *J. Am. Chem. Soc.* **2006**, *128*, 2115-2120.

(28) Jokerst, J. V.; Lobovkina, T.; Zare, R. N.; Gambhir, S. S.: Nanoparticle PEGylation for imaging and therapy. *Nanomedicine (London, U. K.)* **2011**, *6*, 715-728.

(29) van Vlerken, L. E.; Vyas, T. K.; Amiji, M. M.: Poly(ethylene glycol)-modified Nanocarriers for Tumor-targeted and Intracellular Delivery. *Pharm. Res.* **2007**, *24*, 1405-1414.

(30) Davis, S.; Abuchowski, A.; Park, Y. K.; Davis, F. F.: Alteration of the circulating life and antigenic properties of bovine adenosine-deaminase in mice by attachment of polyethylene-glycol. *Clin. Exp. Immunol.* **1981**, *46*, 649-652.

(31) Murray, K. F.; Rodrigue, J. R.; Gonzalez-Peralta, R. P.; Shepherd, J.; Barton, B. A.; Robuck, P. R.; Schwarz, K. B.; Network, P.-C. C. R.: Design of the PEDS-C trial: pegylated interferon +/- ribavirin for children with chronic hepatitis C viral infection. *Clin. Trials* **2007**, *4*, 661-673.

(32) Lutz, J. F.: Thermo-Switchable Materials Prepared Using the OEGMA-Platform. *Adv. Mater.* **2011**, *23*, 2237-2243.

(33) Cai, T.; Marquez, M.; Hu, Z. B.: Monodisperse thermoresponsive microgels of poly(ethylene glycol) analogue-based biopolymers. *Langmuir* **2007**, *23*, 8663-8666.

(34) Zhou, T.; Wu, W. T.; Zhou, S. Q.: Engineering oligo(ethylene glycol)-based thermosensitive microgels for drug delivery applications. *Polymer* **2010**, *51*, 3926-3933.

(35) Murthy, N.; Xu, M.; Schuck, S.; Kunisawa, J.; Shastri, N.; Frechet, J. M. J.: A macromolecular delivery vehicle for protein-based vaccines: acid-degradable protein-loaded microgels. *Proc Natl Acad Sci U S A* **2003**, *100*, 4995-5000.

(36) Riley, T.; Stolnik, S.; Heald, C. R.; Xiong, C. D.; Garnett, M. C.; Illum, L.; Davis, S. S.; Purkiss, S. C.; Barlow, R. J.; Gellert, P. R.: Physicochemical evaluation of nanoparticles assembled from poly(lactic acid)-poly(ethylene glycol) (PLA-PEG) block copolymers as drug delivery vehicles. *Langmuir* **2001**, *17*, 3168-3174.

(37) Riley, T.; Heald, C. R.; Stolnik, S.; Garnett, M. C.; Illum, L.; Davis, S. S.; King, S. M.; Heenan, R. K.; Purkiss, S. C.; Barlow, R. J.; Gellert, P. R.; Washington, C.: Core-shell structure of PLA-PEG nanoparticles used for drug delivery. *Langmuir* **2003**, *19*, 8428-8435.

(38) Smith, M. H.; Lyon, L. A.: Multifunctional Nanogels for siRNA Delivery. *Accounts of Chemical Research* **2012**, *45*, 985-993.

(39) Slatopolsky, E. A.; Burke, S. K.; Dillon, M. A.; RenaGel Study, G.: RenaGel (R), a nonabsorbed calcium- and aluminum-free phosphate binder, lowers serum phosphorus and parathyroid hormone. *Kidney Int.* **1999**, *55*, 299-307.

(40) Mandeville, W. H.; Goldberg, D. I.: The sequestration of bile acids, a non-absorbed method for cholesterol reduction. A review. *Curr. Pharm. Design* **1997**, *3*, 15-28.

(41) Seymour, L. W.; Ferry, D. R.; Anderson, D.; Hesslewood, S.; Julyan, P. J.; Poyner, R.; Doran, J.; Young, A. M.; Burtles, S.; Kerr, D. J.; Canc Res Campaign Phase, I. I. I. C.: Hepatic drug targeting: Phase I evaluation of polymer-bound doxorubicin. *J. Clin. Oncol.* **2002**, *20*, 1668-1676.

(42) Duncan, R.; Seymour, L. C. W.; Scarlett, L.; Lloyd, J. B.; Rejmanova, P.; Kopecek, J.: Fate of n-(2-hydroxypropyl)methacrylamide copolymers with pendent galactosamine residues after intravenous administration to rats. *Biochimica Et Biophysica Acta* **1986**, *880*, 62-71.

(43) Kataoka, K.; Harada, A.; Nagasaki, Y.: Block copolymer micelles for drug delivery: design, characterization and biological significance. *Adv. Drug Deliv. Rev.* **2001**, *47*, 113-131.

(44) Kabanov, A. V.; Batrakova, E. V.; Meliknubarov, N. S.; Fedoseev, N. A.; Dorodnich, T. Y.; Alakhov, V. Y.; Chekhonin, V. P.; Nazarova, I. R.; Kabanov, V. A.: A New class of drug carriers - micelles of poly(oxyethylene)-poly(oxypropylene) block copolymers as microcontainers for drug targeting from blood in brain. *J. Control. Release* **1992**, *22*, 141-157.

(45) Batrakova, E. V.; Dorodnych, T. Y.; Klinskii, E. Y.; Kliushnenkova, E. N.; Shemchukova, O. B.; Goncharova, O. N.; Arjakov, S. A.; Alakhov, V. Y.; Kabanov, A. V.: Anthracycline antibiotics non-covalently incorporated into the block copolymer micelles: In vivo evaluation of anti-cancer activity. *Br. J. Cancer* **1996**, *74*, 1545-1552.

(46) Alakhov, V.; Klinski, E.; Li, S. M.; Pietrzynski, G.; Venne, A.; Batrakova, E.; Bronitch, T.; Kabanov, A.: Block copolymer-based formulation of doxorubicin. From cell screen to clinical trials. *Colloid Surf. B-Biointerfaces* **1999**, *16*, 113-134.

(47) Klingstedt, T.; Nilsson, K. P. R.: Conjugated polymers for enhanced bioimaging. *Biochim. Biophys. Acta-Gen. Subj.* **2011**, *1810*, 286-296.

(48) Nasongkla, N.; Bey, E.; Ren, J.; Ai, H.; Khemtong, C.; Guthi, J. S.; Chin, S.-F.; Sherry, A. D.; Boothman, D. A.; Gao, J.: Multifunctional Polymeric Micelles as Cancer-Targeted, MRI-Ultrasensitive Drug Delivery Systems. *Nano Lett.* **2006**, *6*, 2427-2430.

(49) Wiener, E. C.; Brechbiel, M. W.; Brothers, H.; Magin, R. L.; Gansow, O. A.; Tomalia, D. A.; Lauterbur, P. C.: Dendrimer-based metal chelates: a new class of magnetic resonance imaging contrast agents. *Magn. Reson. Med.* **1994**, *31*, 1-8.

(50) Weissleder, R.; Tung, C.-H.; Mahmood, U.; Bogdanov, A., Jr.: In vivo imaging of tumors with protease-activated near-infrared fluorescent probes. *Nat. Biotechnol.* **1999**, *17*, 375-378.

(51) Feng, X.; Liu, L.; Wang, S.; Zhu, D.: Water-soluble fluorescent conjugated polymers and their interactions with biomacromolecules for sensitive biosensors. *Chem. Soc. Rev.* **2010**, *39*, 2411-2419.

(52) Wu, C.; Bull, B.; Szymanski, C.; Christensen, K.; McNeill, J.: Multicolor Conjugated Polymer Dots for Biological Fluorescence Imaging. *ACS Nano* **2008**, *2*, 2415-2423.

(53) Meid, J.; Dierkes, F.; Cui, J.; Messing, R.; Crosby, A. J.; Schmidt, A.; Richtering, W.: Mechanical properties of temperature sensitive microgel/polyacrylamide composite hydrogels-from soft to hard fillers. *Soft Matter* **2012**, *8*, 4254-4263.

(54) Bachman, H.; Brown, A. C.; Clarke, K. C.; Dhada, K. S.; Douglas, A.; Hansen, C. E.; Herman, E.; Hyatt, J. S.; Kodlekere, P.; Meng, Z. Y.; Saxena, S.; Spears, M. W.; Welsch, N.; Lyon, L. A.: Ultrasoft, highly deformable microgels. *Soft Matter* **2015**, *11*, 2018-2028.

(55) Gao, J.; Hu, Z.: Optical Properties of N-Isopropylacrylamide Microgel Spheres in Water. *Langmuir* **2002**, *18*, 1360-1367.

(56) Zhang, Q. M.; Li, X.; Islam, M. R.; Wei, M.; Serpe, M. J.: Light switchable optical materials from azobenzene crosslinked poly(N-isopropylacrylamide)-based microgels. *J. Mater. Chem. C* **2014**, *2*, 6961-6965.

(57) Boyko, V.; Richter, S.; Burchard, W.; Arndt, K.-F.: Chain dynamics in microgels: Poly(N-vinylcaprolactam-co-N-vinylpyrrolidone) microgels as examples. *Langmuir* **2007**, *23*, 776-784.

(58) Lowe, J. S.; Chowdhry, B. Z.; Parsonage, J. R.; Snowden, M. J.: The preparation and physico-chemical properties of poly(N-ethylacrylamide) microgels. *Polymer* **1998**, *39*, 1207-1212.

(59) Miao, C.; Chen, X.; Pelton, R.: Adhesion of poly(vinylamine) microgels to wet cellulose. *Ind. Eng. Chem. Res.* **2007**, *46*, 6486-6493.

(60) Nolan, C. M.; Serpe, M. J.; Lyon, L. A.: Thermally modulated insulin release from microgel thin films. *Biomacromolecules* **2004**, *5*, 1940-1946.

(61) Li, X.; Gao, Y.; Serpe, M. J.: Responsive Polymer-Based Assemblies for Sensing Applications. *Macromolecular Rapid Communications* **2015**, *36*, 1382-1392.

(62) Capriles-Gonzalez, D.; Sierra-Martin, B.; Fernandez-Nieves, A.; Fernandez-Barbero, A.: Coupled deswelling of multiresponse microgels. *J Phys Chem B* **2008**, *112*, 12195-200.

(63) Gaulding, J. C.; South, A. B.; Lyon, L. A.: Hydrolytically degradable shells on thermoresponsive microgels. *Colloid and Polymer Science* **2013**, *291*, 99-107.

(64) Smith, M. H.; Herman, E. S.; Lyon, L. A.: Network Deconstruction Reveals Network Structure in Responsive Microgels. *J. Phys. Chem. B* **2011**, *115*, 3761-3764.

(65) South, A. B.; Lyon, L. A.: Direct Observation of Microgel Erosion via in-Liquid Atomic Force Microscopy. *Chemistry of Materials* **2010**, *22*, 3300-3306.

(66) Knipe, J. M.; Chen, F.; Peppas, N. A.: Enzymatic Biodegradation of Hydrogels for Protein Delivery Targeted to the Small Intestine. *Biomacromolecules* **2015**, *16*, 962-972.

(67) Pelton, R. H.; Chibante, P.: Preparation of aqueous lattices with n-isopropylacrylamide. *Colloids and Surfaces* **1986**, *20*, 247-256.

(68) Schmidt, S.; Zeiser, M.; Hellweg, T.; Duschl, C.; Fery, A.; Mohwald, H.: Adhesion and Mechanical Properties of PNIPAm Microgel Films and Their Potential Use as Switchable Cell Culture Substrates. *Advanced Functional Materials* **2010**, *20*, 3235-3243.

(69) Rao, K. S. V. K.; Naidu, B. V. K.; Subha, M. C. S.; Sairam, M.; Aminabhavi, T. M.: Novel chitosan-based pH-sensitive interpenetrating network microgels for the controlled release of cefadroxil. *Carbohydr. Polym.* **2006**, *66*, 333-344.

(70) Iwai, K.; Matsumura, Y.; Uchiyama, S.; Prasanna de Silva, A.: Development of fluorescent microgel thermometers based on thermo-responsive polymers and their modulation of sensitivity range. *J. Mater. Chem.* **2005**, *15*, 2796-2800.

(71) Dickerson, E. B.; Blackburn, W. H.; Smith, M. H.; Kapa, L. B.; Lyon, L. A.; McDonald, J. F.: Chemosensitization of cancer cells by siRNA using targeted nanogel delivery. *BMC Cancer* **2010**, *10*.

(72) Rodriguez, B. E.; Wolfe, M. S.; Fryd, M.: Nonuniform swelling of alkali swellable microgels. *Macromolecules* **1994**, *27*, 6642-6647.

(73) Ma, X. M.; Cui, Y. J.; Zhao, X.; Zheng, S. X.; Tang, X. Z.: Different deswelling behavior of temperature-sensitive microgels of poly(N-isopropylacrylamide) crosslinked by polyethyleneglycol dimethacrylates. *J. Colloid Interface Sci.* **2004**, *276*, 53-59.

(74) Nayak, S.; Gan, D. J.; Serpe, M. J.; Lyon, L. A.: Hollow thermoresponsive microgels. *Small* **2005**, *1*, 416-421.

(75) Liu, R.; Saunders, J. M.; Freemont, T. J.; Saunders, B. R.: Doubly crosslinked microgel-polyelectrolyte complexes: three simple methods to tune and improve gel mechanical properties. *Soft Matter* **2012**, *8*, 10932-10940.

(76) Meunier, F.; Pichot, C.; Elaissari, A.: Effect of thiol-containing monomer on the preparation of temperature-sensitive hydrogel microspheres. *Colloid and Polymer Science* **2006**, *284*, 1287-1292.

(77) Gao, J.; Frisken, B. J.: Cross-linker-free N-isopropylacrylamide gel nanospheres. *Langmuir* **2003**, *19*, 5212-5216.

(78) Gao, J.; Frisken, B. J.: Influence of reaction conditions on the synthesis of self-cross-linked N-isopropylacrylamide microgels. *Langmuir* **2003**, *19*, 5217-5222.

(79) McPhee, W.; Tam, K. C.; Pelton, R.: Poly(n-isopropylacrylamide) latices prepared with sodium dodecyl-sulfate. *J. Colloid Interface Sci.* **1993**, *156*, 24-30.

(80) Duracher, D.; Elaissari, A.; Mallet, F.; Pichot, C.: Preparation of thermosensitive latexes by copolymerization of N-isopropylmethacrylamide with a chelating monomer. *Macromolecular Symposia* **2000**, *150*, 297-303.

(81) Hoare, T.; Pelton, R.: Functional group distributions in carboxylic acid containing poly(N-isopropylacrylamide) microgels. *Langmuir* **2004**, *20*, 2123-2133.

(82) Thaiboonrod, S.; Berkland, C.; Milani, A. H.; Ulijn, R.; Saunders, B. R.: Poly(vinylamine) microgels: pH-responsive particles with high primary amine contents. *Soft Matter* **2013**, *9*, 3920-3930.

(83) Heller, D. A.; Levi, Y.; Pelet, J. M.; Doloff, J. C.; Wallas, J.; Pratt, G. W.; Jiang, S.; Sahay, G.; Schroeder, A.; Schroeder, J. E.; Chyan, Y.; Zurenko, C.; Querbes, W.; Manzano, M.; Kohane, D. S.; Langer, R.; Anderson, D. G.: Modular 'Click-in-Emulsion' Bone-Targeted Nanogels. *Adv. Mater.* **2013**, *25*, 1449-1454.

(84) Hoare, T.; Pelton, R.: Titrametric characterization of pH-induced phase transitions in functionalized microgels. *Langmuir* **2006**, *22*, 7342-7350.

(85) Elmas, B.; Onur, M. A.; Senel, S.; Tuncel, A.: Temperature controlled RNA isolation by N-isopropylacrylamide-vinylphenyl boronic acid copolymer latex. *Colloid and Polymer Science* **2002**, *280*, 1137-1146.

(86) Garcia, A.; Marquez, M.; Cai, T.; Rosario, R.; Hu, Z. B.; Gust, D.; Hayes, M.; Vail, S. A.; Park, C. D.: Photo-, thermally, and pH-responsive microgels. *Langmuir* **2007**, *23*, 224-229.

(87) Eke, I.; Elmas, B.; Tuncel, M.; Tuncel, A.: A new, highly stable cationic-thermosensitive microgel: Uniform isopropylacrylamide-dimethylaminopropylmethacrylamide copolymer particles. *Colloid Surf. A-Physicochem. Eng. Asp.* **2006**, *279*, 247-253.

(88) Pikabea, A.; Ramos, J.; Forcada, J.: Production of Cationic Nanogels with Potential Use in Controlled Drug Delivery. *Particle & Particle Systems Characterization* **2014**, *31*, 101-109.

(89) Hemmati, K.; Masoumi, A.; Ghaemy, M.: pH responsive tragacanth gum and poly(methyl methacrylate-co-maleic anhydride)-g-poly(caprolactone) co-network microgel for in vitro quercetin release. *Polymer* **2015**, *59*, 49-56.

(90) Srinivas, R. L.; Chapin, S. C.; Doyle, P. S.: Aptamer-Functionalized Microgel Particles for Protein Detection. *Anal. Chem. (Washington, DC, U. S.)* **2011**, *83*, 9138-9145.

(91) Ali, M. M.; Aguirre, S. D.; Xu, Y.; Filipe, C. D. M.; Pelton, R.; Li, Y.: Detection of DNA using bioactive paper strips. *Chem. Commun. (Cambridge, U. K.)* **2009**, 6640-6642.

(92) Hoare, T.; Pelton, R.: Engineering glucose swelling responses in poly(N-isopropylacrylamide)-based microgels. *Macromolecules* **2007**, *40*, 670-678.

(93) Sorrell, C. D.; Serpe, M. J.: Glucose sensitive poly(N-isopropylacrylamide) microgel based etalons. *Anal. Bioanal. Chem.* **2012**, *402*, 2385-2393.

(94) Chen, K.; Merkel, T. J.; Pandya, A.; Napier, M. E.; Luft, J. C.; Daniel, W.; Sheiko, S.; DeSimone, J. M.: Low Modulus Biomimetic Microgel Particles with High Loading of Hemoglobin. *Biomacromolecules* **2012**, *13*, 2748-2759.

(95) Brown, A. C.; Stabenfeldt, S. E.; Ahn, B.; Hannan, R. T.; Dhada, K. S.; Herman, E. S.; Stefanelli, V.; Guzzetta, N.; Alexeev, A.; Lam, W. A.; Lyon, L. A.; Barker, T. H.: Ultrasoft microgels displaying emergent platelet-like behaviours. *Nat. Mater.* **2014**, *13*, 1108-1114.

(96) Pelton, R.: Temperature-sensitive aqueous microgels. *Advances in Colloid and Interface Science* **2000**, *85*, 1-33.

(97) Blackburn, W. H.; Lyon, L. A.: Size-controlled synthesis of monodisperse core/shell nanogels. *Colloid and Polymer Science* **2008**, *286*, 563-569.

(98) Lehmann, S.; Seiffert, S.; Richtering, W.: Diffusion of guest molecules within sensitive core-shell microgel carriers. *J. Colloid Interface Sci.* **2014**, *431*, 204-208.

(99) Schachschal, S.; Balaceanu, A.; Melian, C.; Demco, D. E.; Eckert, T.; Richtering, W.; Pich, A.: Polyampholyte Microgels with Anionic Core and Cationic Shell. *Macromolecules* **2010**, *43*, 4331-4339.

(100) Zhu, P. W.; Napper, D. H.: studies of aggregation kinetics of polystyrene latices sterically stabilized by poly(n-isopropylacrylamide). *Phys. Rev. E* **1994**, *50*, 1360-1366.

(101) Duracher, D.; Sauzedde, F.; Elaissari, A.; Perrin, A.; Pichot, C.: Cationic amino-containing N-isopropylacrylamide-styrene copolymer latex particles: 1 - Particle size and morphology vs. polymerization process. *Colloid and Polymer Science* **1998**, *276*, 219-231.

(102) Lu, Y.; Mei, Y.; Drechsler, M.; Ballauff, M.: Thermosensitive core-shell particles as carriers for Ag nanoparticles: Modulating the catalytic activity by a phase transition in networks. *Angew. Chem.-Int. Edit.* **2006**, *45*, 813-816.

(103) Ballauff, M.; Lu, Y.: "Smart" nanoparticles: Preparation, characterization and applications. *Polymer* **2007**, *48*, 1815-1823.

(104) Zha, L. S.; Zhang, Y.; Yang, W. L.; Fu, S. K.: Monodisperse temperature-sensitive microcontainers. *Adv. Mater.* **2002**, *14*, 1090-+.

(105) Kim, J. H.; Lee, T. R.: Thermo- and pH-responsive hydrogel-coated gold nanoparticles. *Chemistry of Materials* **2004**, *16*, 3647-3651.

(106) Berndt, I.; Richtering, W.: Doubly temperature sensitive core-shell microgels. *Macromolecules* **2003**, *36*, 8780-8785.

(107) Clarke, K. C.; Dunham, S. N.; Lyon, L. A.: Core/Shell Microgels Decouple the pH and Temperature Responsivities of Microgel Films. *Chemistry of Materials* **2015**, *27*, 1391-1396.

(108) Mei, Y.; Lu, Y.; Polzer, F.; Ballauff, M.; Drechsler, M.: Catalytic activity of palladium nanoparticles encapsulated in spherical polyelectrolyte brushes and core-shell microgels. *Chemistry of Materials* **2007**, *19*, 1062-1069.

(109) Zhou, X. F.; Su, F. Y.; Tian, Y. Q.; Meldrum, D. R.: Dually Fluorescent Core-Shell Microgels for Ratiometric Imaging in Live Antigen-Presenting Cells. *Plos One* **2014**, *9*.

(110) Jones, C. D.; Lyon, L. A.: Shell-restricted swelling and core compression in poly(N-isopropylacrylamide) core-shell microgels. *Macromolecules* **2003**, *36*, 1988-1993.

(111) Tripathi, B. P.; Dubey, N. C.; Stamm, M.: Hollow Microgel Based Ultrathin Thermoresponsive Membranes for Separation, Synthesis, and Catalytic Applications. *ACS Appl. Mater. Interfaces* **2014**, *6*, 17702-17712.

(112) De Geest, B. G.; De Koker, S.; Demeester, J.; De Smedt, S.; Hennink, W. E.: Self-exploding capsules. *Polym. Chem.* **2010**, *1*, 137-148.

(113) De Geest, B. G.; Dejugnat, C.; Verhoeven, E.; Sukhorukov, G. B.; Jonas, A. M.; Plain, J.; Demeester, J.; De Smedt, S. C.: Layer-by-layer coating of degradable microgels for pulsed drug delivery. *J. Controlled Release* **2006**, *116*, 159-169.

(114) Hu, X. B.; Tong, Z.; Lyon, L. A.: Multicompartment Core/Shell Microgels. *J. Am. Chem. Soc.* **2010**, *132*, 11470-11472.

(115) Wang, D.; Liu, T.; Yin, J.; Liu, S.: Stimuli-Responsive Fluorescent Poly(N-isopropylacrylamide) Microgels Labeled with Phenylboronic Acid Moieties as Multifunctional Ratiometric Probes for Glucose and Temperatures. *Macromolecules (Washington, DC, U. S.)* **2011**, *44*, 2282-2290.

(116) Gui, R.; An, X.; Gong, J.; Chen, T.: Thermosensitive, reversible luminescence properties and bright fluorescence imaging of water-soluble quantum dots/microgels nanocompounds. *Mater. Lett.* **2012**, *88*, 122-125.

(117) Wu, W.; Zhou, T.; Shen, J.; Zhou, S.: Optical detection of glucose by CdS quantum dots immobilized in smart microgels. *Chem. Commun. (Cambridge, U. K.)* **2009**, 4390-4392.

(118) Zheng, X.; Qian, J.; Tang, F.; Wang, Z.; Cao, C.; Zhong, K.: Microgel-Based Thermosensitive MRI Contrast Agent. *ACS Macro Lett.* **2015**, *4*, 431-435.

(119) van Elk, M.; Lorenzato, C.; Ozbakir, B.; Oerlemans, C.; Storm, G.; Nijsen, F.; Deckers, R.; Vermonden, T.; Hennink, W. E.: Alginate microgels loaded with temperature sensitive liposomes for magnetic resonance imageable drug release and microgel visualization. *Eur. Polym. J.* **2015**, Ahead of Print.

(120) Ibrahim, N. K.; Frye, D. K.; Buzdar, A. U.; Walters, R. S.; Hortobagyi, G. N.: Doxorubicin-based chemotherapy in elderly patients with metastatic breast cancer - Tolerance and outcome. *Arch. Intern. Med.* **1996**, *156*, 882-888.

(121) Matsumura, Y.; Maeda, H.: A new concept for macromolecular therapeutics in cancer-chemotherapy - mechanism of tumoritropic accumulation of proteins and the antitumor agent smancs. *Cancer Res.* **1986**, *46*, 6387-6392.

(122) Nayak, S.; Lee, H.; Chmielewski, J.; Lyon, L. A.: Folate-mediated cell targeting and cytotoxicity using thermoresponsive microgels. *J. Am. Chem. Soc.* **2004**, *126*, 10258-10259.

(123) Lu, S.; Neoh, K. G.; Huang, C.; Shi, Z.; Kang, E.-T.: Polyacrylamide hybrid nanogels for targeted cancer chemotherapy via co-delivery of gold nanoparticles and MTX. *J. Colloid Interface Sci.* **2013**, *412*, 46-55.

(124) Das, M.; Mardyani, S.; Chan, W. C. W.; Kumacheva, E.: Biofunctionalized pH-responsive microgels for cancer cell targeting: Rational design. *Adv. Mater. (Weinheim, Ger.)* **2006**, *18*, 80-83.

(125) Zhang, H.; Mardyani, S.; Chan, W. C. W.; Kumacheva, E.: Design of biocompatible chitosan microgels for targeted pH-mediated intracellular release of cancer therapeutics. *Biomacromolecules* **2006**, *7*, 1568-1572.

(126) Cook, M. T.; Schmidt, S. A.; Lee, E.; Samprasit, W.; Opanasopit, P.; Khutoryanskiy, V. V.: Synthesis of mucoadhesive thiol-bearing microgels from 2-(acetylthio)ethylacrylate and 2-hydroxyethylmethacrylate: novel drug delivery systems for chemotherapeutic agents to the bladder. *J. Mater. Chem. B* **2015**, *3*, 6599-6604.

(127) Fire, A.; Xu, S. Q.; Montgomery, M. K.; Kostas, S. A.; Driver, S. E.; Mello, C. C.: Potent and specific genetic interference by double-stranded RNA in Caenorhabditis elegans. *Nature* **1998**, *391*, 806-811.

(128) Liu, J.; Valencia-Sanchez, M. A.; Hannon, G. J.; Parker, R.: MicroRNA-dependent localization of targeted mRNAs to mammalian P-bodies. *Nat Cell Biol* **2005**, *7*, 719-23.

(129) Blackburn, W. H.; Dickerson, E. B.; Smith, M. H.; McDonald, J. F.; Lyon, L. A.: Peptide-Functionalized Nanogels for Targeted siRNA Delivery. *Bioconjugate Chem.* **2009**, *20*, 960-968.

(130) Rubio-Retama, J.; Zafeiropoulos, N. E.; Serafinelli, C.; Rojas-Reyna, R.; Voit, B.; Lopez Cabarcos, E.; Stamm, M.: Synthesis and characterization of thermosensitive PNIPAm microgels covered with superparamagnetic γ-Fe2O3 nanoparticles. *Langmuir* **2007**, *23*, 10280-10285.

(131) Teng, D.; Hou, J.; Zhang, X.; Wang, X.; Wang, Z.; Li, C.: Glucosamine-carrying temperature- and pH-sensitive microgels: Preparation, characterization, and in vitro drug release studies. *J. Colloid Interface Sci.* **2008**, *322*, 333-341.

(132) Kupal, S. G.; Cerroni, B.; Ghugare, S. V.; Chiessi, E.; Paradossi, G.: Biointerface Properties of Core-Shell Poly(vinyl alcohol)-hyaluronic Acid Microgels Based on Chemoselective Chemistry. *Biomacromolecules* **2012**, *13*, 3592-3601.

(133) Wang, Z.; Li, Y.; Chen, L.; Xin, X.; Yuan, Q.: A Study of Controlled Uptake and Release of Anthocyanins by Oxidized Starch Microgels. *J. Agric. Food Chem.* **2013**, *61*, 5880-5887.

(134) Zhang, B.; Li, H.; Li, X.; Cheng, C.; Jin, Z.; Xu, X.; Tian, Y.: Preparation, characterization, and in vitro release of carboxymethyl starch/β-cyclodextrin microgel-ascorbic acid inclusion complexes. *RSC Adv.* **2015**, *5*, 61815-61820.

(135) Wang, D.; Miller, S. C.; Kopeckova, P.; Kopecek, J.: Bone-targeting macromolecular therapeutics. *Adv. Drug Deliv. Rev.* **2005**, *57*, 1049-1076.

# CHAPTER 2

# DESIGN AND PHYSICOCHEMICAL CHARACTERIZATION OF FUNCTIONAL CATIONIC MICROGEL CONSTRUCTS

*(**Purva Kodlekere**, Anabel Liyen Cartelle, L. Andrew Lyon; Design of functional cationic microgel constructs for utilization as conjugation agents)*

*To be submitted to: Journal of Materials Chemistry B*

## 2.1 Introduction

The widespread applicability of colloidal conjugates has led to the development of a range of systems that can be utilized in controlled conjugations. Through different routes, such constructs have been developed for various purposes like the delivery of therapeutics, imaging, and solubilization of active agents.[1-6] A number of these constructs have the advantage of being in the nano- to micro- range, which makes them increasingly attractive for employment in conjunction with biological systems due to their similarity in dimensions to specific cells and cellular components, and thus increased control over processes happening at this scale.[7-10] Furthermore, the opportunity to tune their size to match specific applications provides additional advantages.[11] Microgels constitute a promising sub-class of such materials. Similar to their bulk hydrogels counterparts, microgels are water swollen, yet can be synthesized to have sizes ranging from tens of nanometers to a few microns.[12,13] They have been demonstrated to be beneficial in a wide array of biological applications, including tumor targeting for delivery of therapeutic agents,[14] bioresponsive microlenses,[15] artificial platelets[16] and in non-fouling coatings.[17]

The versatility in their synthesis also makes it possible to make them more 'biofriendly' through the utilization of biocompatible constituent polymers[18] and degradable crosslinkers,[19,20] further enhancing their suitability for use in biological systems.

A number of species such as single chain antibodies,[21] peptides[22] and biologically relevant small molecules[23] have been conjugated to microgels through suitable reactions in order to make the resulting constructs useful for some of the applications mentioned above. This has primarily been made possible through the introduction of functional groups within the microgel matrices during synthesis, by copolymerization with molecules containing the desirable functionalities. Thus, microgels with versatile functionalities such as carboxylic acid groups, amine groups and others[24,25] have been synthesized in the past. Microgels being porous networks, the presence of these entities throughout their matrix provides the potential for multivalency to an even higher extent than that observed in comparable hard sphere microparticles, which are only capable of displaying functionalities on their surface. This high density display of functional groups is useful for development of conjugates with very high local concentrations of the relevant biomolecules. One such functional group that can be incorporated in microgel networks is the amine group. The incorporation of amine groups brings with it the opportunity to perform numerous conjugation reactions to a range of functional groups on the biomolecules, such as NHS esters, isocyanates or isothiocyanates, acyl azides, carbodiimides, and aldehydes.[26] Thus, keeping the potential of these systems in mind, cationic polymeric particles containing amine groups have been synthesized and characterized by several groups in the past.[27-30] Both N-isopropylacrylamide (NIPAm) and N-isopropylmethacrylamide (NIPMAm) have been used along with comonomers like

N-(3-aminopropyl)methacrylamide hydrochloride (APMA),[31] 2-aminoethylmethacrylate hydrochloride (AEMA),[32-34] and N-vinylformamide.[35,36] A detailed description of the various constructs that have been synthesized from several different constituent monomers has been provided by Ramos et al.[37] In spite of their manifold merits though, the extensive utilization of amine functionalized microgels has been hindered due to the inherent limitations of their syntheses as noted by Thaiboonrod et al.[36] and Farley et al.[38] The main issue relates to the stunted incorporation of amine containing comonomers during synthesis and therefore, an inability to generate stable, monodisperse solutions of large colloids with a high density of amine groups. Microgels with diameters of ~ 1 μm particularly, have remarkable potential in being useful for the visualization and manipulation of biological processes occurring at this length scale. However, a simple, reproducible, one step reaction for generation of colloidally stable microgels in the micrometer range, with a high density of amine groups has remained largely elusive. This has necessitated the employment of multi-step, complicated pathways in order to achieve the desirable end products.[38,39]

In the work presented here, a series of primary amine functionalized microgels were developed in different size ranges and with varying amounts of amine groups. Having been synthesized primarily from the monomer N-isopropylmethacrylamide (NIPMAm) leading to the formation of the thermoresponsive polymer pNIPMAm, the loosely crosslinked microgels are swollen at 37 $^{0}$C, which makes them viable candidates for applications requiring colloidally stable particles at the physiological temperature. We have demonstrated that simple one step syntheses can be utilized to generate monodisperse solutions of cationic microgels in a reproducible manner, with synthesis conditions being altered to optimize formation of the end product. For comparison, a two-step approach for the synthesis of core/shell microgels is also investigated. All microgels

were analyzed in detail for their primary amine content. This analysis is crucial for any system that has the potential to be used for well controlled conjugations.

## 2.2 Experimental section

### 2.2.1 Materials

All materials were purchased from Sigma-Aldrich unless specified otherwise. The primary monomer N-isopropylmethacrylamide (NIPMAm) was purified via recrystallization from *n*-hexane (J.T. Baker). The comonomer N-(3-aminopropyl)methacrylamide hydrochloride (APMA, Polysciences, Inc.), crosslinker N,N′-methylenebis(acrylamide) (BIS), NaCl, cationic initiator 2,2'-azobis(2-methylpropionamidine)dihydrochloride (V50), anionic initiator ammonium persulfate (APS), buffer preparation materials sodium dihydrogen phosphate, N-(2-hydroxyethyl)piperazine-N′-(2-ethanesulfonic acid) (HEPES), 3-(cyclohexylamino)-1-propanesulfonic acid (CAPS) and sodium borate, 3-aminopropyltrimethoxysilane (APTMS) and poly(4-styrenesulfonic acid) sodium salt (PSS) for substrate functionalization for AFM imaging, ethanol, isopropanol and acetone were all used as received. Solutions were prepared using distilled water, deionized to a resistance of 18 MΩ (Barnstead E-Pure system) and were filtered through a 0.2 μm Acrodisc syringe filter before use.

### 2.2.2 Microgel synthesis

Microgels were synthesized by free radical precipitation polymerization. In a typical synthesis, NIPMAm, BIS and APMA in the relevant molar compositions (refer to

Table 2.1 for monomer feed ratios) were dissolved in 49 mL distilled, deionized water to a total monomer concentration of 140 mM (except for μgel11 and μgel12) along with sodium chloride, where pertinent, at the indicated concentration. The resulting solution was filtered through a 0.8 μm Acrodisc syringe filter and introduced into a 100 mL three necked, round bottom flask along with a magnetic stirrer. The flask was fitted with a thermometer, condenser and $N_2$ inlet and introduced into an oil bath, which was heated at 100 $^0$C/h. Stirring was kept constant at 400 RPM and the solution was purged with $N_2$. Once the temperature was stable at 70 $^0$C, 1 mL of the initiator (APS or V50) was added after filtration through a 0.2 μm Acrodisc syringe filter. The reaction was allowed to proceed for 4 h under a $N_2$ blanket, after which it was cooled down to room temperature. The solution was then filtered through glass wool.

For the syntheses performed on a temperature ramp, a similar procedure was utilized. The monomer solution was heated until it reached a stable starting temperature of 50 °C. Polymerization was initiated at this temperature with the addition of 1 mL of a filtered V50 or APS solution and following initiation, the reaction solution was heated to a final temperature of 70 °C using a ramp rate of 30 °C/h.

Core/shell synthesis details have been previously reported.[22,40] In a typical synthesis, 39 mL of a filtered monomer solution consisting of NIPMAm, BIS and APMA was introduced into a reaction flask along with 10 mL of the purified core (μgel10) solution. This reaction solution was heated to a stable temperature of 65 °C while being continuously stirred and purged with $N_2$. Polymerization was initiated at this temperature with the addition of 1 mL of filtered V50 solution.

All microgels were purified by pelleting via ultracentrifugation (Beckman Coulter Optima MAX-XP) at 120,700 - 214,600 × *g* for 30 - 60 minutes, depending on the microgel type. This was followed by removal of the supernatant and resuspension in DI water. This process was repeated four times, after which the microgels were lyophilized prior to characterization.

### 2.2.3 Dynamic Light Scattering

Hydrodynamic radii ($R_H$) of the microgels were determined via dynamic light scattering (DLS, DynaPro, Protein Solutions) measurements in pH 7.4 HEPES (6 mM ionic strength) and pH 11 CAPS (6 mM ionic strength) buffers in order to observe pH responsivity. Microgel samples in the respective buffers were equilibrated for 20 minutes, following which scattering intensity fluctuations based on Brownian motion of the microgels were detected at a scattering angle of $90^0$. 25 acquisitions of 20 seconds each were obtained and used to generate intensity time correlation functions. Cumulants analysis was then used to attain diffusion coefficients and the Stokes-Einstein equation was utilized to calculate the $R_H$ values. The procedure was repeated 3 more times on the same sample in order to generate a total of 100 $R_H$ values for each microgel sample and averages of these $R_H$ values along with standard deviations are presented.

### 2.2.4 Atomic Force Microscopy

Atomic Force Microscopy (AFM) was performed using an MFP-3D AFM (Asylum Research). Images were acquired in air and under ambient conditions in the tapping mode, using pyramidal cantilevers (Nanoworld, Force Constant 42 N/m) made of

heavily doped silicon. Image processing was performed using software written in an IgorPro environment (Wavemetrics, Inc.).

Samples were prepared on 22 mm × 22 mm glass coverslips (VWR). The coverslips were first cleaned by sequential sonication in Alconox solution, DI water, acetone, 95% ethanol, and isopropanol for 20 minutes each. They were then functionalized in a 1% (v/v) APTMS/absolute ethanol solution on a shaker table for 2 h, and subsequently modified with a 0.1 mg/mL PSS solution in pH 7 phosphate buffer (50 mM ionic strength) for 30 minutes in order to render the glass surface anionic. The coverslips were then washed with DI water. Microgel solutions prepared in the same phosphate buffer described above were then used for submonolayer deposition onto the glass substrates by centrifugation at 2250 × *g* for 15 - 20 minutes (depending on the microgel type) at 25 $^{0}$C using a plate rotor. The coverslips were rinsed well with DI water and dried with nitrogen before imaging.

### 2.2.5 CBQCA assay for quantification of amines

The efficiency of APMA incorporation during polymerization was determined by quantifying the accessible amine groups in the microgels using a fluorescence-based assay (Life Technologies), based on the reaction of ATTO-TAG$^{TM}$ CBQCA (3-(4-carboxybenzoyl)quinoline-2-carboxaldehyde) with primary amines. A reference standard curve was generated using monomeric APMA solutions (sample volume = 135 μL) prepared in sodium borate buffer (pH 9.3, 100 mM ionic strength). The reagent solutions of KCN (20 mM) and ATTO-TAG$^{TM}$ CBQCA (working solution of 5 mM concentration) were also prepared in the same buffer and following addition of these reagents, all sample

solutions (total volume = 150 μL) were incubated at room temperature with shaking for 60-90 minutes and kept protected from light. Microgel solutions prepared in borate buffer were treated in an identical manner as the standards. The fluorescence of all solutions was then measured using a plate reader (Infinite® 200 PRO NanoQuant™, Tecan Group LTD., San Jose, CA) at excitation and emission wavelengths of 465 nm and 550 nm, respectively. After correcting these values for background from the buffer, the percent efficiencies of APMA incorporation in the microgels were determined.

## 2.3 Results and discussion

### 2.3.1 Synthesis and fundamental characterization of amine functionalized microgels

Cationic microgels synthesized with varying monomer molar feed ratios of NIPMAm:APMA and under numerous experimental conditions (Tables 2.1.1, 2.1.2, 2.1.3) were purified and analyzed for their hydrodynamic radii ($R_H$) using dynamic light scattering.

**Table 2.1.1** Reaction conditions and $R_H$ values of microgels synthesized at constant temperature

| Microgel identity | [APMA] (mol %) | [NIPMAm] (mol %) | [BIS] (mol %) | [V50] (mM) | [APS] (mM) | [NaCl] (mM) | $R_H$ (nm) at pH 7.4 | $R_H$ (nm) at pH 11 |
|---|---|---|---|---|---|---|---|---|
| **µgel1** | 1 | 97 | 2 | 0.50 | -- | 25 | 563±33 | 559±40 |
| **µgel2** | 5 | 97 | 2 | 0.50 | -- | 50 | 436±23 | 419±21 |
| **µgel3** | 7 | 91 | 2 | 0.25 | -- | 85 | 433±17 | 380±13 |
| **µgel4** | 7 | 91 | 2 | -- | 4 | -- | 425±16 | 397±17 |
| **µgel5** | 9 | 89 | 2 | 0.25 | -- | -- | 94±2 | 86±3 |
| **µgel6** | 9 | 89 | 2 | 0.25 | -- | 100 | 311±12 | 296±9 |
| **µgel7** | 9 | 89 | 2 | -- | 3 | -- | 261±8 | 244±7 |

*[Total monomer] = 140 mM, Temperature = 70 °C*

**Table 2.1.2** Reaction conditions and $R_H$ values of microgels synthesized with a temperature ramp

| Microgel identity | [APMA] (mol %) | [NIPMAm] (mol %) | [BIS] (mol %) | [V50] (mM) | [APS] (mM) | $R_H$ (nm) at pH 7.4 | $R_H$ (nm) at pH 11 |
|---|---|---|---|---|---|---|---|
| **µgel8** | 9 | 89 | 2 | 0.25 | -- | 64±2 | 58±1 |
| **µgel9** | 9 | 89 | 2 | -- | 3 | 184±5 | 160±4 |

*[Total monomer] = 140 mM, Reaction initiation temperature = 50 °C, Reaction final temperature: 70 °C*

**Table 2.1.3** Reaction conditions for microgel cores (μgel10) and shells synthesized on μgel10 cores

| Microgel identity | [APMA] (mol %) | [NIPMAm] (mol %) | [BIS] (mol %) | [V50] (mM) |
|---|---|---|---|---|
| **μgel10*** | 0 | 98 | 2 | 1.0 |
| **μgel11** | 1 | 97 | 2 | 0.5 |
| **μgel12** | 5 | 93 | 2 | 0.5 |

*[Total monomer] = 50 mM, Temperature = 65 °C*
**[Total monomer] = 140 mM*

The pH responsivity observed in low ionic strength pH 7.4 HEPES and pH 11 CAPS buffers (pKa of APMA ≈ 10) demonstrated successful incorporation of the cationic comonomer APMA. Buffers of low, 6 mM ionic strength were used in order to reduce the effects of charge screening, thus facilitating observation of pH responsivity to a greater extent. The motivation behind the development of a large range of microgels was two-fold. Firstly, modifications in synthesis conditions generated microgels of different dimensions. This versatility with respect to size is a desirable quality, particularly for particles that have the potential to be used in different environments in biological systems. Secondly, the variation in APMA incorporation within the particles during synthesis provides tunability with regards to degree of functionality and thus further bioconjugation. Since it has been shown that cationic polymers can potentially be toxic to cells,[41] a definitive control on the density of amine groups present in the microgels can also be leveraged for utilization of these constructs in biological environments. The interplay between the aforementioned microgel features was quantified by measuring the $R_H$ and amine content of the microgels. The 'knobs' that were tuned to achieve differences in microgel characteristics included monomer ratios,

concentration of NaCl, concentration and identity of the initiator, initiation temperature and microgel architecture.

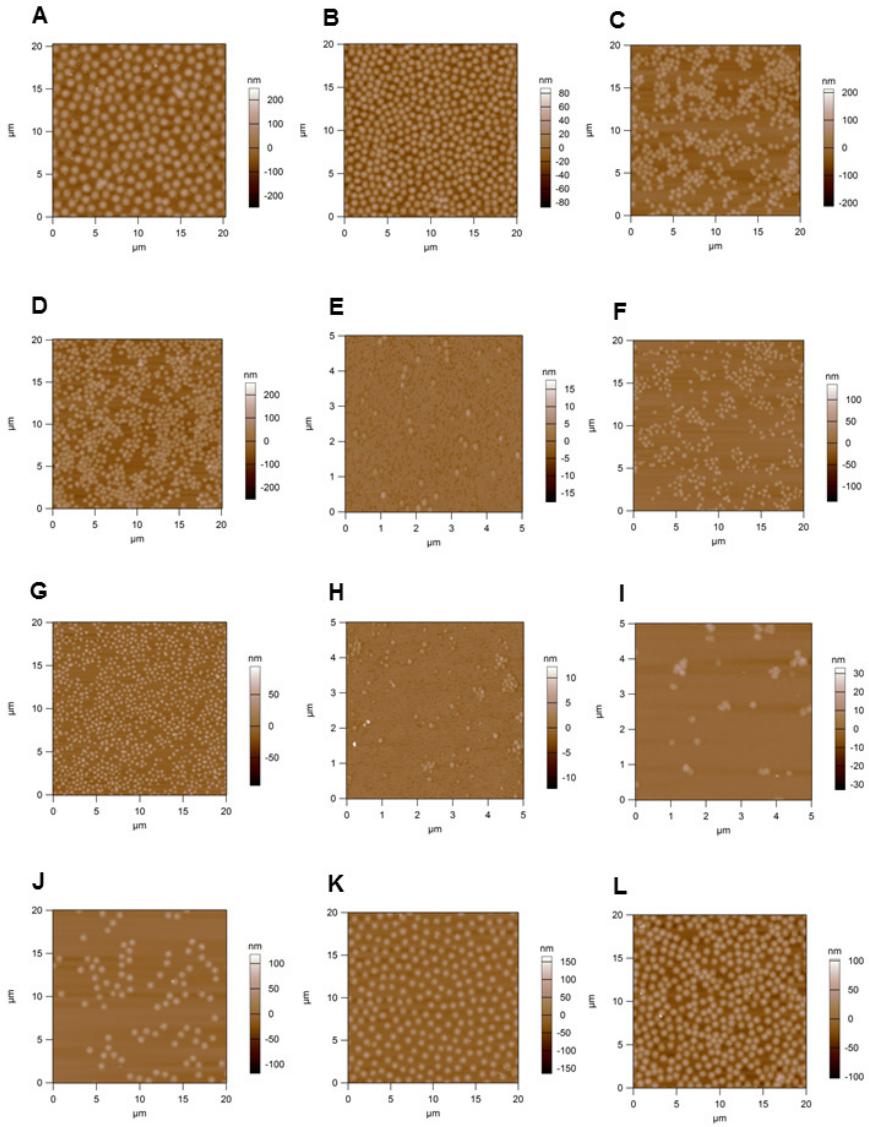


**Figure 2.1.** AFM height traces of µgel1 to µgel12 (A to L respectively) deposited on pre-functionalized glass by centrifugal deposition at 2250 × *g* for 15 - 20 minutes at 25 $^{0}$C, depending on the microgel type. Images qualitatively demonstrated monodispersity of individual microgel suspensions and size differences in particles depending on changes in synthesis conditions

Figure 2.1 presents images of microgels obtained using atomic force microscopy. Owing to their deformability, microgels deposited on functionalized glass substrates are often seen to be flattened (~hemispherical), as illustrated by these images. Within the group of microgels synthesized using V50 as an initiator, an increase in NaCl concentration during synthesis led to an increase in particle diameter. This is indicated by the $R_H$ values of μgel5 and μgel6. This trend can be attributed to the screening of charges caused by NaCl, leading to a decrease in Coulombic repulsion between APMA-containing polymer chains. The electrostatic repulsion when uninhibited, prevents chain collapse due to positioning of like positive charges along the polymer backbone. This leads to free polymer chains in solution and thus smaller microgel size resulting from less polymer incorporation in the particles.[32] Additionally, the charged monomer in solution acts as a polymerizable surfactant and displays behavior similar to that of an ionic surfactant, thus further limiting the growth of particle size.[42,43] The $R_H$ values of microgels μgel1, μgel2, μgel3 and μgel6 are demonstrative of this effect of NaCl concentration on particle size. However, above a threshold concentration, deformation of microgels was observed (Figure B.1.A, **Appendix B**). This threshold varied with monomer feed concentrations and its occurrence can likely be attributed to the formation of block copolymers at the periphery of the microgels in a charge screening environment, which leads to the development of particles that are not perfectly spherical.[31,44] These artifacts in structure, while well demonstrated in the AFM images, were also revealed by an inconsistency in $R_H$ values obtained using DLS. This is because the Stokes-Einstein equation relates the diffusion coefficient D of a spherical 'Stokes' particle to its $R_H$. Upon increasing the NaCl concentration further, macroscopic aggregation of the polymer was

observed, demonstrating disappearance of electrostatic stabilization in the system due to increased charge screening.

For syntheses initiated using the anionic initiator APS, microgel size increased with increasing concentration of the initiator. At first glance this is counterintuitive, as ordinarily an increase in initiator concentration would be expected to lead to a higher rate of nucleation than propagation, which leads to a large number of smaller particles. There are two possible explanations for the observation of a reverse trend in the case of these microgels. Firstly, proton abstraction from the carbon adjacent to the primary amine group in APMA, causes the generation of secondary reactive sites. This occurs due to the nucleophilicity of the radical center oxygen in the persulfate radical. Self crosslinking and larger particle size result from this phenomenon due to an increase in the efficiency of polymer incorporation. Hu et al. observed larger yields in cases of reactions initiated using APS when compared to those initiated using V50.[31] These observations were also demonstrative of better polymer incorporation in the microgels. Secondly, the process of stabilization of microgels by positive charges contributed by APMA is hindered by the presence of negatively charged sulfate groups from APS. This necessitates the accumulation of a larger number of primary particles to generate a microgel stabilizing net positive charge, causing build-up of particle size. This reasoning is supported by the observations of Still et al. concerning positive zeta potential values obtained in syntheses of p(NIPAm-co-AEMA) and negative values obtained in a similar synthesis conducted in the absence of AEMA.[33] Above a threshold concentration of APS, this 'neutralization' of charges leads to an effect similar to that observed with higher NaCl concentrations in syntheses described previously, i.e. the formation of misshapen microgels (Figure B.1.B,

**Appendix B**). Microgels were also synthesized using a different crosslinker Poly(ethylene glycol) (200) diacrylate (Polysciences, Inc.) or PEG-DA, and were designated μgelPEG. This synthesis was performed with molar feed ratios of 93:2:5 corresponding to NIPMAm:PEG-DA:APMA and in the presence of 50 mM NaCl. These microgels were also analyzed for their $R_H$ via DLS and their hemispherical profile via AFM (Figure B.2, A), in order to demonstrate the versatility of the approach.

Microgels synthesized by means of a temperature ramp commencing after initiation (μgel8 and μgel9) were found to be smaller than their counterparts obtained via traditional syntheses. pNIPAm and pNIPMAm based microgels have been synthesized in a similar manner before,[13,45] with initiation at a temperature lower than that used for conventional syntheses, followed by a gradual, steady increase in solution temperature as the reaction progresses. In these cases, large microgels were obtained due to a bias created towards particle growth through chain propagation vs. the generation of nucleation sites. A continuous increase in temperature during the synthesis ensures that the propagation rate is not sacrificed due to consumption of the monomer, by increasing the number of radicals generated. It is noteworthy that these ramp syntheses performed in the past have involved the use of an anionic comonomer. The observation of a somewhat reverse trend in the case of p(NIPMAm-co-APMA) microgels synthesized on a temperature ramp (50-70 $^0$C) via initiation with the cationic initiator V50 (μgel5 and μgel8) or anionic initiator APS (μgel7 and μgel9) may be attributed to the heavy influence of cationic comonomers on the formation of water soluble polymers during the synthesis. A similar phenomenon was observed by Mai-ngam et al. when analyzing the phase separation of p(NIPAm-co-APMA) polymers.[44] In their experiment,

conformational collapse was not observed at temperatures up to 45 $^0$C in pure water, in spite of the LCST of pNIPAm being 31 $^0$C. This was due to strong electrostatic repulsion between the positively charged amine groups along the polymer chain. The addition of salt however, facilitated phase separation through charge screening. The same argument may be extended to microgel synthesis of μgel8 and μgel9, since these were conducted in the absence of any salt. At the temperature of initiation, Coulombic repulsion between the positively charged amine groups along the polymer chain dominates over the collapse of polymer chains. Thus, a majority of the monomer is utilized in the formation of polymer chains in solution. This can be observed as a temperature driven amplified effect of the same phenomenon discussed earlier, that leads to the generation of small microgels when a high feed ratio of amine containing comonomer is used. Despite the fact that the syntheses discussed here were initiated at a temperature higher than the ones conducted by Mai-ngam et al., the same reasoning may be considered applicable because of the higher LCST of pNIPMAm (≈ 44 $^0$C). As the temperature gradually increases, the coil to globule transition of the polymer begins to occur. However, by the time this stage of the synthesis is reached, another factor, namely the incorporation of the crosslinker BIS into the particles, comes into play. It has been postulated by Meunier et al. that the depletion of free BIS through incorporation into the polymer, acts as a deterrent towards any further capture of free polymers by the microgels from solution.[32] Thus particle growth is further impeded. All these factors contribute to the formation of microgels smaller than those generated through a conventional synthesis, under similar conditions. It is worthwhile to note that the reactivity ratios of NIPAm and BIS are different from those of NIPMAm and BIS. However, the results obtained here indicate that these differences

may not be a major contributing factor due to the overpowering effect of the comonomer APMA on the syntheses.

### 2.3.2 Quantification of primary amine incorporation in microgels during synthesis

Following analysis of the physical characteristics of all microgels, the ATTO-TAG™ CBQCA reagent was used to determine the content of accessible primary amines on the microgels via a fluorescence based assay.[46] This reagent is non-fluorescent by itself in aqueous solutions. However, it reacts with primary amines in the presence of cyanide to yield a fluorescent derivative, and is capable of detecting proteins in nanogram quantities though primary amine derivatization. Historically, the incorporation of primary amine functional groups during microgel synthesis has not been very efficient, as described above. Moreover, the low magnitude of pH responsivity, when observed for the microgel solutions (Table 2.1) indicated that the degree of APMA incorporation during the synthesis of almost all microgels was fairly low. Hence, the CBQCA assay was the analysis method of choice, due to its low detection limit, which should permit the quantitative analysis of amines even if incorporation degrees were low. A standard curve was generated using APMA solutions in borate buffer and used for analysis.

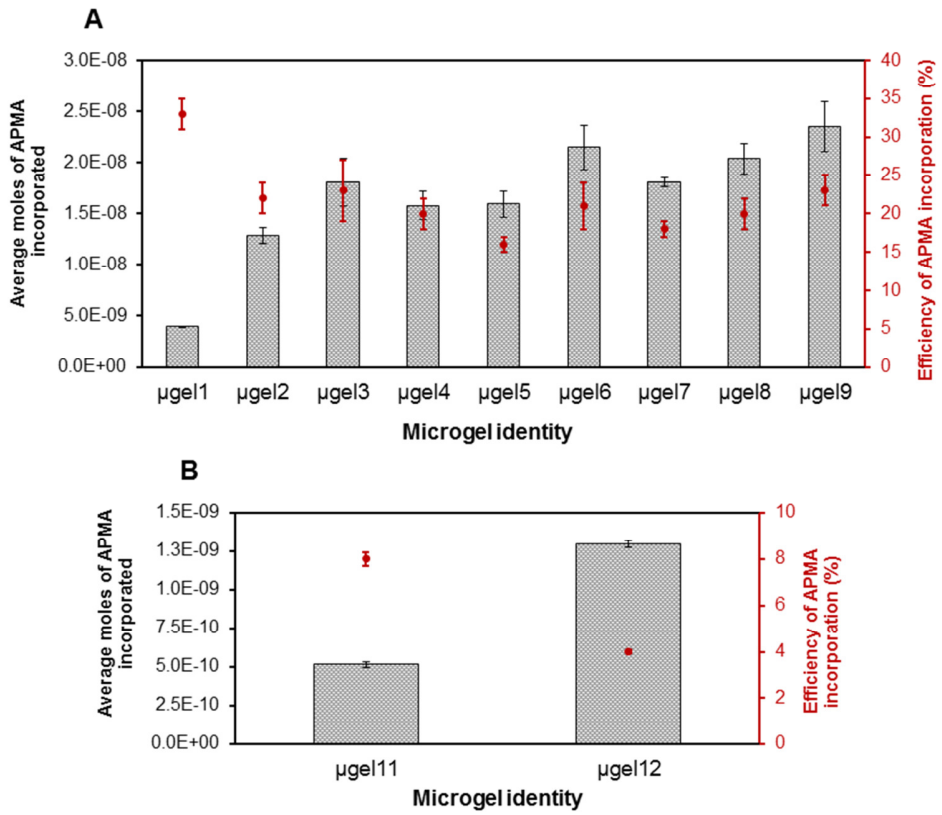


**Figure 2.2.** Incorporation of APMA in moles, in 135 µL of 1 mg/mL solutions of the respective microgels (grey bars) and percent efficiency of incorporation of APMA (red circles) in conventional microgel populations with varying APMA feed ratios (A) and core/shell microgel architectures (B), analyzed via CBQCA assay *(values presented as averages of 3 trials, error bars represent standard deviations of these three values)*

Taking into consideration the monomer feed ratios during the syntheses, the efficiencies of incorporation of APMA during polymerization were calculated and are presented in Figure 2.2. Analysis on µgel10 solutions demonstrated fluorescence close to that of the background, thus indicating the absence of any interference from non-primary amine groups, at the concentrations under consideration. A general upward trend in the moles of APMA incorporated within the microgels is observed, based on the monomer feed ratio of APMA, in microgels µgel1 (1 mol % feed APMA), µgel2 (5 mol % feed

APMA) and microgels μgel3 and μgel4 (7 mol % feed APMA). For μgel5, μgel6, μgel7, μgel8 and μgel9, the absence of a clear trend can be attributed to the stark difference in $R_H$ values of these microgels compared to the others, and thus dissimilar number densities. With a low feed ratio of APMA in μgel1, a low amount of amine groups are successfully assimilated within the microgel network, but a high incorporation efficiency of 33% is observed. This result is in agreement with the argument put forth by Meunier et al., described earlier. At lower APMA feed ratios, the electrostatic repulsion between positively charged amine groups randomly positioned along the forming polymer chains is minimal and polymer collapse is not impeded. This results in higher APMA incorporation efficiency and larger microgels. Therefore, in spite of a lower concentration of NaCl being used in the synthesis, μgel1 have larger $R_H$ values (in comparison to μgel2, μgel3 and μgel6). As the APMA feed ratio is increased, the percent efficiency of amine incorporation within the microgels remains within a range from 16-23%, despite differences in the microgel sizes, hinting at the fact that in the syntheses, a compromise of microgel size is favored over that of the APMA incorporation efficiency.

In order to analyze variants of microgel architecture, two core/shell structures were synthesized using a 'seed and feed' method. Microgels with such architectures have been demonstrated to be useful for applications requiring dual functionality, such as loading of therapeutics in the core, and cell specific targeting through conjugation of relevant molecules to the shell,[14] and for ratiometric imaging.[47] The cores used for both syntheses were the same and were synthesized with no APMA (μgel10). They were found to have an $R_H$ value of 459 ± 24 nm in pH 7.4 HEPES buffer of 6 mM ionic strength. Core/shell architectures μgel11 and μgel12 were generated by depositing two

different shells on μgel10 with APMA feed ratios of 1 mol % and 5 mol %, respectively. The AFM images of the core/shell structures revealed well-defined, hemispherical particles (Figure 2.1 K, L). Reliable $R_H$ values could not be obtained for these microgels, which may be attributed to their larger size leading to a combination of non-random movement, i.e. sedimentation and number fluctuations due to low particle concentration in the DLS measurement volume. Analysis of the primary amine content of these microgels via the CBQCA assay revealed the moles of APMA incorporated in μgel11 and μgel12 to be approximately an order of magnitude below their conventional microgel counterparts, μgel1 and μgel2 (Figure 2.2 A, B). The inclusion of APMA only in microgel shells is a possible explanation for this observation. However, the trend observed was similar, i.e. a lower feed ratio of APMA resulted in a lower number of moles being incorporated. The percent efficiency of APMA incorporation was found to be 8 ± 0.31 % and 4 ± 0.08 in % μgel11 and μgel12 respectively. This low efficiency may be due to a reasoning similar to that proposed by Meunier et al. as explained above, relating to the formation of polymer chains in solution. Additionally, the formation of secondary 'core' microgels in solution (detected via DLS on supernatants following ultracentrifugation) may be responsible for a further decrease in incorporation efficiency of APMA within the shells formed on pre-existing cores.

## 2.4 Conclusion

We have successfully synthesized and characterized a large range of cationic microgels with varying amounts of primary amine groups incorporated within the polymer networks. These microgels have potential applications in bioconjugation reactions. The syntheses were optimized to generate monodisperse, stable microgels and

the particles were analyzed in detail with the goal of generating information about the incorporation efficiency of the amine containing comonomer. Furthermore, the effects of various synthesis conditions on microgel size and APMA incorporation efficiency were also investigated. All these studies have helped in the establishment of a toolbox of amine functionalized microgels, with constructs being suited to a wide range of applications. In particular, these investigations have revealed previously unknown aspects of these systems, with extensive studies providing corroboration through trends observed in microgel behaviors. Due to the large number of possible reactions with primary amines, the opportunities of conjugations to these microgels are boundless, with ample flexibility available for a vast array of systems. These particles thus have prospective utility in a number of significant biomedical applications such as the delivery of therapeutics and bioimaging.

## 2.5 References

(1) Magnusson, J. P.; Bersani, S.; Salmaso, S.; Alexander, C.; Caliceti, P.: In Situ Growth of Side-Chain PEG Polymers from Functionalized Human Growth Hormone-A New Technique for Preparation of Enhanced Protein-Polymer Conjugates. *Bioconjugate Chem.* **2010**, *21*, 671-678.

(2) Meng, F.; Hennink, W. E.; Zhong, Z.: Reduction-sensitive polymers and bioconjugates for biomedical applications. *Biomaterials* **2009**, *30*, 2180-2198.

(3) Lutz, J.-F.; Zarafshani, Z.: Efficient construction of therapeutics, bioconjugates, biomaterials and bioactive surfaces using azide-alkyne "click" chemistry. *Adv. Drug Delivery Rev.* **2008**, *60*, 958-970.

(4) Escriou, V.; Carriere, M.; Scherman, D.; Wils, P.: NLS bioconjugates for targeting therapeutic genes to the nucleus. *Adv. Drug Delivery Rev.* **2003**, *55*, 295-306.

(5) Chau, Y.; Tan, F. E.; Langer, R.: Synthesis and characterization of dextran-peptide-methotrexate conjugates for tumor targeting via mediation by matrix metalloproteinase II and matrix metalloproteinase IX. *Bioconjugate Chem.* **2004**, *15*, 931-941.

(6) Jin, Y. D.; Jia, C. X.; Huang, S. W.; O'Donnell, M.; Gao, X. H.: Multifunctional nanoparticles as coupled contrast agents. *Nat. Commun.* **2010**, *1*.

(7) Biju, V.: Chemical modifications and bioconjugate reactions of nanomaterials for sensing, imaging, drug delivery and therapy. *Chem. Soc. Rev.* **2014**, *43*, 744-764.

(8) Cheng, L.; Gong, H.; Zhu, W. W.; Liu, J. J.; Wang, X. Y.; Liu, G.; Liu, Z.: PEGylated Prussian blue nanocubes as a theranostic agent for simultaneous cancer imaging and photothermal therapy. *Biomaterials* **2014**, *35*, 9844-9852.

(9) Erathodiyil, N.; Ying, J. Y.: Functionalization of Inorganic Nanoparticles for Bioimaging Applications. *Accounts of Chemical Research* **2011**, *44*, 925-935.

(10) Farokhzad, O. C.; Cheng, J.; Teply, B. A.; Sherifi, I.; Jon, S.; Kantoff, P. W.; Richie, J. P.; Langer, R.: Targeted nanoparticle-aptamer bioconjugates for cancer chemotherapy in vivo. *Proc. Natl. Acad. Sci. U. S. A.* **2006**, *103*, 6315-6320.

(11) Matsumura, Y.; Maeda, H.: A new concept for macromolecular therapeutics in cancer-chemotherapy - mechanism of tumoritropic accumulation of proteins and the antitumor agent smancs. *Cancer Res.* **1986**, *46*, 6387-6392.

(12) Li, L.; Chang, A.; Hu, Y.; Zhang, L.; Wu, W.: One-pot aqueous synthesis of sub-10 nm responsive nanogels. *Chem. Commun.* **2013**, *49*, 6534-6536.

(13) Meng, Z. Y.; Smith, M. H.; Lyon, L. A.: Temperature-programmed synthesis of micron-sized multi-responsive microgels. *Colloid and Polymer Science* **2009**, *287*, 277-285.

(14) Dickerson, E. B.; Blackburn, W. H.; Smith, M. H.; Kapa, L. B.; Lyon, L. A.; McDonald, J. F.: Chemosensitization of cancer cells by siRNA using targeted nanogel delivery. *BMC Cancer* **2010**, *10*.

(15) Hendrickson, G. R.; Lyon, L. A.: Bioresponsive hydrogels for sensing applications. *Soft Matter* **2009**, *5*, 29-35.

(16) Brown, A. C.; Stabenfeldt, S. E.; Ahn, B.; Hannan, R. T.; Dhada, K. S.; Herman, E. S.; Stefanelli, V.; Guzzetta, N.; Alexeev, A.; Lam, W. A.; Lyon, L. A.; Barker, T. H.: Ultrasoft microgels displaying emergent platelet-like behaviours. *Nat. Mater.* **2014**, *13*, 1108-1114.

(17) Bridges, A. W.; Singh, N.; Burns, K. L.; Babensee, J. E.; Lyon, L. A.; Garcia, A. J.: Reduced acute inflammatory responses to microgel conformal coatings. *Biomaterials* **2008**, *29*, 4605-4615.

(18) Lutz, J. F.: Thermo-Switchable Materials Prepared Using the OEGMA-Platform. *Adv. Mater.* **2011**, *23*, 2237-2243.

(19) Smith, M. H.; Herman, E. S.; Lyon, L. A.: Network Deconstruction Reveals Network Structure in Responsive Microgels. *J. Phys. Chem. B* **2011**, *115*, 3761-3764.

(20) South, A. B.; Lyon, L. A.: Direct Observation of Microgel Erosion via in-Liquid Atomic Force Microscopy. *Chemistry of Materials* **2010**, *22*, 3300-3306.

(21) Brown, A. C.; Stabenfeldt, S. E.; Ahn, B.; Hannan, R. T.; Dhada, K. S.; Herman, E. S.; Stefanelli, V.; Guzzetta, N.; Alexeev, A.; Lam, W. A.; Lyon, L. A.; Barker, T. H.: Ultrasoft microgels displaying emergent platelet-like behaviours. *Nat Mater* **2014**, *advance online publication*.

(22) Blackburn, W. H.; Dickerson, E. B.; Smith, M. H.; McDonald, J. F.; Lyon, L. A.: Peptide-Functionalized Nanogels for Targeted siRNA Delivery. *Bioconjugate Chem.* **2009**, *20*, 960-968.

(23) Nayak, S.; Lee, H.; Chmielewski, J.; Lyon, L. A.: Folate-mediated cell targeting and cytotoxicity using thermoresponsive microgels. *J. Am. Chem. Soc.* **2004**, *126*, 10258-10259.

(24) Hoare, T.; Pelton, R.: Functional group distributions in carboxylic acid containing poly(N-isopropylacrylamide) microgels. *Langmuir* **2004**, *20*, 2123-2133.

(25) Sahiner, N.; Demirci, S.; Sahiner, M.; Al-Lohedan, H.: The synthesis of desired functional groups on PEI microgel particles for biomedical and environmental applications. *Applied Surface Science* **2015**.

(26) Hermanson, G. T.: *Bioconjugate Techniques*; 2nd edition ed.; Academic Press: San Diego, CA, 2008.

(27) Antonietti, L.; Aymonier, C.; Schlotterbeck, U.; Garamus, V. M.; Maksimova, T.; Richtering, W.; Mecking, S.: Core-shell-structured highly branched poly(ethylenimine amide)s: Synthesis and structure. *Macromolecules* **2005**, *38*, 5914-5920.

(28) Hahn, M.; Gornitz, E.; Dautzenberg, H.: Synthesis and properties of ionically modified polymers with LCST behavior. *Macromolecules* **1998**, *31*, 5616-5623.

(29) Nabzar, L.; Duracher, D.; Elaissari, A.; Chauveteau, G.; Pichot, C.: Electrokinetic properties and colloidal stability of cationic amino-containing N-isopropylacrylamide-styrene copolymer particles bearing different shell structures. *Langmuir* **1998**, *14*, 5062-5069.

(30) Pinschmidt, R. K.: Polyvinylamine at Last. *J. Polym. Sci. Pol. Chem.* **2010**, *48*, 2257-2283.

(31) Hu, X. B.; Tong, Z.; Lyon, L. A.: Synthesis and physicochemical properties of cationic microgels based on poly(N-isopropylmethacrylamide). *Colloid and Polymer Science* **2011**, *289*, 333-339.

(32) Meunier, F.; Elaissari, A.; Pichot, C.: Preparation and characterization of cationic poly(n-isopropylacrylamide) copolymer latexes. *Polym. Adv. Technol.* **1995**, *6*, 489-496.

(33) Still, T.; Chen, K.; Alsayed, A. M.; Aptowicz, K. B.; Yodh, A. G.: Synthesis of micrometer-size poly(N-isopropylacrylamide) microgel particles with homogeneous crosslinker density and diameter control. *J. Colloid Interface Sci.* **2013**, *405*, 96-102.

(34) Duracher, D.; Sauzedde, F.; Elaissari, A.; Perrin, A.; Pichot, C.: Cationic amino-containing N-isopropylacrylamide-styrene copolymer latex particles: 1 - Particle size and morphology vs. polymerization process. *Colloid and Polymer Science* **1998**, *276*, 219-231.

(35) Xu, J. J.; Pelton, R.: A new route to poly(N-isopropylacrylamide) microgels supporting a polyvinylamine corona. *J. Colloid Interface Sci.* **2004**, *276*, 113-117.

(36) Thaiboonrod, S.; Berkland, C.; Milani, A. H.; Ulijn, R.; Saunders, B. R.: Poly(vinylamine) microgels: pH-responsive particles with high primary amine contents. *Soft Matter* **2013**, *9*, 3920-3930.

(37) Ramos, J.; Forcada, J.; Hidalgo-Alvarez, R.: Cationic Polymer Nanoparticles and Nanogels: From Synthesis to Biotechnological Applications. *Chemical Reviews* **2014**, *114*, 367-428.

(38) Farley, R.; Saunders, B. R.: A general method for functionalisation of microgel particles with primary amines using click chemistry. *Polymer* **2014**, *55*, 471-480.

(39) Miraballes-Martinez, I.; Martin-Molina, A.; Galisteo-Gonzalez, F.; Forcada, J.: Synthesis of amino-functionalized latex particles by a multistep method. *J. Polym. Sci. Pol. Chem.* **2001**, *39*, 2929-2936.

(40) Gan, D. J.; Lyon, L. A.: Tunable swelling kinetics in core-shell hydrogel nanoparticles. *J. Am. Chem. Soc.* **2001**, *123*, 7511-7517.

(41) Fischer, D.; Li, Y. X.; Ahlemeyer, B.; Krieglstein, J.; Kissel, T.: In vitro cytotoxicity testing of polycations: influence of polymer structure on cell viability and hemolysis. *Biomaterials* **2003**, *24*, 1121-1131.

(42) McPhee, W.; Tam, K. C.; Pelton, R.: Poly(n-isopropylacrylamide) latices prepared with sodium dodecyl-sulfate. *J. Colloid Interface Sci.* **1993**, *156*, 24-30.

(43) Gao, J.; Frisken, B. J.: Influence of secondary components on the synthesis of self-cross-linked N-isopropylacrylamide microgels. *Langmuir* **2005**, *21*, 545-551.

(44) Mai-ngam, K.; Boonkitpattarakul, K.; Sakulsombat, M.; Chumningan, P.; Mai-ngam, B.: Synthesis and phase separation of amine-functional temperature responsive copolymers based on poly(N-isopropylacrylamide). *European Polymer Journal* **2009**, *45*, 1260-1269.

(45) Bachman, H.; Brown, A. C.; Clarke, K. C.; Dhada, K. S.; Douglas, A.; Hansen, C. E.; Herman, E.; Hyatt, J. S.; Kodlekere, P.; Meng, Z. Y.; Saxena, S.; Spears, M. W.; Welsch, N.; Lyon, L. A.: Ultrasoft, highly deformable microgels. *Soft Matter* **2015**, *11*, 2018-2028.

(46) You, W. W.; Haugland, R. P.; Ryan, D. K.; Haugland, N. P.: 3-(4-carboxybenzoyl)quinoline-2-carboxaldehyde, a reagent with broad dynamic range for the assay of proteins and lipoproteins in solution. *Anal. Biochem.* **1997**, *244*, 277-282.

(47) Zhou, X. F.; Su, F. Y.; Tian, Y. Q.; Meldrum, D. R.: Dually Fluorescent Core-Shell Microgels for Ratiometric Imaging in Live Antigen-Presenting Cells. *Plos One* **2014**, *9*.

# CHAPTER 3

# MICROGEL-DYE CONJUGATES AS VIABLE CANDIDATES FOR THE GENERATION OF HIGH INTENSITY PHOTOACOUSTIC SIGNALS

*Portions of this to be included in submission to Journal of Materials Chemistry B*

## 3.1 Introduction

In Chapter 2, we developed a range of amine functionalized microgels and characterized them with respect to their sizes and amine incorporation during synthesis. These studies provided information on the effects of various synthesis conditions on microgel stability, size and functional group incorporation. On the basis of these studies, a model microgel system was used for further characterization with respect to molecular weight and number density. Two different dyes, malachite green and rose bengal were then conjugated to this microgel system, in order to demonstrate availability of the primary amine groups for conjugation reactions. These dyes were selected because their optical properties make them suitable candidates for photoacoustic imaging.[1,2] We found that the local concentrations of these dyes were nearly three orders of magnitude above their overall concentration in solution, demonstrating the merit of using microgels as the conjugation scaffolds that enable the local concentration of active agents. The viability of NIH3T3 fibroblasts in the presence of these microgel-dye constructs was also studied. This investigation was carried out particularly to address the toxicity of polycations, which has previously been observed to occur due to their interactions with the cell

membrane.[3] Through qualitative analysis via imaging, the microgel-dye constructs were found to be less toxic to cells compared to the primary amine functionalized microgels containing no dye, presumably due to consumption of amine groups during conjugation, which is a promising outcome for their utilization in conjunction with biological systems.

## 3.2 Experimental section

### 3.2.1 Materials

For information on common materials, refer to Chapter 2, section 2.2.1. Buffer preparation materials 2-(cyclohexylamino)ethanesulfonic acid (CHES) and 4-Morpholineethanesulfonic acid (MES), dyes malachite green isothiocyanate (MGITC, Life Technologies) and rose bengal (RB), coupling reagents N-(3-dimethylaminopropyl)-N′-ethylcarbodiimide hydrochloride (EDC) and N-hydroxysulfosuccinimide sodium salt (NHSS), calcium nitrate, 1X PBS (phosphate buffered saline, Corning Cellgro), Dulbecco's Modified Eagle Medium (DMEM, Corning Cellgro), methanol, dimethyl sulfoxide (DMSO) and dyes from the live/dead cytotoxicity kit (Life Technologies) calcein AM and ethidium homodimer-1 (EthD-1) were all used as received.

### 3.2.2 Microgel synthesis

Microgels were synthesized using a procedure similar to that utilized for μgel2, described in Chapter 2, section 2.2.2.

### 3.2.3 Dynamic Light Scattering

$R_H$ values for microgels were obtained in a manner identical to that described in Chapter 2, section 2.2.3

### 3.2.4 Atomic Force Microscopy

AFM images of microgels deposited on pre-functionalized glass substrates were obtained usng a procedure similar to that described in Chapter 2, section 2.2.4.

### 3.2.5 CBQCA assay for quantification of amines

The incorporation of amine groups in microgel matrices during synthesis was quantified using the CBQCA assay, in a manner identical to that described in Chapter 2, section 2.2.5.

### 3.2.6 Tunable resistive pulse sensing

The qNano (IZON Science, Oxford, UK) was utilized for performing resistive pulse sensing via examination of translocation events of particles through a tunable polyurethane nanopore (IZON Science Ltd. NZ) NP400, which is suitable for analysis of particles with diameters between 200 and 800 nm. HEPES buffer (pH 7, 150 mM ionic strength) was first introduced in the cells on both sides of the nanopore, in order to generate a stable baseline current. Following this, the buffer in the cell above the nanopore was replaced with 40 μL of the relevant sample solution. All microgel solutions were used at a concentration of 0.2 mg/mL, and the measurements were standardized against solutions of the reference, carboxylated polystyrene beads at a known number

density of $7.5\times10^{-8}$ particles/mL and a mean diameter of 350 nm, by performing sample and standard measurements under identical conditions of voltage, nanopore stretch and pressure. The proprietary software provided by Izon was utilized for sample and data analysis. Three sets of measurements generated a total of ~ 215 values for $R_{qNano}$ for each sample. The $R_{qNano}$ distribution from these values is presented. The three sets also provided three values of microgel number density per sample. The averages and standard deviations of these values are presented.

### 3.2.7 Conjugation of dyes to microgels

*Malachite green:* The lyophilized microgels were weighed and resuspended overnight in pH 9.8 CHES buffer (pH 9.8, 20 mM ionic strength) to a concentration of ~ 3 - 5 mg/mL. Following this, MGITC dissolved in DMSO was added to the microgel solution in a 4.5X molar excess based on the amount of amine groups in the microgels. The conjugation reaction was allowed to proceed overnight at 4 $^0$C on a shaker after which the solution was dialyzed against DI water for 2 – 4 weeks at 4 $^0$C in order to get rid of excess dye and buffer.

*Rose bengal:* For conjugation to RB, the lyophilized microgels were weighed and resuspended in phosphate buffer (pH 7, 50 mM ionic strength) to a concentration of ~ 2 – 4 mg/mL. The dye was then conjugated to the microgels by dissolving it in the same buffer and adding it to the microgel solution in a 4X molar excess (for µgel1-RB, µgel2-RB and µgel6-RB) or a 10.5X molar excess (for µgel2b-RB) based on the concentration of amines. EDC and NHSS were also used in the same molar excess as RB, for the respective conjugations. The reaction was allowed to proceed overnight at room

temperature on a shaker, after which the solution was dialyzed against CAPS (pH 11, 500 mM ionic strength) for 3 - 5 weeks to remove excess dye and then against DI water for 2 - 3 weeks to remove buffer components.

The dialyzed dye conjugated microgel solutions were left on a shaker overnight in order to ensure homogeneity after which small portions of the solutions were lyophilized to determine the concentration of the 'stock' solutions.

### 3.2.8 Absorbance measurements

The dye conjugated microgel solutions of known concentrations were analyzed for dye content via absorbance measurements done in a plate reader (Infinite® 200 PRO NanoQuant™, Tecan Group LTD., San Jose, CA). Standard curves were generated by using dye solutions of MGITC (stock solution in DMSO, remaining dilutions in DI water) and RB (in water). Upon determining the $\lambda_{max}$ values (625 nm for MGITC and 540 nm for Rose Bengal), absorbance measurements were performed at the corresponding wavelengths. Absorbance values of the dye conjugated microgels were then determined at these wavelengths, after ensuring that scattering by microgels was not causing perturbation of the obtained results and the moles of dye conjugated, and conjugation efficiencies were calculated.

### 3.2.9 Cell culture

NIH3T3 cells were grown in DMEM (supplemented with 10% Fetal Bovine Serum and 1% penicillin streptomycin) on T75 flasks until they were 80% confluent. The medium was then removed from the flask, after which the cells were split through

treatment with 5 mL trypsin/EDTA (0.25%) followed by a 5 min incubation at 37 $^0$C. The cell count was then determined using a hemocytometer (Reichert Bright Line), and then pelleted down by centrifugation at 1200 × g for 5 minutes. The supernatant was aspirated out and the cells were resuspended in medium to a concentration of 1 million cells/mL. The cells were further diluted using medium and plated to a concentration of 10000 cells/cm$^2$ in a 96 well plate and allowed to spread on the surface for 3 - 4 h. Following this, the medium was removed via aspiration and the microgel solutions diluted in medium were added to the corresponding wells. A change of medium was made for the control wells to maintain uniformity in procedure. The well plate was then incubated for 24 h at 37 $^0$C and the live dead assay was performed on the cells.

### 3.2.10 Viability studies

The live/dead assay protocol (Life Technologies) was performed in a sterile tissue culture hood. The medium was aspirated from the sample wells and controls and the wells were washed gently with 200 µL 1X PBS. The cells in the dead control wells were then killed by incubating them with 100 µL of 70% methanol for 30 minutes. 100 µL 1X PBS was added to the remaining wells for the same period of time. The methanol and 1X PBS were then removed gently with a pipette, following which single or both dye solutions (Calcein AM and EthD-1) were added to the corresponding wells with controls and samples. The 96 well plate was subsequently incubated at room temperature for 45 min and protected from light. The solutions from all wells were then gently removed using a pipette and all wells were washed gently with 200 µL 1X PBS, following which a 4% v/v formaldehyde/1X PBS solution was introduced into the wells for the purpose of

fixing the cells. After an incubation of 15 minutes, the formaldehyde was pipetted out and all wells were gently washed twice with 200 µL 1X PBS. 100 µL 1X PBS was added to all the wells before conducting fluorescence measurements. The excitation and emission wavelengths of Calcein, 528 nm and 645 nm respectively, were utilized for the measurements and the percent viability values of the cells were calculated.

### 3.2.11 Confocal microscopy

The samples were prepared in a sterile tissue culture hood. Round coverslips (12 mm diameter, 0.17-0.25 mm thickness, Electron Microscopy Sciences) were immersed in 70% ethanol for 30 minutes, after which they were dried and introduced into a 24 well plate. They were incubated in DMEM for 1 h at 37 $^{0}$C in order to facilitate cell attachment. The cells were then plated at a concentration of 10000 cells/cm$^2$ in each well and were allowed to spread for 3 - 4 h. Following this, a similar procedure as the one for the 96 well plate was used for incubation with microgels and staining of the cells, with volume adjustments. The coverslips were then air dried and preserved in ProLong® Gold Antifade reagent (Life Technologies). The samples were sealed with nail polish and kept protected from light, at 4 $^{0}$C until they were imaged.

Images were obtained on a Confocal Laser Scanning Microscopy (CLSM, Zeiss LSM 700) by setting the pinhole diameter to 1 airy unit. Image processing was performed using the Zen 2012 (Carl Zeiss, SP1) software.

### 3.2.12 Generation of photoacoustic signals using microgel-dye conjugates

Photoacoustic signal generation was performed by Aida Demissie, from the Dickson research group at Georgia Tech. Tissue phantoms with optical properties similar to those of human skin tissue, were made using sodium alginate Protanal LF 10/60 (FMC Biopolymer, Drammen, Norway) and cross-linked in an 80 mM solution of calcium nitrate. Solutions of microgel dye conjugates (1 mg/mL for μgel 2a-MGITC and 2 mg/mL for μgel 2a-RB) were added to the alginate solution prior to crosslinking and then placed in the calcium nitrate solution for 30 minutes.

Photoacoustic signals from phantoms were measured on an inverted microscope (IX70-S1F2, Olympus) through a 40X dry objective. In order to generate signals, a pulsed laser was used to satisfy both thermal and stress relaxation time conditions. Photoacoustic signals were generated by a pulsed primary laser (532 nm, 10 kHz repetition) and were detected by a broadband submersible piezoelectric transducer with central frequency 10MHz (U8427003, Olympus NDT Inc, USA). Signals were amplified with a broadband amplifier (U8120004, Olympus NDT Inc, USA) and recorded on an oscilloscope (TDS5104B, Tektronix)

## 3.3 Results and discussion

In chapter 3, we demonstrated the development and characterization of several amine functionalized microgels. Based on the microgel sizes, profiles and primary amine contents , μgel2 was selected as a model system for further characterization and conjugations. The reasons behind this selection were multi-fold. Firstly, the content of primary amine groups in these microgels was intermediate in the range of microgels

studied. This content measured via the CBQCA assay was corroborated with the help of a second technique, pH titrations (Figure B.3, **Appendix B**). The comparative results from both these analysis methods are presented in Table 3.1. The agreement in these values demonstrated the quantitative accuracy of the CBQCA assay.

**Table 3.1** Comparative values of percentage efficiency of primary amine incorporation during microgel synthesis using two different techniques (data from μgel2)

| Method used for primary amine quantification | Calculated % efficiency of primary amine incorporation |
|---|---|
| **CBQCA assay** | 22 ± 2 |
| **pH titrations** | 20 ± 2 |

*Values presented as averages of 3 trials*

Another reason why μgel2 were selected as a model system, was because of their convenient size for analysis and imaging, reproducibility of synthesis, and good amine incorporation.

### 3.3.1 Synthesis and detailed characterization of μgel2a and μgel2b

Two batches of the model system μgel2, described in Chapter 2, were synthesized, μgel2a and μgel2b (feed ratios of NIPMAm:BIS:APMA :: 93:2:5). Their $R_H$ values in pH 7.4 HEPES and pH 11 CAPS buffers were found to be 413 ± 29 nm and 377 ± 24 nm for μgel2a and 409 ± 19 nm and 387 ± 15 nm for μgel2b respectively. The incorporation of APMA during synthesis is qualitatively evident from these values.

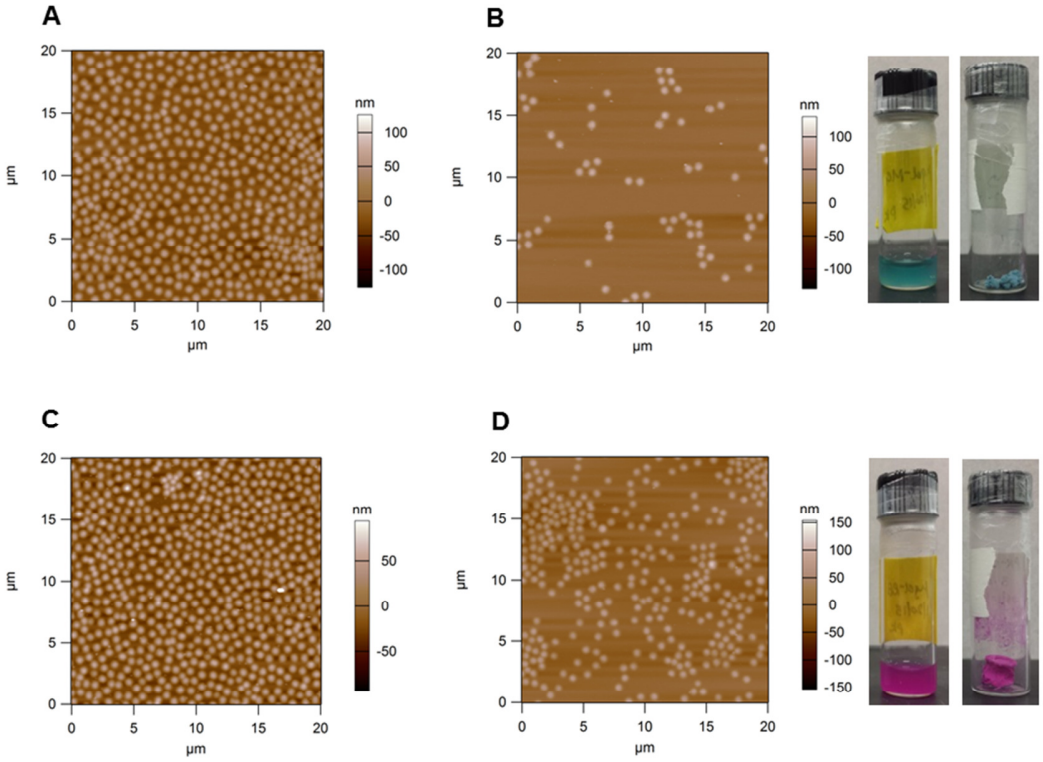


**Figure 3.1.** AFM height traces of µgel2a (A), µgel2a-MGITC (B), µgel2b (C) and µgel2b-RB (D) deposited on APTMS-functionalized glass by centrifugal deposition at 2250 × *g* for 15 minutes at 25 $^{0}$C. Images qualitatively demonstrated monodispersity of individual microgel suspensions. Solutions of µgel2a-MGITC and µgel2b-RB and dried microgel samples are shown adjacent to the corresponding images

The microgels were also observed via AFM imaging following centrifugal deposition on pre-functionalized glass. They were found to be monodisperse with a spherical profile (Figure 3.1 A, C).

To determine the physical radii of individual microgels and number densities of microgel solutions, dispersions of both µgel2a and µgel2b were subjected to tunable resistive pulse sensing in a high ionic strength buffer. This technique based on the Coulter principle detects passage of single particles through a nanopore. A decrease in the

intensity of current whenever a particle passes through the pore, detected as a blockade event, provides information about the population density of the dispersion and properties of individual particles. The distributions of microgel radii as obtained by this method are presented in Figure 3.2.

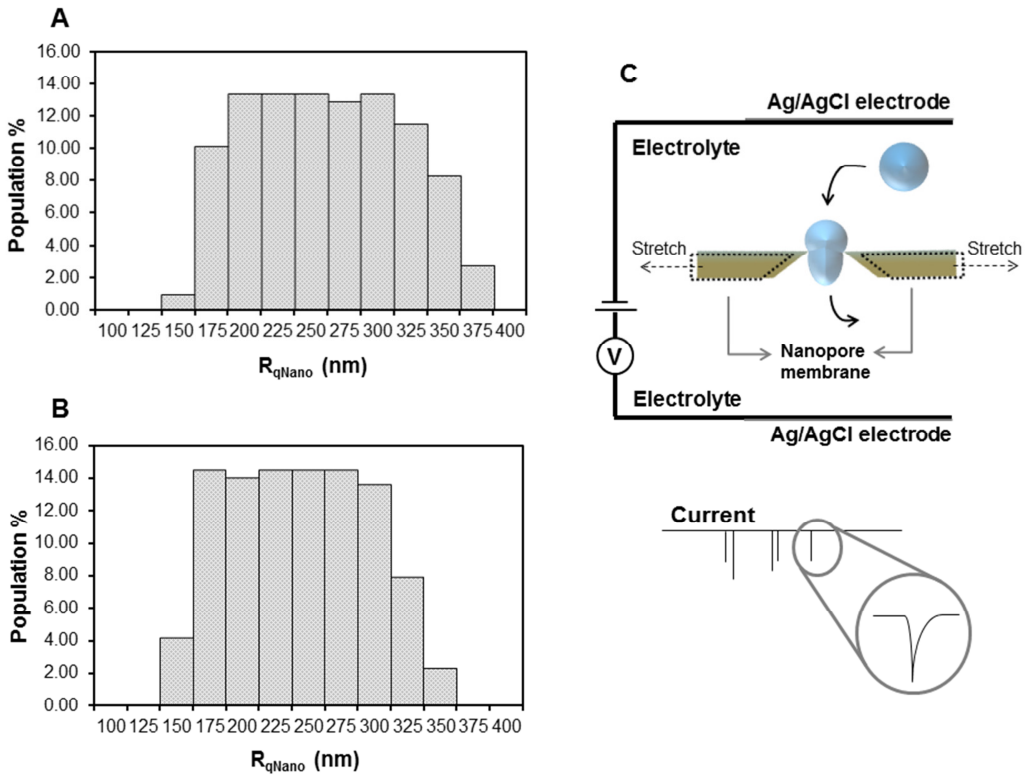


**Figure 3.2.** Particle size distribution of dispersions of µgel2a (A) and µgel2b (B) as determined through tunable resistive pulse sensing (each graph represents a distribution of ~ 215 $R_{qNano}$ values obtained through a total of 3 trials) and a schematic demonstrating working of the qNano (C)

All measurements were calibrated against standard solutions of polystyrene beads of relevant dimensions and values were obtained as averages from three sets of measurements on the qNano. When compared to the hydrodynamic diameters ($D_H$) of the microgels in similar conditions of ionic strength, the diameters obtained via the qNano ($D_{qNano}$) were seen to be smaller by ≈ 35% for µgel2a and ≈ 38% for and µgel2b (Table 3.2).

**Table 3.2** Population characteristics of µgel2a and µgel2b with comparative microgel sizes obtained via tunable resistive pulse sensing using the qNano and hydrodynamic diameter obtained using DLS

| Microgel identity | Number density (Particles/mL) | Molecular weight (g/mol) | $D_{qNano}$ (nm) | $D_H$ (nm) |
|---|---|---|---|---|
| **µgel2a** | $(7.83 \pm 2.42)\times10^{9}$ | $(8.31\pm 3.04)\times10^{10}$ | 499 ± 114 | 764 ± 42 |
| **µgel2b** | $(1.30 \pm 6.90)\times10^{10}$ | $(5.39 \pm 2.19)\times10^{10}$ | 461 ± 103 | 746 ± 32 |

*Values presented as averages of 3 sets of trials*
*All measurements performed in HEPES buffer (pH 7, 150 mM ionic strength)*

This difference in measured microgel dimensions can be attributed to the fact that the $R_H$ measured by dynamic light scattering takes into account the dangling polymer chains around the microgels and hence tends to be an overestimation of the microgel radius when compared to the physical size. Furthermore, since resistive pulse analysis involves standardization against hard spheres, it does not take into account the volume of buffer within the porous microgels, which is responsible for making them conductive. Thus, when examined in parallel to the resistive pulse due to a hard sphere, that observed

for a comparable microgel is of lower magnitude due to its buffer content and therefore, its volume is underestimated, leading to a further discrepancy in size. Based on the number density obtained via the qNano and the weight percent of the starting microgel solutions, the molecular weights of μgel2a and μgel2b were found to be (8.31± 3.04)×$10^{10}$ g/mol and (5.39 ± 2.19)×$10^{10}$ g/mol respectively (Table 3.2).

Further analysis of μgel2a and μgel2b with respect to their primary amine content was undertaken using the ATTO-TAG™ CBQCA reagent.[4] A standard curve was generated using APMA solutions in pH 9.3 borate buffer and the efficiency of APMA incorporation in the microgels was found to be 25 ± 3 % for μgel2a and 20 ± 2 % for μgel2b. The average number of moles of APMA in the microgels were found to be (1.27 ± 0.16)×$10^{-8}$ and (1.05 ± 0.11)×$10^{-8}$ respectively.

### 3.3.2 Conjugation of dyes to microgels and characterization of microgel-dye constructs

Following characterization of the cationic microgels, two dyes, malachite green and rose bengal were conjugated to μgel2a and μgel2b respectively. The conjugations were performed via the amine groups in the polymer matrices, using different techniques. This study was performed to determine the applicability of these microgels as agents of conjugation through a demonstration of the accessibility of their primary amines for covalent conjugations. Malachite green (MG) was conjugated in the form of its derivative MGITC (4.5X molar excess) in a manner similar to that utilized by Nayak et al.[5] RB was conjugated in its native form by carbodiimide coupling using EDC in the presence of NHSS (10.5X molar excess of reagents used) (Scheme B.2, **Appendix B**). The two

conjugates thus obtained, µgel2a-MGITC and µgel2b-RB have potential applications in bioimaging through techniques like photoacoustic and fluorescence imaging.[1,6] The conjugations were followed by purification through dialysis. µgel2a-MGITC was dialyzed against DI water, while µgel2b-RB was subjected to a two step dialysis method due to the non-specific interactions between free dye and the microgels. The first step involved dialyzing the microgel-dye conjugate solution against pH 11 CAPS buffer of very high ionic strength (500 mM). This buffer served the purpose of decreasing Coulombic interactions between the two species through the deprotonation of the amine groups on the microgels and by decreasing the Debye screening length of the charged species. Following this first step of dialysis, the second step involved dialysis against DI water to facilitate replacement of the buffer.

**Table 3.3** Concentrations of conjugated dyes (MGITC and RB) per microgel in comparison to dye concentration in solution and efficiency of conjugation reactions expressed as a percentage

| Microgel identity | 'Overall' concentration of dye in solution (mM) | Concentration of dye/microgel (mM) | % Efficiency of dye conjugation |
|---|---|---|---|
| **µgel2a-MGITC** | 0.035 ± 0.010 | 20.88 ± 7.66 | 42.50 ± 11.50 |
| **µgel2b-RB** | 0.034 ± 0.001 | 13.99 ± 5.67 | 46.41 ± 2.61 |

*Values presented as averages of measurements on two sample dilutions*

After purification, µgel2a-MGITC and µgel2b-RB were analyzed for their hydrodynamic radii by DLS in low ionic strength buffers. The results obtained are

summarized in Table 3.3. The pH responsivity of μgel2a-MGITC can be attributed partially to the free amine groups remaining post conjugation. Additionally, it may also be ascribed to the pKa of malachite green being 6.9,[7] leading to the presence of the charged dye species $R=N(CH_3)_2^+$ at pH 7.4. $R_H$ measurements performed on μgel2b-RB in pH 11 CAPS buffer did not yield reliable results, which may be due to aggregate formation through charge screening at the higher pH, leading to enhanced hydrophobic interactions. AFM on μgel2a-MGITC and μgel2b-RB following deposition on functionalized glass demonstrated no distortion in the hemispherical profile of the microgels post dye conjugation (Figure 3.1 B, D).

In order to determine the conjugation efficiencies of MGITC and RB, absorbance measurements were performed. For these, the concentrations of microgel-dye constructs used were low enough to prevent interference due to scattering from the colloidal microgel particles. Measurements were done on μgel2a-MGITC and μgel2b-RB solutions alongside standard absorbance curves prepared using MGITC and RB solutions, at $\lambda_{max}$ values of 625 nm and 540 nm respectively (Figure B.4, **Appendix B**). These revealed that the dye concentrations of the stock 1 mg/mL microgel solutions were 0.035 ± 0.010 mM and 0.034 ± 0.001 mM respectively. For comparison, μgel1, μgel2 and μgel6 (AFM height traces in Figure S6, Supporting Information) from the original series described in Chapter 2, were also conjugated to RB, but with a lower molar excess of the conjugation agents (4X). The motivation behind the synthesis of these microgels was to demonstrate the trend in primary amine group availability for reactions in two ways. First, through the conjugation of RB to microgels with different starting amounts of amines (μgel1-RB, μgel2-RB and μgel6-RB) and second, through the analysis of microgels with the same

starting density of amines but varying amounts of reagents used for conjugations (µgel2-RB and µgel2b-RB). The results obtained from absorbance measurements are presented in Figure 3.3.

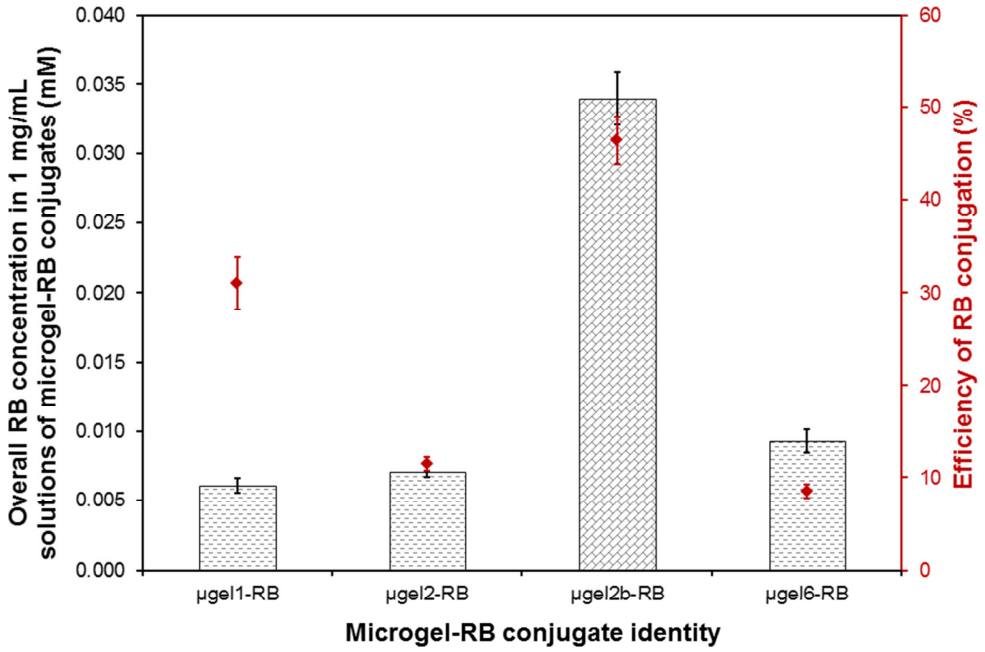


**Figure 3.3.** Microgel-RB conjugates analyzed for dye content via absorbance measurements at $\lambda_{max}$ = 540 nm. Bars with dashed pattern represent conjugates µgel1-RB, µgel2-RB and µgel6-RB generated using low ratios of conjugation reagents. The brick pattern represents µgel2b-RB with primary amine content identical to µgel2-RB, but conjugated to RB using higher concentrations of conjugation reagents. Red diamonds represent percent efficiencies of RB conjugations to microgels *(Values presented as averages of measurements on two different dilutions, error bars represent standard deviations of these two values)*

A similar trend as that observed for APMA incorporation (refer to Chapter 2, Figure 2.2) was seen for µgel1-RB, µgel2-RB and µgel6-RB. The percent efficiency of

conjugation was found to decrease with an increase in the number of APMA units in the microgels, which may be a result of differences in accessibility, particularly due to differences in microgel $R_H$ values and thus surface presentation of functional groups. Additionally, µgel2-RB and µgel2b-RB showed differences in RB conjugation amounts as expected, due to differences in reaction equilibria. Consequently, the efficiency of conjugation was also seen to be higher in µgel2b-RB, synthesized with a larger starting concentration of the reagents.

When considering utility in an imaging application like photoacoustics, the dye content in a specific, concentrated volume is a more relevant parameter than the overall dye concentration in solution. This is because in photoacoustic imaging, signals are generated by irradiation of a region of the sample with very small dimensions (~ 1 µm diameter), defined either by a point source such as a highly focused laser beam or by excitation of a small ~ 1 µm sized contrast agent. Thus, the concentration of dye per microgel was determined from the absorbance measurements using Beer-Lambert's law, the molecular weights of the microgels determined previously using the qNano (Table 3.2) and the volume of the microgels, which was calculated from their hydrodynamic radii. The dye concentration per microgel were found to be 20.88 ± 7.66 mM for µgel2a-MGITC and 13.99 ± 5.67 mM for µgel2b-RB, which were almost three orders of magnitude above the 'overall' solution concentrations for the microgel dispersions. Based on these values and the efficiency of APMA incorporation obtained via the CBQCA assay, the efficiency of dye conjugation was found to be 42.50 ± 11.50 % for µgel2a-MGITC and 46.41 ± 2.61% for µgel2b-RB. These efficiencies observed were similar in spite of different conjugative approaches and molar excesses of reagents being used for

both dyes. This may be partially due to the inherent reaction efficiencies of the conjugation reactions utilized, but the accessibility of the amine groups in the microgels may also be a major contributing factor in determining the number of dye molecules attached per microgel.

### 3.3.3 Viability studies with NIH3T3 fibroblasts

The development of new constructs for use in conjunction with biological systems brings with it the necessity to examine their potential toxic effects on cells. A viability assay was performed using NIH3T3 fibroblasts. These particular cells were utilized because they have been studied extensively as model systems for analysis of cell function in regards to adhesion, movement, and proliferation. They have also often been used to examine the toxicity of different kinds of nanoparticles.[8,9]

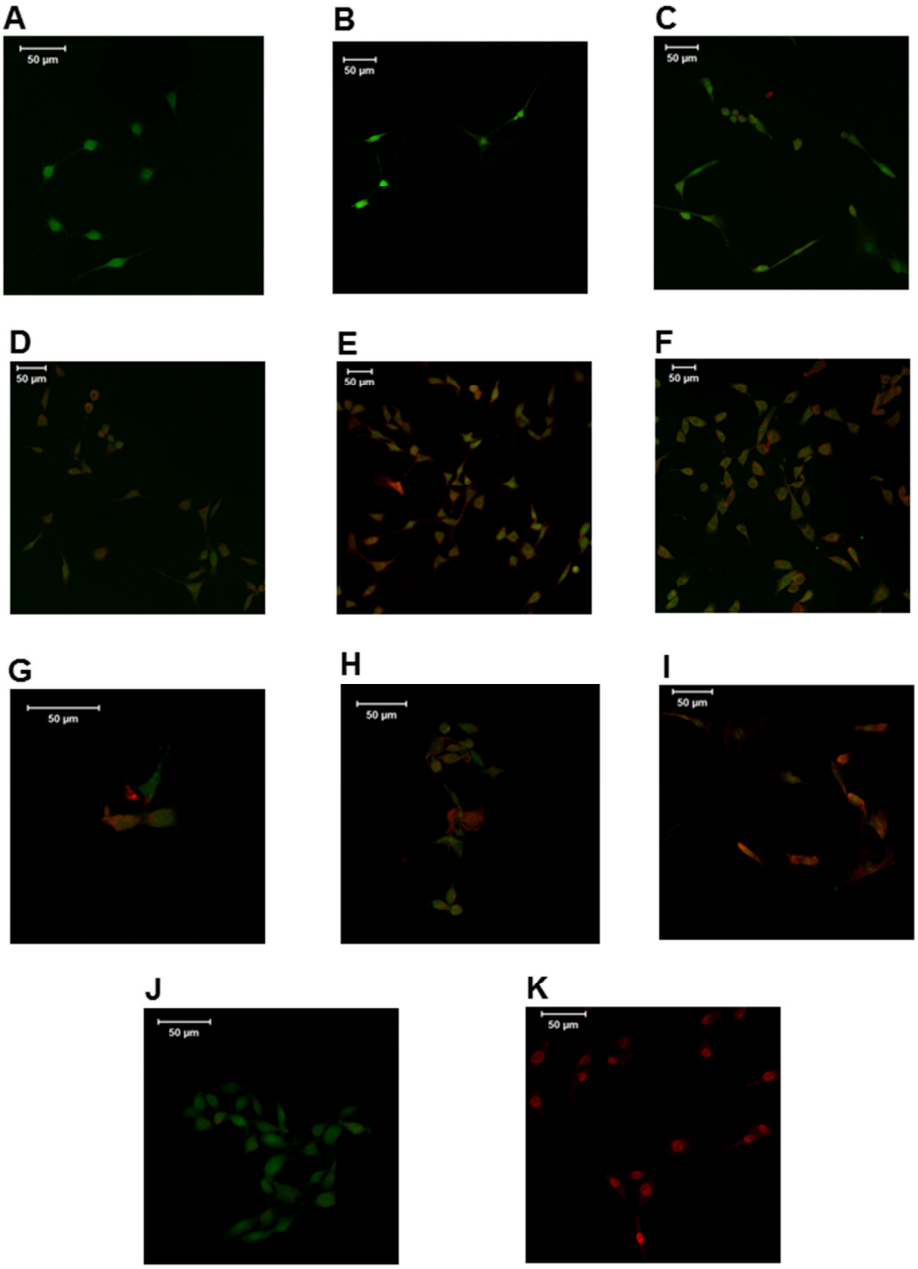


**Figure 3.4.** CLSM images of NIH3T3 fibroblasts incubated with varying microgel conjugates and concentrations for 24 h, and then stained using Calcein AM (green, live cell stain) and EthD-1 (red, dead cell stain) for determination of viability. Cells grown at a concentration of 10000 cells/cm$^2$ were incubated with 0.125 mg/mL µgel2a-MGITC (A), 0.25 mg/mL µgel2a-MGITC (B), 0.5 mg/mL µgel2a-MGITC (C), 0.125 mg/mL µgel2b-RB (D), 0.25 mg/mL µgel2b-RB (E), 0.5 mg/mL µgel2b-RB (F), 0.125 mg/mL µgel2b (G), 0.25 mg/mL µgel2b (H) and 0.5 mg/mL µgel2b (I). 'All live' and 'all dead' controls (J and K) shown for comparison

In the current study, NIH3T3 fibroblasts were grown on a multi-well plate at a uniform density of 10000 cells/cm$^2$ and were allowed to adhere and spread, after which they were incubated with the relevant microgels for 24 hours. The microgel solutions were subsequently removed from the wells and the cells were stained with Calcein AM and EthD-1 homodimer to determine viability. The measurements performed at $\lambda_{ex}$ = 528 nm and $\lambda_{em}$ = 645 nm for Calcein AM were normalized against 'all live' and 'all dead' cell controls and the percent viabilities were obtained (Figure B.6, **Appendix B**). Images of cells obtained via confocal microscopy following staining with the dyes, are presented in Figure 3.4. These images demonstrated red fluorescence from all microgels that had been incubated with μgel2b-RB (Figure 3.4 D, E, F). A closer examination of the images revealed that this red fluorescence was emanating from the cytoplasm of the cell and not from the nucleus. Since EthD-1 is known to stain the nucleus of dead cells (Figure 3.4 K), this observation along with the high Calcein fluorescence exhibited by these cells suggested that the cells were 'live' and that the red fluorescence was emanating from the RB in μgel2b-RB particles within the cells, rather than the membrane penetrating EthD-1. Therefore, we concluded that the microgels had been engulfed by the cells during the incubation period. This observation could be validated only with the μgel2b-RB particles, because the unconjugated cationic microgels μgel2b are non-fluorescent and the μgel2a-MGITC particles are conjugated to MG, which has a very low quantum yield and is hence virtually non-fluorescent. We hypothesize that both these species of microgels had been engulfed by the fibroblasts as well. In the interest of avoiding any interference from engulfed μgel2-RB particles, all viability calculations were performed based only on fluorescence intensities obtained from Calcein AM.

A statistical examination via one way ANOVA analysis rendered the quantitative viability results inconclusive, presumably due to variability in cell cultures (Figure B.6, **Appendix B**). However, the assay revealed low viability when the cells were incubated with the unconjugated, cationic microgels. This is not unexpected since polycations are known to be cytotoxic, as mentioned earlier. Qualitatively, via imaging, this cytotoxicity was seen to escalate with increasing concentrations of these microgel solutions incubated with the cells. However, when incubated with dye-conjugated microgels, the images of the fibroblasts obtained hinted at the comparative lower toxicity of these constructs, especially at lower concentrations. At higher concentrations of the microgel-dye conjugates, the results indicated that the microgels might be toxic to the cells, which may be due to the ability of the dyes to generate biologically harmful reactive oxygen species in solution.[10,11] However, in spite of its toxicity, RB has been used in biological systems in the past.[12] At the lowest concentration of the μgel-dye conjugates (0.125 mg/mL) used for these viability studies, low cytotoxicity was observed. This was encouraging, since the local concentrations of the dyes were very high as described in the earlier section. Thus, decreasing weight percent during introduction into a biological system may be feasible, in order to improve cell viability further. If the microgel-dye constructs need to be utilized at concentrations higher than 0.125 mg/mL, microgels synthesized from biocompatible materials like polyethylene glycol (PEG)[13,14] may present lower toxicity to the cells and thus may be the material of choice moving forward. Additionally, dyes that do not generate ROS can be conjugated to the microgels to serve the same purpose.

### 3.3.4 Generation of photoacoustic signals from microgel-dye constructs

Both microgel-dye constructs, μgel2a-MGITC and μgel2b-RB were incorporated into tissue phantoms and attempts were made to generate photoacoustic signals (Figure B.7, **Appendix B**). These signals were not reproducible, presumably due to background interference. Therefore, the signals represented in Figure B.7 are not reliable, warranting further optimization of the signal generation system for utilization with microgel-dye conjugates.

## 3.4 Conclusion

Controlled bioconjugation reactions can be performed using well characterized amine functionalized microgels, as demonstrated through conjugation to the two different dyes utilized in this study. Absorbance measurements provided information about the availability of functional groups for conjugation. Local concentrations of the dyes calculated through analysis of the molecular weights of the microgels were found to be almost three orders of magnitude higher than the concentration of dye in solution. This was very promising for applications like photoacoustic imaging, for the generation of high intensity signals. This high local concentration of the conjugated entity may also be useful for phenomena requiring multivalency for efficient targeting in biological systems. Additionally, it may be beneficial for heightened interactions with biological materials leading to events such as clot contraction, such as that observed by Brown et al. when they developed artificial platelets.[15] Viability studies conducted with NIH3T3 fibroblasts indicated that microgel-dye conjugates were not toxic to cells, especially when concentrations of 0.125 mg/mL were used for incubation with the cells.

## 3.5 References


(1) Indig, G. L.; Jay, D. G.; Grabowski, J. J.: The efficiency of malachite green, free and protein bound, as a photon-to-heat converter. *Biophys. J.* **1992**, *61*, 631-8.

(2) Richards, C. I.; Hsiang, J. C.; Dickson, R. M.: Synchronously Amplified Fluorescence Image Recovery (SAFIRe). *J. Phys. Chem. B* **2010**, *114*, 660-665.

(3) Fischer, D.; Li, Y. X.; Ahlemeyer, B.; Krieglstein, J.; Kissel, T.: In vitro cytotoxicity testing of polycations: influence of polymer structure on cell viability and hemolysis. *Biomaterials* **2003**, *24*, 1121-1131.

(4) You, W. W.; Haugland, R. P.; Ryan, D. K.; Haugland, N. P.: 3-(4-carboxybenzoyl)quinoline-2-carboxaldehyde, a reagent with broad dynamic range for the assay of proteins and lipoproteins in solution. *Anal. Biochem.* **1997**, *244*, 277-282.

(5) Nayak, S.; Lyon, L. A.: Photoinduced phase transitions in poly(N-isopropylacrylamide) microgels. *Chemistry of Materials* **2004**, *16*, 2623-2627.

(6) Serafini, A. N.; Smoak, W. M.; Hupf, H. B.; Beaver, J. E.; Holder, J.; Gilson, A. J.: Iodine-123-Rose bengal: An improved hepatobiliary imaging agent. *J Nucl Med* **1975**, *16*, 629-32.

(7) Nguyen, M. C.; Shoji, I.; Noboru, K.: Donnan Electric Potential Dependence of Intraparticle Diffusion of Malachite Green in Single Cation Exchange Resin Particles: A Laser Trapping-Microspectroscopy Study. *American Journal of Analytical Chemistry* **2012**, *2012*.

(8) Drescher, D.; Orts-Gil, G.; Laube, G.; Natte, K.; Veh, R. W.; Oesterle, W.; Kneipp, J.: Toxicity of amorphous silica nanoparticles on eukaryotic cell model is determined by particle agglomeration and serum protein adsorption effects. *Anal. Bioanal. Chem.* **2011**, *400*, 1367-1373.

(9) Fletcher, D. A.; Mullins, D.: Cell mechanics and the cytoskeleton. *Nature* **2010**, *463*, 485-492.

(10) Dhamgaye, S.; Devaux, F.; Manoharlal, R.; Vandeputte, P.; Shah, A. H.; Singh, A.; Blugeon, C.; Sanglard, D.; Prasad, R.: In Vitro Effect of Malachite Green on Candida albicans Involves Multiple Pathways and Transcriptional Regulators UPC2 and STP2. *Antimicrob. Agents Chemother.* **2012**, *56*, 495-506.

(11) Lambert, C.; Sarna, T.; Truscott, T. G.: Rose-bengal radicals and their reactivity. *J. Chem. Soc.-Faraday Trans.* **1990**, *86*, 3879-3882.

(12) Savini, G.; Prabhawasat, P.; Kojima, T.; Grueterich, M.; Espana, E.; Goto, E.: The challenge of dry eye diagnosis. *Clin Ophthalmol* **2008**, *2*, 31-55.

(13) Lutz, J. F.: Thermo-Switchable Materials Prepared Using the OEGMA-Platform. *Adv. Mater.* **2011**, *23*, 2237-2243.

(14) Hu, Z. B.; Cai, T.; Chi, C. L.: Thermoresponsive oligo(ethylene glycol)-methacrylate- based polymers and microgels. *Soft Matter* **2010**, *6*, 2115-2123.

(15) Brown, A. C.; Stabenfeldt, S. E.; Ahn, B.; Hannan, R. T.; Dhada, K. S.; Herman, E. S.; Stefanelli, V.; Guzzetta, N.; Alexeev, A.; Lam, W. A.; Lyon, L. A.; Barker, T. H.: Ultrasoft microgels displaying emergent platelet-like behaviours. *Nat. Mater.* **2014**, *13*, 1108-1114.

# CHAPTER 4

# MICROGEL CORE/SHELL ARCHITECTURES AS TARGETED AGENTS FOR THROMBOLYSIS

*(**Purva Kodlekere**, L. Andrew Lyon; Microgel core/shell architectures as targeted agents for thrombolysis)*

*To be submitted to: Biomaterials*

## 4.1 Introduction

Fibrin is a biopolymer that plays a vital role in hemostasis. In the occurrence of an injury, fibrinogen, its soluble precursor, gets converted to insoluble fibrin through the action of the proteolytic enzyme, thrombin. On activation, thrombin cleaves fibrinopeptides in the central domain of fibrinogen. This exposes knobs that are complementary to holes that are always exposed, present at the distal domains of the molecule. The intermolecular interactions between the knobs and holes result in the formation of a half-staggered structure and this in turn leads to the formation of a protofibril. On reaching a particular length, the protofibrils aggregate laterally, leading to the formation of fibers. The last step involves covalent ligation by the action of activated factor XIII.[1]

Dissolution of fibrin clots in the body is carried out by the fibrinolytic system, which primarily functions through the action of plasmin on fibrin clots, following activation of its precursor plasminogen. A delicate balance between the formation of clots and their dissolution is extremely crucial for maintaining normal bodily function. An

imbalance can either cause massive hemorrhages or the generation of thrombi, that can block the flow of blood through vessels. The latter leads to physiological diseased states such as deep vein thrombosis, atherosclerosis and stroke. In order to dissolve abnormal thrombi, plasminogen activators such as streptokinase, urokinase and tissue-type plasminogen activator (tPA) are commonly used, but direct intravenous administration of these agents can cause off target effects and lead to massive hemorrhages.[2] In order to increase efficacy of these agents and reduce off-target effects, a number of delivery agents have been developed. For example, Wang et al. synthesized magnetic mesoporous silica nanoparticles or M-MSNs for magnetically guided, targeted delivery of urokinase to thrombi.[3] McCarthy et al. utilized specific targeting to activated factor XIII, by conjugating crosslinked dextran coated iron oxide nanoparticles to peptide affinity ligands, for the delivery of tPA.[4] Similarly, Absar et al. utilized peptide-grafted liposomes for targeted delivery of tPA to thrombi.[5]

Microgels form an important class of materials that have been utilized for targeted delivery of therapeutics in the past.[6-8] They are colloidally stable, solvent swollen polymer-based hydrogel microparticles that demonstrate tremendous versatility in synthesis. This can be leveraged to the generation of microgels of different sizes, architectures and with responsivity to different stimuli such as temperature and pH.[9-11] Core/shell microgels have been synthesized before[12-14] and provide the advantage of localizing functionalities and hence potential targeting agents on their surface. Additionally, the porous nature of the core makes it possible to load therapeutics like drugs[15] or siRNA[16] and use the resulting system for targeted delivery.

The incorporation of colloidal particles such as microgels in matrices of polymeric scaffolds provides the opportunity to tune properties of the matrix.[17] Such modular systems are thus gaining increasing importance. The interactions of colloidal particles with pre-formed fibrin clots have also been studied before.[18,19] Additionally, colloids have also been employed to generate imaging agents targeted to fibrin.[20,21] The knowledge that fibrin clots behave as equilibrium polymers,[22] with monomers or oligomers associating and/or dissociating from pre-formed fibers, has provided opportunities for remodeling of the structural components of fibrin. Radical-generating nanoparticles have therefore, also been used to bring about remodeling of fibrin without the help of enzymes.[23]

Herein, we present the development of core/shell microgels in three different size ranges, to be used in fibrinolysis. Investigations have been carried out with regards to their pH responsivity in buffers of two different ionic strengths to demonstrate the incorporation of AAc moieties in the microgel shells during synthesis. Atomic force microscopy was employed to examine the profile of these particles. The microgel solutions were then allowed to flow through fibrin clots, in order to examine the interplay between their dimensions, their deformability and the pore size of the clots. Differences in microgel residence were observed as a function of microgel size. Following this, a proof of principle encapsulation study was conducted using +6 GFP in order to investigate the role of electrostatic interactions in loading of therapeutics within the microgels, with possible potential in triggered release. Finally, microgels with the largest $R_H$ among those analyzed, conjugated to three different peptides, GPRP (fibrin knob A mimic), GPSP (control peptide) and AHRP (fibrin knob B mimic), were subjected to

flow through fibrin clots. The particles conjugated to the knob A mimic were found to successfully disrupt the fibrin clots. These results are promising because this is a novel system that exploits the nature of fibrin as an equilibrium polymer,[22] in order to cause clot disruption in the presence of micromolar concentrations of targeting peptide density in less than 3 hours. We hypothesize that the multivalent display of peptide moieties on the microgels are responsible for this enhanced effect. Moreover, the presence of a core in the microgels has the potential to be loaded with a secondary therapeutic if essential, for supplementing fibrinolysis, or for delivering other agents that could be used in applications such as imaging to the clots, further improving the scope of this system.

## 4.2 Experimental section

### 4.2.1 Materials

All materials were purchased from Sigma-Aldrich unless specified otherwise. Details of common materials are available in Chapter 2, section 2.2.1 and Chapter 3, section 3.2.1. The comonomer used for shell synthesis acrylic acid (AAc, Fluka), $CaCl_2$, KCl, buffer preparation material formic acid (EMD Millipore), 2-maleimidoethylamine trifluoroacetate salt (AEM), methacryloxyethyl thiocarbamoyl rhodamine B (mRhoB, Poly Fluor 570, Polysciences Inc.), human fibrinogen (FIB3, Enzyme Research Laboratories), human α-thrombin (Enzyme Research Laboratories, HT 1002a) and peptides from GenScript GPRPFPAC (GPRP), GPSPFPAC (GPSP) and AHRPYAAC (AHRP) were all used as received. The solutions were prepared using distilled water,

deionized to a resistance of 18 MΩ (Barnstead E-Pure system). Solutions were filtered through a 0.2-μm Acrodisc syringe filter before use.

### 4.2.2 Microgel core synthesis

Microgel cores were synthesized by free radical precipitation polymerization, by a process similar to that described in Chapter 2, section 2.2. For the syntheses under consideration here, NIPMAm and BIS in molar compositions of 98% and 2% respectively were dissolved in 48.5 mL distilled, deionized water, to a total monomer concentration of 140 mM, along with SDS at the relevant concentration (refer to Table 4.1). The resulting solution was filtered through a 0.8 μm Acrodisc syringe filter and synthesis was carried out in conditions identical to those described in Chapter 2, section 2.2.2, with the only change being the introduction of 0.5 mL of a solution of mRhoB in DMSO, to a final concentration of 0.1 mM, once the solution temperature was stable at 70 $^{0}$C. After reaction completion, the solution was cooled and then filtered through glass wool.

### 4.2.3 Microgel shell synthesis

Core/shell microgels were synthesized using the previously established 'seed and feed' method,[12,24] in a manner similar to that described in Chapter 2, section 2.2.2. The shell monomer solution used in this case was prepared by dissolving NIPMAm, BIS and AAc in feed ratios of 93%, 2% and 5% respectively, in distilled, deionized water, to a total monomer concentration of 50 mM, along with SDS at a total concentration of 2 mM, and filtering it through a 0.8 μm Acrodisc syringe filter. The microgel core and

monomer shell mixture was heated to 70 $^0$C in a manner similar to the core synthesis and was initiated with 0.5 mL APS once temperature stability was achieved. After allowing it to proceed for 4 h under a $N_2$ blanket, with constant stirring at 400 RPM, it was cooled down to room temperature and the solution was filtered through glass wool. The microgels were then purified by pelleting via ultracentrifugation at 104000 – 417000 × *g* for 20 – 70 minutes, depending on the microgel type. Every run of ultracentrifugation was followed by removal of the supernatant and resuspension in DI water. After repeating this process six times, the microgels were lyophilized prior to characterization.

### 4.2.4 Dynamic Light Scattering

Hydrodynamic radii ($R_H$) of the microgels were determined via dynamic light scattering (DLS, DynaPro, Protein Solutions). Measurements were performed in the following buffers: pH 7 phosphate (50 mM ionic strength), pH 7.4 HEPES (6 mM ionic strength), pH 3 formate (50 mM ionic strength), pH 3 formate (6 mM ionic strength), in a manner similar to that described in Chapter 2, section 2.2.3

### 4.2.5 Atomic Force Microscopy

Atomic Force Microscopy (AFM) was performed using an MFP-3D AFM (Asylum Research), in a manner similar to that utilized in Chapter 2, section 2.2.4. Similar coverslips were cleaned and functionalized in a 1% (v/v) APTMS/absolute ethanol solution on a shaker table for 2 h, following which they were washed with DI water. The microgel solutions prepared in phosphate buffer (pH 7, 50 mM ionic strength) were then used for submonolayer deposition onto the glass substrates by centrifugation at

2250 × *g* for 10 – 25 minutes (depending on the microgel type) at 25 $^{0}$C using a plate rotor. The coverslips were rinsed well with DI water and dried with nitrogen before imaging.

### 4.2.6 Fibrin clot formation

Solutions of fibrinogen (13.51 mg/mL) and thrombin (10 U/mL) were thawed to room temperature. These were mixed with $CaCl_2$ (final concentration 5 mM) and HEPES (final concentration 25 mM HEPES, 150 mM NaCl) to concentrations of 3 mg/mL or 2 mg/mL (fibrinogen, size-based localization studies and clot disruption studies respectively) and 1 U/mL (thrombin) and clots were formed in plastic capillary tubes (Globe Scientific, Inc., I.D. = 0.85 mm). They were allowed to polymerize overnight in a humid environment, to avoid drying out of clots. For the experiments, they were cut into 1.5 cm pieces for utilization with each sample solution.

### 4.2.7 Permeability measurements and perfusion studies

Flow studies were performed using the experimental setup represented in Scheme 4.1. HEPES buffer (same as that used for clot preparation) was first perfused through the 1.5 cm clots and following a 15 minute equilibration, flow rates of buffer post traversal through the fibrin clots were measured for 3 – 5 minutes (depending on the clot formation conditions), from a solution reservoir height of 18 inches. Three measurements were made for every clot and clot permeability values were calculated using Darcy's law,

$$Q = \frac{k}{\mu} A \frac{\Delta P}{L}$$

where Q is the volumetric flow ($m^3/s$), k is Darcy's constant or the Darcy permeability ($m^2$), μ is the liquid viscosity (kg/ms), A is the cross-sectional area of the clot ($m^2$), ΔP is the pressure gradient across the clot ($kg/ms^2$) and L is the length of the cylindrical clot (m).

Following confirmation of consistency in clot permeabilities, buffer solutions in the reservoirs were replaced by microgel solutions at a concentration of 0.1 mg/mL and were allowed to pass through the clots. After equilibration for 15 minutes, eluent collection was begun and was conducted every 30 minutes. The eluents were analyzed for their fluorescence using a plate reader (Infinite® 200 PRO NanoQuant™, Tecan Group LTD., San Jose, CA) at excitation and emission wavelengths of 540 nm and 575 nm, respectively. Following background corrections for buffer, fluorescence intensities normalized to that of the respective reservoir microgel solutions (0.1 mg/mL) were calculated. Three trials were performed and values of normalized fluorescence intensities are presented as averages of values obtained at the respective time points from these trials. Standard deviations were also obtained from these values and are presented.

### 4.2.8 Production and purification of +6 GFP

Plasmids with genes encoding for +6 GFP from Prof. David Liu's research group (Howard Hughes Medical Institute, Harvard University) were used for transformation of *E.coli*, following which the production and purification of the protein was performed in a manner similar to that utilized by Cronican et al.[25] with slight modifications. Briefly, transformed *E.coli* were grown to an OD of 0.6 in LB broth (Lennox, Alfa Aesar), following which they were induced with 1 mM IPTG (Isopropyl β-D-

thiogalactopyranoside, ThermoFisher) at 30 $^0$C for 4 h. The cells were then harvested and preserved as pellets at -80 $^0$C. These pellets were thawed in a solution of 1X PBS with 2M NaCl and sonication was employed to lyse them. Following centrifugation at 10000 × *g* for 8 minutes, the supernatant was mixed with Ni-NTA resin (Fisher Scientific) for 30 minutes at 4 $^0$C. The removal of resin by centrifugation was followed by multiple washes with 2 M NaCl and 20 mM imidazole (Fisher Scientific) and then a 2 M NaCl + 500 mM imidazole solution was used for detachment of the protein from the resin. Dialysis against PBS for 18 h at 4 $^0$C was then carried out, followed by SDS-PAGE staining with Simply Blue (ThermoFisher).

### 4.2.9 +6 GFP encapsulation studies

Lyophilized core/shell microgels were weighed and resuspended in 0.20 μM +6 GFP solution in the respective buffer (6 mM ionic strength HEPES or 150 mM ionic strength HEPES). After a 20 h equilibration, the microgel solutions were centrifuged at 104000 – 417000 × *g* for 20 – 70 minutes, depending on the microgel type. The supernatants were analyzed for presence of +6 GFP by fluorescence measurements at λex = 475 nm and λex = 520 nm. Normalization was performed against stock +6 GFP solutions in the respective buffer conditions.

### 4.2.10 Conjugation of peptides to microgels

Microgels (small, intermediate and large core/shell) were divided into three sections each and were resuspended in MES buffer (20 mM ionic strength) and conjugated to AEM through carbodiimide coupling, using a 2X molar excess of EDC and

NHSS and a 1:1 –COOH:AEM molar ratio, based on the theoretical number of AAc moieties incorporated in the microgel shells. This conjugation was allowed to proceed for 2 h, following which dialyses for all 9 solutions were performed against MES buffer for 15 h. The MES buffer was then replaced with phosphate buffer (pH 7, 140 mM ionic strength) and following equilibration for ~ 8 h, peptide conjugations to GPRP, GPSP and AHRP (1:0.2 molar ratio of theoretical –COOH:peptide) were performed overnight. The resulting solutions were dialyzed against DI water for one week and placed on a shaker for homogeneity. A small portion of each solution was lyophilized in order to determine concentration of the stock solutions.

### 4.2.11 Clot disruption studies under flow

These studies were performed in a manner similar to the permeability measurements described in section 4.2.7. 1.5 cm fibrin clots were first analyzed for their consistency in permeability by conducting flow rate measurements using HEPES buffer. The Darcy constant k was determined for each clot, following which reservoir solutions (at an 18 inch height) were replaced with the respective peptide-conjugated microgel solutions (0.1 mg/mL). After equilibration for 10 minutes, flow rate measurements (3 minutes each) were conducted for each microgel solution, after passage through the clot. This was repeated every 10 minutes until clot disruption was observed. Pictures of clots were also taken at various time points during the experiment. Two separate trials were performed and the results from these are presented.

## 4.3 Results and discussion

### 4.3.1 Development and characterization of core/shell microgels with different dimensions

Core/shell microgels in three different size ranges were synthesized and analyzed. The shell was synthesized to have carboxylic acid functionalities that facilitate conjugation of pertinent moieties to the microgels with the display being predominantly localized to the surface. In this study, the goal was to utilize these groups for conjugation of fibrin-specific peptides, thus generating a micro- scale system for enabling targeted fibrinolysis. Three size ranges of microgels were analyzed in order to visualize their size-based differential localization in and around the clots. The hypothesis was that the porosity of fibrin clots would cause differences in microgel residence in them.

Core/shell microgels have been synthesized using a seed-and-feed mechanism.[13] The synthesis conditions for small, intermediate and large core and core/shell microgels are presented in Table 4.1. Rhodamine was incorporated in its polymerizable form while synthesizing the cores, to aid microgel visualization in flow experiments. Different concentrations of the surfactant SDS and initiator APS were utilized in order to generate cores of three different sizes. Higher concentrations of both led to a decrease in size of the resultant microgels. The presence of a high concentration of surfactant like SDS is known to lead to smaller microgels through early particle stabilization.[26] Additionally, a higher concentration of initiator causes a large number of nucleation sites to be formed, and this process being favored over chain propagation results in the formation of a large number of small microgels.

**Table 4.1** Synthesis conditions for small, intermediate and large core particles and core/shell microgels

| Microgel type | | [Total monomer] (mM) | Volume of core solution (mL) | [NIPMAm] (mol %) | [BIS] (mol %) | [mRhoB] (mM) | [AAc] (mol %) | [SDS] (mM) | [APS] (mM) |
|---|---|---|---|---|---|---|---|---|---|
| **Small** | Core | 140 | - | 98 | 2 | 0.1 | - | 8 | 8 |
| | Core/Shell | 50 | 10 | 93 | 2 | - | 5 | 2 | 0.5 |
| **Intermediate** | Core | 140 | - | 98 | 2 | 0.1 | - | 2 | 2 |
| | Core/Shell | 50 | 10 | 93 | 2 | - | 5 | 2 | 0.5 |
| **Large** | Core | 140 | - | 98 | 2 | 0.1 | - | 0.5 | 0.5 |
| | Core/Shell | 50 | 10 | 93 | 2 | - | 5 | 2 | 0.5 |

*Volume = 50cm$^3$ , Temp. = 70 $^0$C, Stir rate = 400 RPM*

Following synthesis, the core/shell microgels were purified to remove excess reagents, oligomers and secondary cores formed during the synthesis (disappearance of secondary cores was confirmed via DLS on supernatant solutions after centrifugation). The microgels were then deposited on pre-functionalized glass through centrifugation and imaged via AFM. Figure 4.1 A, B and C represent the AFM images of small core/shell (S C/S), intermediate core/shell (I C/S) and large core/shell (L C/S) microgels respectively. The differences in microgel size were evident from the images and height profiles. Deposition on functionalized substrates causes microgels to appear flattened, due to their deformability. They thus appear hemispherical, as observed in these images. The I C/S microgels seemed to be slightly polydisperse, but their sizes obtained through analysis of these images and DLS revealed that their diameters were still ‘intermediate’ between those of S C/S and L C/S microgels.

In order to measure particle size and qualitatively assess incorporation of –COOH groups into microgel matrices during the syntheses, DLS measurements were performed in buffers of 6 mM and 50 mM ionic strength, at pH values above and below the pKa of AAc, which is ≈ 4.

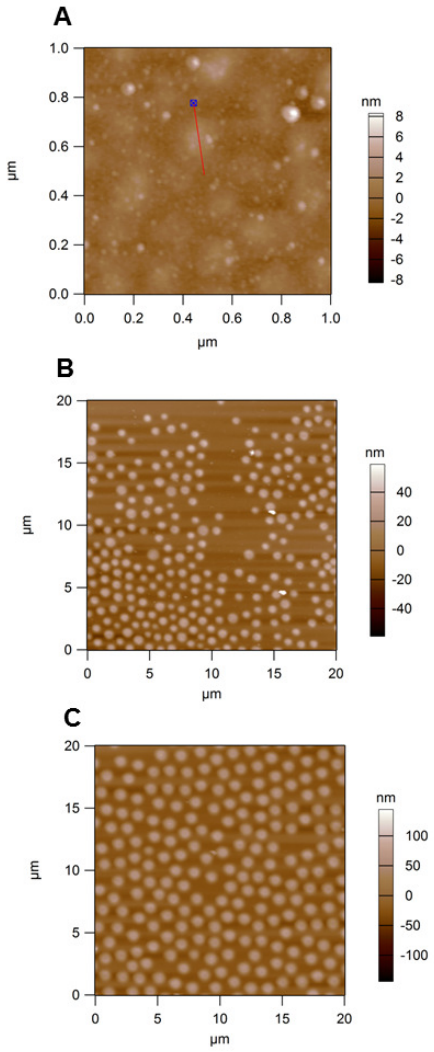


**Figure 4.1.** AFM height traces of S C/S, I C/S and L C/S microgels deposited on APTMS-functionalized glass by centrifugal deposition at 2250 × *g* for 10 - 25 minutes at 25 $^{0}$C, depending on the microgel type. Images demonstrated spherical particles in all three size ranges

The values from DLS measurements are presented in Figure 4.2. Microgels were seen to be pH responsive at both ionic strengths, demonstrating successful incorporation of AAc. The low magnitude of change in $R_H$ values can be attributed to the presence of –COOH groups only in microgel shells, which causes microgel deswelling in response to pH to be primarily shell-localized. This manifests as low pH responsivity.

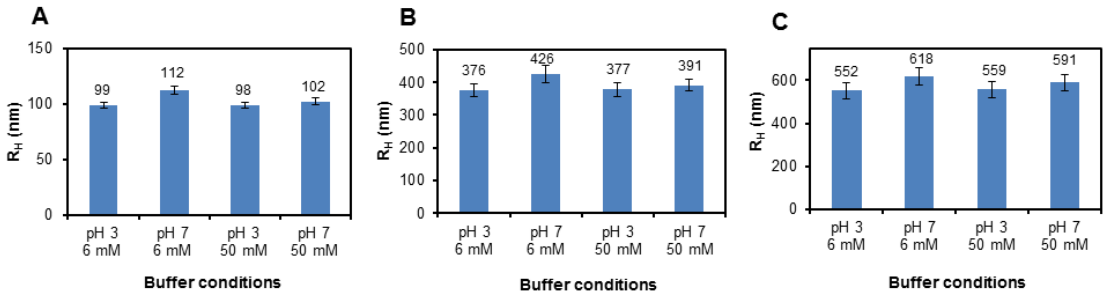


**Figure 4.2.** DLS measurements performed on S C/S (A), I C/S (B) and L C/S (C) microgels generated $R_H$ values that demonstrated a slightly greater magnitude of pH responsivity at 6 mM ionic strength, than at 50 mM ionic strength

Microgels were, however, observed to be slightly more responsive to changes in the pH, when measurements were conducted in low ionic strength (6 mM) buffers, compared to those taken in buffers of higher ionic strength (50 mM). This can be explained on the basis of partial screening of charges in the presence of a higher concentration of ionic species in solution, leading to inhibition of microgel deswelling under these conditions.

### 4.3.2 Flow experiments for analysis of size-based differential localization of microgels in fibrin clots

The abnormal formation of thrombi warrants the need for the delivery of thrombolytic agents to bring about clot lysis, to mitigate impedance of blood flow through blood vessels. The utilization of microgels for this purpose is very promising (refer to section 4.1). However, development of an effective system for this purpose requires an investigation into microgel localization in and around clots. This is vital to determine the efficacy of microgels for the purpose of fibrinolysis, because the rate of clot degradation will depend on the region of the clot from where it commences and how it progresses. Just as microgel size is an important parameter when considering this application, clot porosity also has a major role to play. The interplay between these two factors is thus extremely crucial, particularly because microgels are known to be deformable and hence have the potential to undergo more intricate interactions with the clots than comparable hard sphere colloids.[27]

Porosity of fibrin clots depends on the clot formation conditions.[28] Thus, a higher starting concentration of fibrinogen leads to the formation of denser clots. Utilization of different thrombin concentrations also has distinct effects on the physical and mechanical properties of the clots, through changes in the thickness of clot fibers.[29,30] In the study described here, microgel dispersions were allowed to flow through fibrin clots and the eluent was analyzed to examine microgel residence within the clots. The concentration of fibrinogen used was 3 mg/mL, which is close to the physiological range of ~ 2.5 mg/mL and clots were made using 1 U/mL thrombin.

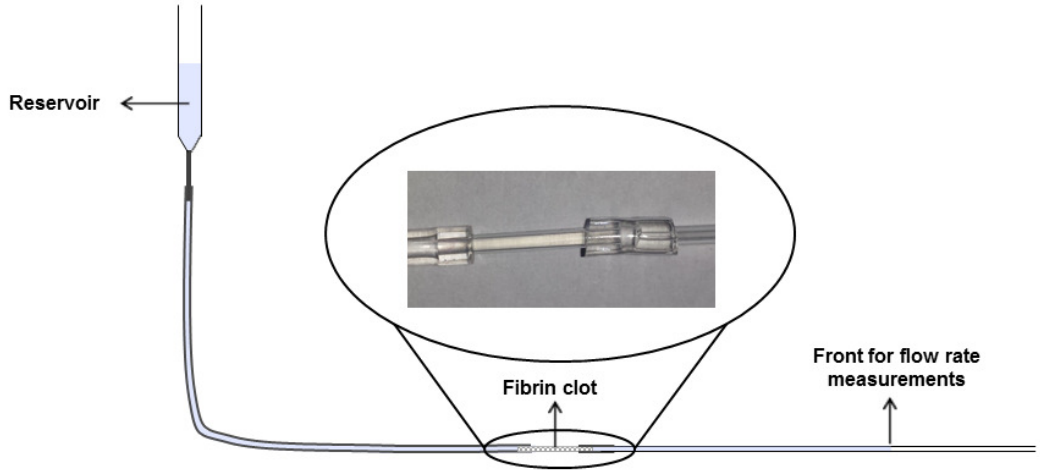


**Scheme 4.1.** Experimental setup used for examination of perfusion through fibrin clots. Permeability measurements on the clots were first performed using HEPES buffer and then the respective microgel solutions were allowed to flow through the clots

Scheme 4.1 represents the experimental set up for the flow studies. In a typical experiment, the permeability of fibrin clots was first analyzed through measurements of buffer flow rate through the clots. Darcy's law, which relates the average interstitial fluid velocity to permeability of the medium, was used for this purpose. The average value of Darcy's constant 'k', i.e. permeability, for all clots used in three trials of the experiment was found to be $(4.027 \pm 0.389)\times10^{-13}$ $m^2$, which was in the same range as values that have been obtained for fibrin clots in previous studies.[19,31] Once uniformity in clot permeabilities was ensured, the buffer solutions in reservoirs were replaced with S C/S, I C/S and L C/S microgel solutions at a concentration of 0.1 mg/mL. Following equilibration, eluents were collected at different time points and were analyzed based on the fluorescence of mRhoB at $\lambda_{ex}$ = 540 nm and $\lambda_{em}$ = 575 nm. The results obtained are presented in Figure 4.3.

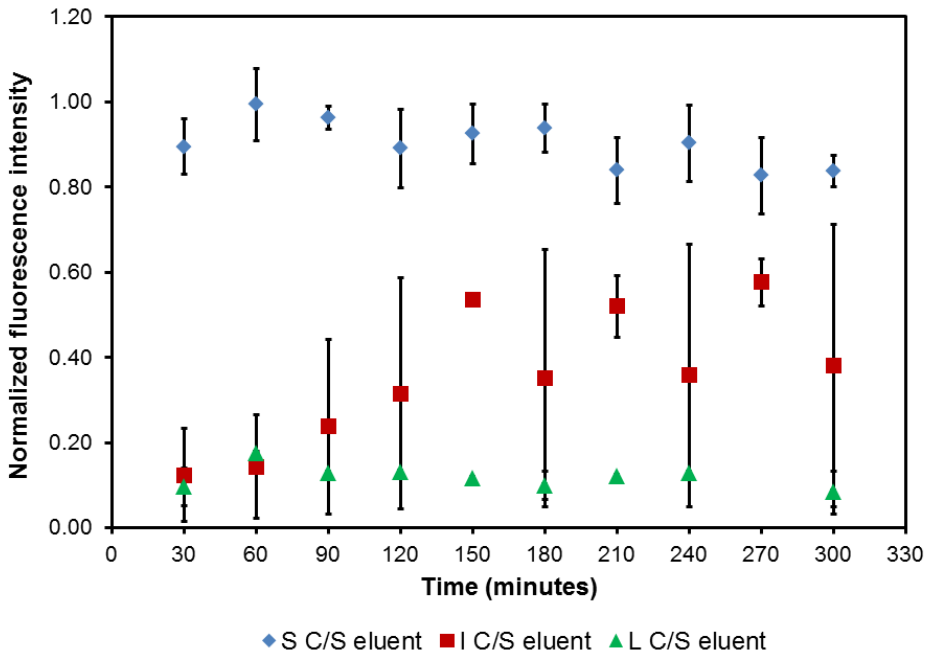


**Figure 4.3.** Flow studies performed on fibrin clots formed at 3 mg/mL fibrinogen and 1 U/mL thrombin demonstrated differences in microgel-clot interactions based on particle size. Measurements performed at $\lambda_{ex}$ = 540 nm, $\lambda_{em}$ = 575 nm. Fluorescence intensities were normalized to those of respective (S C/S, I C/S, L C/S) reservoir solutions (0.1 mg/mL) *(Values presented as average of 3 trials, error bars represent standard deviations of these three values)*

Flow studies revealed differences in microgel passage and residences within fibrin clots, based on microgel dimensions. S C/S microgels were observed to pass through the clots easily, appearing in the eluent almost immediately. This suggests that these particles undergo minimal interactions with the clot, possibly due to their diameters being significantly smaller than the average pore size of the clot. I C/S microgels traversed through the clot slower than the S C/S microgels, appearing in the eluent only beyond the one hour time point and in seemingly smaller numbers. This suggests that their

dimensions may be in the range of the average pore size of fibrin clots formed under the aforementioned conditions. Thus, I C/S microgels appear to interact heavily with clot fibers. The variability observed with regards to the flow of I C/S microgels, between different trials, may be caused by two contributing factors. Firstly, while the microgel dimensions may be close to the average pore size of the clots, the differences in individual pore sizes, although subtle, may play an important role at the length scale under study. This may cause the microgel path through the clot to be somewhat non-uniform and this may manifest itself in the form of variability in concentration of microgels in the eluent at different time points. Secondly, as mentioned in the previous section, dispersions of I C/S microgels were somewhat polydisperse. This may also be responsible for the discrepancies observed between different trials. L C/S microgels were unable to enter the clot and did not appear in the eluent in the five hour time frame of the experiment. Instead, these microgels concentrated at the entrance of the clot through the experiment, forming a macroscopically visible boundary (visualized via the color of mRhoB, similar to that observed in Figure 4.5 C). It is worth nothing that I C/S microgels also formed a similar boundary at the beginning of the experiment, which can be correlated to their absence in the eluent during the first hour. Over time, however, while the L C/S microgels were unable to enter the clot, the I C/S microgels were successful in doing so, presumably due to a combination of their size and deformability. Therefore, S C/S, I C/S and L C/S microgels showed variations in interactions with the clots due to the differences in their dimensions. When considering applicability, fibrin targeting could potentially be achieved by all three kinds of microgels. For the utilization of S C/S particles, attachment of affinity ligands may be necessary to observe interactions and

long term residence in the clots. Furthermore, S C/S microgels have the potential for utilization in targeting to internal regions of denser clots than the ones under consideration, with smaller pore sizes. Interactions of I C/S microgels may be enhanced with the conjugation of an affinity ligand on their shell, for increasing residence time for delivery, if required. Based on this study, L C/S microgels also may demonstrate potential utility for targeting with affinity ligands on their shells, with the interactions commencing at surfaces of the clots. Furthermore, the visibility to these interactions is hypothesized to be enhanced when clots of greater porosity are under consideration.

### 4.3.3 Encapsulation of +6 GFP in core/shell microgels of different sizes

In order to investigate the ability of the core/shell constructs to encapsulate relevant therapeutics, a proof of principle study was performed with positively charged green fluorescent protein (GFP). GFP is a well characterized protein and has been utilized in innumerable biomedical examinations, since its discovery in 1962, by Shimomura et al.[32] GFP has a molecular weight of ~ 27 kDa and an $R_H$ of ~ 2.3 nm,[33] and it consists of 11 β-strands that form a hollow cylinder. This cylinder has an α-helix along its axis, containing the chromophore, *p*-hydroxybenzylideneimidazolinone.[34,35] This chromophore is formed by residues 65-67.[36,37]

A range of anionic and cationic supercharged variants of GFP have been developed by Lawrence et al. by carrying out mutations at surface-exposed residues.[38] These were developed primarily as potent delivery vehicles for functional macromolecules, into the cytoplasm of cells.[25,39] In the current study, one of these variants, +6 GFP, was produced using genetically modified *E.coli* and utilized for

encapsulation studies in S C/S, I C/S and L C/S microgels. A positively charged variant was selected in order to provide an insight into the involvement of electrostatic interactions between the loaded protein and anionic microgels. Microgels were equilibrated in buffers of low and high ionic strengths containing +6 GFP, in order to facilitate encapsulation. The fluorescence values of supernatant solutions were analyzed following centrifugation. The results obtained are presented in Figure 4.4.

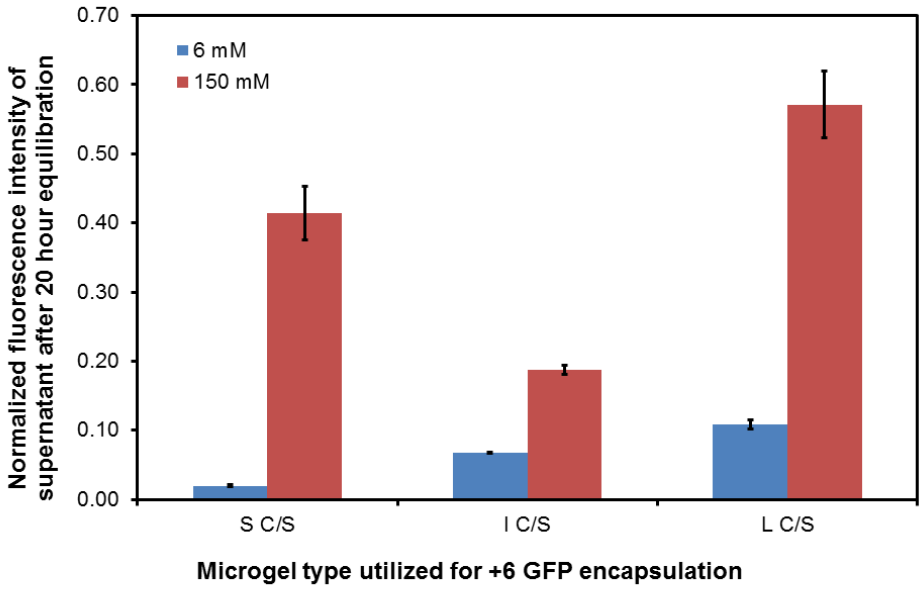


**Figure 4.4.** Analysis of encapsulation of +6 GFP by S C/C, I C/S and L C/S microgels. Fluorescence intensities of supernatants were normalized to those of +6 GFP solutions in the respective buffers. Charge screening at higher ionic strength was found to be effective in causing differences in encapsulation *(Values presented as averages of 3 measurements on single samples, error bars represent standard deviations in these three values)*

Fluorescence analysis revealed low concentration of +6 GFP in the supernatant of microgel solutions incubated with low ionic strength (6 mM) buffer. This indicated high

encapsulation efficiency. In comparison, in the presence of a buffer of greater ionic strength (150 mM), a large amount of +6 GFP was observed to be left over in supernatant, indicating a lower amount of effective encapsulation. This difference may be attributed to greater screening of charges in the presence of a high salt concentration, thus effectively decreasing the electrostatic interactions between the positively charged protein and negatively charged microgels. The same trend was observed for S C/S, I C/S and L C/S microgels. These findings led us to a few different conclusions. Firstly, the size of +6 GFP (~ 27 kDa) is in a range that allows passage into microgels with the crosslinking density used in these experiments. Encapsulation experiments with cytochrome C have been performed earlier, using microgels with carboxylic acid groups distributed throughout their network, with the same crosslinking density as the microgels under consideration.[40] However, the concentration of cytochrome C utilized for encapsulation was higher and the protein is slightly smaller than +6 GFP.[41] Thus, encapsulation of other proteins with dimensions similar to +6 GFP into microgels may be feasible. Secondly, charge interactions play an important role in this encapsulation.

This proof of principle study provided information that can be helpful in developing effective methods for loading of therapeutics and implementing techniques of triggered release of the cargo through a change in the pH environment of the microgels.

### 4.3.4 Clot disruption using microgels conjugated to fibrin-specific peptides

Fibrinogen is converted to the insoluble polymer fibrin thorough the action of thrombin. During this process, the fibrinopeptides in the center of the molecule are cleaved by the proteolytic action of thrombin, leading to the generation of ‘free’ knobs A

and B, which specifically interact with the holes a and b, present at the ends of the molecules. A cascade of linear and lateral arrangements leads to the eventual formation of fibrin.[1] Even following polymerization, though, exposed holes a and b are present in the fibrin structure. Their presence and the specific A:a and B:a knob:hole interactions have been exploited in this study.

Fibrin specificity was imparted to microgels by conjugating peptide mimics of knobs A and B with amino acid sequences GPRPFPAC (GPRP) and AHRPYAAC (AHRP) respectively. These sequences have been studied for their fibrin specificity in the past.[42] The conjugation was performed in a two step process, with the first involving carbodiimide coupling of a heterobifunctional, maleimide containing crosslinker to the microgels. This was followed by attaching the peptides to the microgels by thiol-maleimide coupling, through the cysteines on the peptides. The purified microgel-peptide conjugates were then used in a flow study set up similar to the one represented in scheme 4.1.

The flow studies were performed using fibrin clots made at a concentration of 2 mg/mL fibrinogen and 1 U/mL thrombin. Prior to administering flow of microgel-peptide conjugates through the clots, permeability studies were conducted on the clots to ensure homogeneity. The Darcy constants for trials 1 and 2 represented in Figure 4.5 were found to be $(6.3 \pm 0.18)\times10^{-13}$ $m^2$ and $(8.17 \pm 0.30)\times10^{-13}$ $m^2$ respectively. Following this, the buffer solutions in the reservoirs was replaced with controls and microgel-dye conjugates, namely solutions of L C/S, L C/S-GPRP, L C/S-GPSP and L C/S-AHRP, at 0.1 mg/mL concentrations. The clots were allowed to equilibrate for 10 minutes, following which

flow rates of microgel solutions through the clots were measured. The results of these measurements are presented in Figure 4.5.

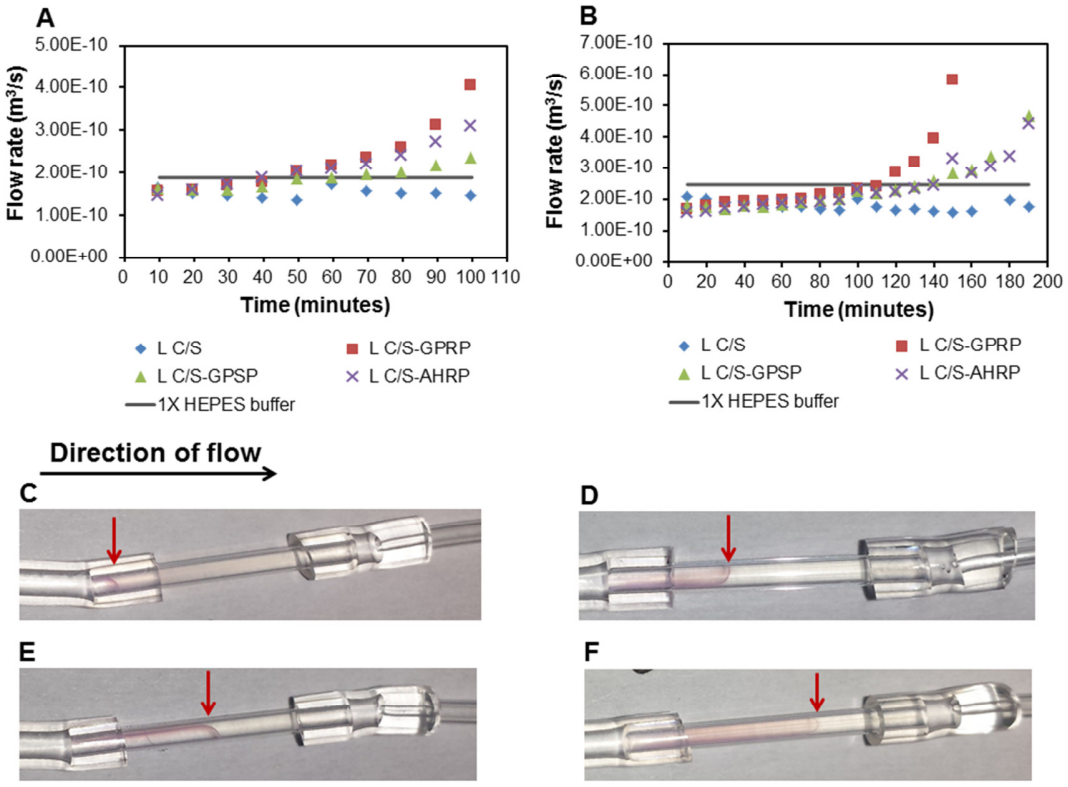


**Figure 4.5.** Trial 1 (A) and trial 2 (B) for flow rate measurements of microgel solutions (0.1 mg/mL) following passage through fibrin clots formed at 2 mg/mL fibrinogen and 1 U/mL thrombin concentrations. Grey lines indicate flow rate of HEPES buffer through the fibrin clots. Pictures of clots after passage of L C/S (C), L C/S-GPSP (D), L C/S-AHRP (E) and L C/S-GPRP (F) solutions for 100 minutes, taken during trial 1. Red arrows indicate extent of microgel passage through clots, bringing about partial (D, E) or complete (F) clot disruption. The pictures are in agreement with corresponding flow rates (A). L C/S-GPRP microgels are seen to be effective in causing complete clot disruption in the time frame of the experiment

Flow rate measurements over time and pictures of clots taken revealed an initial gradual increase in flow rate of solution, followed by the complete disruption of fibrin clots by L C/S-GPRP microgels, over the course of the experiment (Figure 4.5 A, B, F). The commencement of disruption may be assigned at the time point where the increase in flow rate is appreciably higher than that of passage of HEPES buffer through the fibrin clot. Beyond this point, there is a dramatic increase in flow rate. This can be explained in the following manner. It has been assumed, for a long time, that fibrin clot formation is irreversible and that clot disruption can occur only in the presence of the active enzyme plasmin or under non-physiological conditions. The presence of GPRP during polymerization, has been known to inhibit polymer formation through competition with the knobs A for interactions with the complementary holes.[42] However, after clot formation, the effect of GPRP on fibrin has only been studied briefly. In 2012, Chernysh et al. conducted experiments using fluorescence recovery after photobleaching (FRAP), to demonstrate that fibrin clots behave as equilibrium polymers.[22] They observed that bleached regions of clots regained fluorescence in ~ 2 seconds, and thus they hypothesized that fibrin monomers and/or oligomers dissociate and associate with the fibers, behaving as a dynamic system, as opposed to one that is irreversible. Passage of solutions of GPRP though the clot was seen to cause the formation of free fiber ends and at high enough concentrations of GPRP (0.1 mM), the fibrin was seen to dissolve. Bale et al. had similarly observed a decrease in storage moduli of the fibrin clots when 5.8 mM GPRP solution was diffused into them, eventually leading to clot liquefaction after two days.[43] It is worthwhile to note that the clots utilized in both these studies were formed under different conditions and changes in fibrinogen and thrombin concentrations are

known to affect properties of resulting fibrin clots.[28,30] Nevertheless, the dissolution of the clots observed in the experiments presented in this chapter, can be explained by the occurrence of similar phenomena. The presence of deformable microgels with multivalent display of peptides presumably increases the probability of adjacent, dissociated junctions being simultaneously occupied by GPRP moieties on the microgels, leading to an enhanced effect of the phenomena observed by Chernysh et al. and Bale et al. Based on the theoretical moles of AAc, assuming 100% efficiency of peptide conjugation, the upper limit of GPRP concentration in a 0.1 mg/mL microgel-peptide conjugate solution is in the micromolar range, which is at least two orders of magnitude below the free GPRP concentrations used by the aforementioned groups. Additionally, complete clot disruption is observed to take place in less than 3 hours from the beginning of the flow experiment. This further explains the importance of the role played by multivalency of the microgels. The absence of changes in flow rate when solutions of L C/S microgels were utilized is evidence that peptide interactions with the fibrin clot are responsible for the dissolution. There are differences in the time taken for disruption, seen in the two trials represented in Figure 4.5. These may be explained on the basis of the sensitivity of this technique to small variations in clot permeabilities. Also, L C/S-AHRP and L C/S-GPSP microgels are also seen to increase flow rate of solution through the clots, indicating partial clot dissolution (Figure 4.5 E, D respectively). Complete dissolution was not observed in both these cases within the time period of the experiment and additional experiments need to be conducted in order to study the phenomenon in detail over a longer time frame. However, partial dissolution may be explained in the following manner. Firstly, AHRP is known to be a peptide that interacts with the holes b

in fibrin. As Bale et al. noted, if a knob B-specific peptide disrupts B:b interactions, the disruptions are not effective enough to cause large changes in clot moduli. Additionally, AHRP is known to have a lower binding affinity to fibrin than GPRP.[42,44] These may therefore be contributing factors towards partial or slower clot dissolution. The GPSP peptide may be causing partial dissolution due to the similarity in its sequence to GPRP. It may not, thus, be a 'control' with null interactions with the clots.

The experiments conducted, thus indicate the potential of microgel-peptide conjugates to be used as fibrinolytic agents themselves. This is very promising because the presence of peptides on their surface can ensure selective, quick lytic action, only on thrombi. Additionally, the encapsulation of a secondary therapeutic in the cores of the microgels can be employed. This could be a thrombolytic agent such as tPA. More complex systems could include encapsulation of a fibrin-specific imaging agent to be delivered at the site, for enhanced efficacy.

## 4.4 Conclusion

We have developed core/shell microgels in three different size ranges, to be used as fibrinolytic agents. The incorporation of carboxylic acid groups in the shells of these particles was qualitatively assessed through an analysis of their pH responsivity at two different ionic strengths. Following this, flow studies were conducted, which revealed differential residence of microgels in the fibrin clots, depending on the differences between their size and clot porosity. A proof of principle encapsulation study was performed using +6 GFP, in order to demonstrate the involvement of electrostatic interactions in loading therapeutics within microgels. Finally, we demonstrated that

conjugation of knob A peptide mimics to the L C/S microgels generated constructs capable of disrupting fibrin clots through competition with the knobs A on fibrin monomers. This competition was for intermolecular interactions with the holes a, generated during equilibrium dissociation and association of monomers and/or oligomers. The multivalent display of GPRP peptides on microgels likely plays an important role in this disruption, through increasing the probability of the presence of GPRP in the vicinity of multiple adjacent A:a sites, leading to a faster rate of clot dissolution, at a lower overall concentration of peptide in the dispersion, in comparison to previous studies. These constructs thus have the ability to target and dissolve fibrin clots. Moreover, they also have the capability of being loaded with relevant imaging agents for visualization of fibrin clots, or with supplemental thrombolytic agents, with possible pH triggered targeted release at the site of the clots, to facilitate an even faster rate of fibrinolysis.

## 4.5 References

(1) Weisel, J. W.: Fibrinogen and fibrin. *Adv.Protein Chem.* **2005**, *70*, 247-+.

(2) Marler, J. R.; Brott, T.; Broderick, J.; Kothari, R.; Odonoghue, M.; Barsan, W.; Tomsick, T.; Spilker, J.; Miller, R.; Sauerbeck, L.; Jarrell, J.; Kelly, J.; Perkins, T.; McDonald, T.; Rorick, M.; Hickey, C.; Armitage, J.; Perry, C.; Thalinger, K.; Rhude, R.; Schill, J.; Becker, P. S.; Heath, R. S.; Adams, D.; Reed, R.; Klei, M.; Hughes, S.; Anthony, J.; Baudendistel, D.; Zadicoff, C.; Rymer, M.; Bettinger, I.; Laubinger, P.; Schmerler, M.; Meirose, G.; Lyden, P.; Rapp, K.; Babcock, T.; Daum, P.; Persona, D.; Brody, M.; Jackson, C.; Lewis, S.; Liss, J.; Mahdavi, Z.; Rothrock, J.; Tom, T.; Zweifler, R.; Dunford, J.; Zivin, J.; Kobayashi, R.; Kunin, J.; Licht, J.; Rowen, R.; Stein, D.; Grisolia, J.; Martin, F.; Chaplin, E.; Kaplitz, N.; Nelson, J.; Neuren, A.; Silver, D.; Chippendale, T.; Diamond, E.; Lobatz, M.; Murphy, D.; Rosenberg, D.; Ruel, T.; Sadoff, M.; Schim, J.; Schleimer, J.; Atkinson, R.; Wentworth, D.; Cummings, R.; Frink, R.; Heublein, P.; Grotta, J. C.; Degraba, T.; Fisher, M.; Ramirez, A.; Hanson, S.; Morgenstern, L.; Sills, C.; Pasteur, W.; Yatsu, F.; Andrews, K.; Villarcordova, C.; Pepe,

P.; Bratina, P.; Greenberg, L.; Rozek, S.; Simmons, K.; Kwiatkowski, T. G.; Horowitz, S. H.; Libman, R.; Kanner, R.; Silverman, R.; Lamantia, J.; Mealie, C.; Duarte, R.: Tissue-plasminogen activator for acute ischemic stroke. *N. Engl. J. Med.* **1995**, *333*, 1581-1587.

(3) Wang, M. Q.; Zhang, J. X.; Yuan, Z. M.; Yang, W. Z.; Wu, Q.; Gu, H. C.: Targeted Thrombolysis by Using of Magnetic Mesoporous Silica Nanoparticles. *J. Biomed. Nanotechnol.* **2012**, *8*, 624-632.

(4) McCarthy, J. R.; Sazonova, I. Y.; Erdem, S. S.; Hara, T.; Thompson, B. D.; Patel, P.; Botnaru, I.; Lin, C. P.; Reed, G. L.; Weissleder, R.; Jaffer, F. A.: Multifunctional nanoagent for thrombus-targeted fibrinolytic therapy. *Nanomedicine* **2012**, *7*, 1017-1028.

(5) Absar, S.; Nahar, K.; Kwon, Y. M.; Ahsan, F.: Thrombus-Targeted Nanocarrier Attenuates Bleeding Complications Associated with Conventional Thrombolytic Therapy. *Pharm. Res.* **2013**, *30*, 1663-1676.

(6) Dickerson, E. B.; Blackburn, W. H.; Smith, M. H.; Kapa, L. B.; Lyon, L. A.; McDonald, J. F.: Chemosensitization of cancer cells by siRNA using targeted nanogel delivery. *BMC Cancer* **2010**, *10*.

(7) Cook, M. T.; Schmidt, S. A.; Lee, E.; Samprasit, W.; Opanasopit, P.; Khutoryanskiy, V. V.: Synthesis of mucoadhesive thiol-bearing microgels from 2-(acetylthio)ethylacrylate and 2-hydroxyethylmethacrylate: novel drug delivery systems for chemotherapeutic agents to the bladder. *J. Mater. Chem. B* **2015**, *3*, 6599-6604.

(8) Wang, Z.; Li, Y.; Chen, L.; Xin, X.; Yuan, Q.: A Study of Controlled Uptake and Release of Anthocyanins by Oxidized Starch Microgels. *J. Agric. Food Chem.* **2013**, *61*, 5880-5887.

(9) Wang, D.; Liu, T.; Yin, J.; Liu, S.: Stimuli-Responsive Fluorescent Poly(N-isopropylacrylamide) Microgels Labeled with Phenylboronic Acid Moieties as Multifunctional Ratiometric Probes for Glucose and Temperatures. *Macromolecules (Washington, DC, U. S.)* **2011**, *44*, 2282-2290.

(10) Pinaud, F.; Millereux, R.; Vialar-Trarieux, P.; Catargi, B.; Pinet, S.; Gosse, I.; Sojic, N.; Ravaine, V.: Differential Photoluminescent and Electrochemiluminescent Behavior for Resonance Energy Transfer Processes in Thermoresponsive Microgels. *J. Phys. Chem. B* **2015**, *119*, 12954-12961.

(11) Zuo, Y.; Guo, N.; Jiao, Z.; Song, P.; Liu, X.; Wang, R.; Xiong, Y.: Novel reversible thermoresponsive nanogel based on poly(ionic liquid)s prepared via RAFT crosslinking copolymerization. *J. Polym. Sci., Part A: Polym. Chem.* **2015**, Ahead of Print.

(12) Jones, C. D.; Lyon, L. A.: Synthesis and characterization of multiresponsive core-shell microgels. *Macromolecules* **2000**, *33*, 8301-8306.

(13) Blackburn, W. H.; Lyon, L. A.: Size-controlled synthesis of monodisperse core/shell nanogels. *Colloid and Polymer Science* **2008**, *286*, 563-569.

(14) Schachschal, S.; Balaceanu, A.; Melian, C.; Demco, D. E.; Eckert, T.; Richtering, W.; Pich, A.: Polyampholyte Microgels with Anionic Core and Cationic Shell. *Macromolecules* **2010**, *43*, 4331-4339.

(15) Sahiner, N.; Alb, A. M.; Graves, R.; Mandal, T.; McPherson, G. L.; Reed, W. F.; John, V. T.: Core–shell nanohydrogel structures as tunable delivery systems. *Polymer* **2007**, *48*, 704-711.

(16) Blackburn, W. H.; Dickerson, E. B.; Smith, M. H.; McDonald, J. F.; Lyon, L. A.: Peptide-Functionalized Nanogels for Targeted siRNA Delivery. *Bioconjugate Chem.* **2009**, *20*, 960-968.

(17) Kimberly C. Clarke, A. M. D., Ashley C. Brown, Thomas H. Barker, L. Andrew Lyon: Colloid-matrix assemblies in regenerative medicine.

(18) Valentine, M. T.; Perlman, Z. E.; Gardel, M. L.; Shin, J. H.; Matsudaira, P.; Mitchison, T. J.; Weitz, D. A.: Colloid surface chemistry critically affects multiple particle tracking measurements of biomaterials. *Biophys J* **2004**, *86*, 4004-14.

(19) Spero, R. C.; Sircar, R. K.; Schubert, R.; Taylor, R. M.; Wolberg, A. S.; Superfine, R.: Nanoparticle Diffusion Measures Bulk Clot Permeability. *Biophys. J.* **2011**, *101*, 943-950.

(20) Pan, D.; Pramanik, M.; Senpan, A.; Yang, X.; Song, K. H.; Scott, M. J.; Zhang, H.; Gaffney, P. J.; Wickline, S. A.; Wang, L. V.; Lanza, G. M.: Molecular Photoacoustic Tomography with Colloidal Nanobeacons. *Angew. Chem., Int. Ed.* **2009**, *48*, 4170-4173, S4170/1-S4170/9.

(21) Pan, D.; Senpan, A.; Caruthers, S. D.; Williams, T. A.; Scott, M. J.; Gaffney, P. J.; Wickline, S. A.; Lanza, G. M.: Sensitive and efficient detection of thrombus with fibrin-specific manganese nanocolloids. *Chem. Commun. (Cambridge, U. K.)* **2009**, 3234-3236.

(22) Chernysh, I. N.; Nagaswami, C.; Purohit, P. K.; Weisel, J. W.: Fibrin Clots Are Equilibrium Polymers That Can Be Remodeled Without Proteolytic Digestion. *Sci Rep* **2012**, *2*.

(23) Walker, J. M.; Zaleski, J. M.: Non-Enzymatic Remodeling of Fibrin Biopolymers via Photothermally Triggered Radical-Generating Nanoparticles. *Chemistry of Materials* **2014**, *26*, 5120-5130.

(24) Gan, D. J.; Lyon, L. A.: Tunable swelling kinetics in core-shell hydrogel nanoparticles. *J. Am. Chem. Soc.* **2001**, *123*, 7511-7517.

(25) Cronican, J. J.; Thompson, D. B.; Beier, K. T.; McNaughton, B. R.; Cepko, C. L.; Liu, D. R.: Potent Delivery of Functional Proteins into Mammalian Cells in Vitro and in Vivo Using a Supercharged Protein. *Acs Chemical Biology* **2010**, *5*, 747-752.

(26) McPhee, W.; Tam, K. C.; Pelton, R.: Poly(n-isopropylacrylamide) latices prepared with sodium dodecyl-sulfate. *J. Colloid Interface Sci.* **1993**, *156*, 24-30.

(27) Brown, A. C.; Stabenfeldt, S. E.; Ahn, B.; Hannan, R. T.; Dhada, K. S.; Herman, E. S.; Stefanelli, V.; Guzzetta, N.; Alexeev, A.; Lam, W. A.; Lyon, L. A.; Barker, T. H.: Ultrasoft microgels displaying emergent platelet-like behaviours. *Nat. Mater.* **2014**, *13*, 1108-1114.

(28) Ryan, E. A.; Mockros, L. F.; Weisel, J. W.; Lorand, L.: Structural origins of fibrin clot rheology. *Biophys. J.* **1999**, *77*, 2813-2826.

(29) Bateman, R.; Leong, H.; Podor, T.; Hodgson, K.; Kareco, T.; Walley, K.: The effect of thrombin concentration on fibrin clot structure imaged by multiphoton microscopy and quantified by fractal analysis. *Microscopy and Microanalysis* **2005**, *11*, 1018-1019.

(30) Duong, H.; Wu, B.; Tawil, B.: Modulation of 3D Fibrin Matrix Stiffness by Intrinsic Fibrinogen-Thrombin Compositions and by Extrinsic Cellular Activity. *Tissue Eng. Part A* **2009**, *15*, 1865-1876.

(31) Kim, O. V.; Xu, Z. L.; Rosen, E. D.; Alber, M. S.: Fibrin Networks Regulate Protein Transport during Thrombus Development. *PLoS Comput. Biol.* **2013**, *9*.

(32) Shimomura, O.; Johnson, F. H.; Saiga, Y.: Extraction, purification and properties of aequorin, a bioluminescent protein from luminous hydromedusan, aequorea. *Journal of Cellular and Comparative Physiology* **1962**, *59*, 223-&.

(33) Hink, M. A.; Griep, R. A.; Borst, J. W.; van Hoek, A.; Eppink, M. H. M.; Schots, A.; Visser, A.: Structural dynamics of green fluorescent protein alone and fused with a single chain Fv protein. *J. Biol. Chem.* **2000**, *275*, 17556-17560.

(34) Tsien, R. Y.: The green fluorescent protein. *Annu. Rev. Biochem.* **1998**, *67*, 509-544.

(35) Ormo, M.; Cubitt, A. B.; Kallio, K.; Gross, L. A.; Tsien, R. Y.; Remington, S. J.: Crystal structure of the Aequorea victoria green fluorescent protein. *Science* **1996**, *273*, 1392-1395.

(36) Prasher, D. C.; Eckenrode, V. K.; Ward, W. W.; Prendergast, F. G.; Cormier, M. J.: Primary structure of the aequorea-victoria green-fluorescent protein. *Gene* **1992**, *111*, 229-233.

(37) Cody, C. W.; Prasher, D. C.; Westler, W. M.; Prendergast, F. G.; Ward, W. W.: Chemical-structure of the hexapeptide chromophore of the aequorea green-fluorescent protein. *Biochemistry* **1993**, *32*, 1212-1218.

(38) Lawrence, M. S.; Phillips, K. J.; Liu, D. R.: Supercharging proteins can impart unusual resilience. *J. Am. Chem. Soc.* **2007**, *129*, 10110-+.

(39) McNaughton, B. R.; Cronican, J. J.; Thompson, D. B.; Liu, D. R.: Mammalian cell penetration, siRNA transfection, and DNA transfection by supercharged proteins. *Proc. Natl. Acad. Sci. U. S. A.* **2009**, *106*, 6111-6116.

(40) Smith, M. H.; Lyon, L. A.: Tunable Encapsulation of Proteins within Charged Microgels. *Macromolecules* **2011**, *44*, 8154-8160.

(41) Dumetz, A. C.; Snellinger-O'Brien, A. M.; Kaler, E. W.; Lenhoff, A. M.: Patterns of protein - protein interactions in salt solutions and implications for protein crystallization. *Protein Sci.* **2007**, *16*, 1867-1877.

(42) Laudano, A. P.; Doolittle, R. F.: Studies on synthetic peptides that bind to fibrinogen and prevent fibrin polymerization - structural requirements, number of binding-sites, and species-differences. *Biochemistry* **1980**, *19*, 1013-1019.

(43) Bale, M. D.; Muller, M. F.; Ferry, J. D.: Effects of fibrinogen-binding tetrapeptides on mechanical-properties of fine fibrin clots. *Proc. Natl. Acad. Sci. U. S. A.* **1985**, *82*, 1410-1413.

(44) Stabenfeldt, S. E.; Gossett, J. J.; Barker, T. H.: Building better fibrin knob mimics: an investigation of synthetic fibrin knob peptide structures in solution and their dynamic binding with fibrinogen/fibrin holes. *Blood* **2010**, *116*, 1352-1359.

# CHAPTER 5

# OUTLOOK AND FUTURE DIRECTIONS

## 5.1 Development of cationic microgels for dye conjugation and high intensity photoacoustic signal generation

Chapter 2 focused on the development of functional cationic microgels of different sizes and degrees of functionality, for utilization in conjugation reactions. The generation of similar, stable colloidal systems in a reproducible manner has been difficult in the past,[1,2] and hence detailed characterization of these constructs was very important. Therefore, we conducted studies that generated data regarding the efficiency of incorporation of amine groups within microgel matrices during synthesis. Chapter 3 dealt with the development and thorough characterization of one model cationic, amine functionalized microgel system, which was further used for the conjugation of two different dyes with potential applications in photoacoustic imaging.

Microgel-dye conjugates are extremely promising systems for the development of high intensity photoacoustic signals. This is because, through conjugation of multiple dye molecules within the polymer network, microgels can increase the local concentration of contrast agents, while their overall concentration in solution remains low. A point source such as a laser can thus theoretically irradiate a single particle and generate signal equivalent to that obtained from a much higher solution concentration of the contrast agent. This is particularly important when considering that dyes like malachite green and rose bengal, though extremely suitable for photoacoustics, are toxic to cells at higher concentrations due to their ability to generate reactive oxygen species in solution.[3-5]

Therefore, any system that eliminates the need to use such dyes at toxic levels would be advantageous and deserving of further development. However, currently, the photoacoustic signals obtained from this system were not reliable due to interference from the background. Hence, a crucial step to be taken before making changes in the structure or properties of the microgel constructs, would be the generation of reproducible signals, through optimization of the current signal generation system. Once this is accomplished, generation of photoacoustic signals from single microgels will be more straightforward and following this, optimization of conditions, with the use of laser power below the maximum permissible exposure (MPE, which depends on the wavelength of the laser and time of exposure) can be achieved. For rose bengal, utilization of a secondary laser for improving signal intensity via modulation can also be done.[6] Furthermore, dyes that are more biofriendly can be utilized.

When considering further development of the microgel construct, an important step forward could involve the introduction of degradable crosslinkers within microgel matrices. The versatility of microgel syntheses provides several opportunities for this, as has been demonstrated by the development of a number of degradable microgel constructs in the past. The degradation could be triggered by the microgel environment and it could be a slower, controlled process or it could occur almost instantaneously as an immediate response to a stimulus.[7-10] This could potentially generate constructs that can be cleared from the body following imaging. However, in order to ensure their survival until their purpose is served, preliminary investigations can involve the analysis of changes in photoacoustic signals generated over time and changes induced during

degradation. The degradability of the eventual construct may thus need to be tuned, with the use of multiple crosslinkers, for this balance to be achieved.

Photoacoustic imaging is a promising technique that has the capability to generate high resolution images of pathological abnormalities located several centimeters below the surface of the skin. However, when introducing imaging agents such as the microgel-dye conjugates under consideration into biological systems, very often, they are cleared by the immune system before they reach the relevant region of the body.[11] A future step could thus involve the development of microgels entirely synthesized from a polymer like poly(ethyleneglycol) (PEG). PEG has been demonstrated to be biocompatible and recently, the development of PEG-based microgels and their characterization has gained increasing interest.[12-15] Comonomers containing functional groups can also be introduced in such microgels and thus, dye conjugations to PEG-based microgels can also be carried out. Similarly, degradable crosslinkers may also be introduced in the polymer matrices of these microgels for reasons similar to those mentioned above.

Additionally, microgels provide the capability to introduce specific targeting moieties on them, through covalent conjugations. Therefore, another interesting avenue to explore would involve the development of particles conjugated to dye and targeting moieties in the optimum ratios. The two species could also be localized in spatially distinct regions of the microgels, by using microgels with suitably segregated regions.[16] Such constructs can be utilized for dual functionality in the form of targeting and imaging. This targeting can be to utilized for carrying out imaging of tumors, early detection of specific molecular markers,[17-20] or for investigations of other abnormalities.[21]

Thus, cationic microgel constructs for utilization in conjugation reactions have tremendous promise. The 'toolbox' of such particles described in Chapter 2 provides the opportunity to select suitable microgels for conjugation, with a preliminary analysis of the availability of their functional groups for dye conjugations provided in Chapter 3. A number of arenas can be explored by modifying these constructs, as described above, for executing well-controlled conjugations and generating multifunctional constructs.

### 5.2 Microgels conjugated to fibrin-specific peptides as agents of thrombolysis

Chapter 4 looked at the development of core/shell microgels in three different size ranges, with carboxylic acid groups in their shells, for utilization as agents of thrombolysis. These microgels demonstrated differences in their interactions with fibrin clots as observed through perfusion experiments of microgel solutions through fibrin clots. These diverse interactions were a result of the differences between microgel dimensions and clot porosities. A proof of principle encapsulation study with +6 GFP showed that electrostatic interactions were involved in loading into these anionic microgels, demonstrating that they have the potential to be used in release of loaded cargo triggered by a change in pH or ionic strength. Microgels conjugated to the GPRP peptide, which is known to have strong interactions with fibrin, were found to successfully disrupt fibrin clots. It was hypothesized that they were able to do this merely through multiple simultaneous peptide-clot interactions, by taking advantage of the equilibrium nature of fibrin clots[22,23] and competing with momentarily dissociated sites, otherwise involved in fiber formation.

The implications of these results are manifold and yet, a number of studies remain to be done, first in order to understand the intricacies of the processes involved in clot disruption and second, to utilize and optimize this system for temporally controlled and well understood outcomes.

While a basic understanding of the processes involved in remodeling of fibrin clots post polymerization is available,[22,23] and it has been explored to some extent,[24] the studies that have been performed are limited. Additionally, this is the first example of systems like microgels that are able to disrupt clots at a faster rate than systems investigated before, chiefly due to their multivalency, and without the aid of additional agents. This makes it more important to study the role of peptide density, microgel deformability and the relationship between clot porosity, microgel dimensions and the rate of clot dissolution. In order to understand these processes in greater detail, the utilization of computational modeling may prove to be extremely beneficial. This is because it may provide an insight into the kinetics of the interactions and the probability of adjacent knob:hole interactions being disrupted with the peptides on microgels simultaneously interfering with them. Thus, information about distance required between surface presented peptides and the role of microgel surface area, can also be obtained.

In order to fully understand the processes involved in clot disruption by microgels, visualization of the process will be necessary. An experimental setup that utilizes microfluidics combined with confocal imaging can provide details about microgel-clot interactions. For a better understanding, fluorophores such as 5-iodoacetamidofluorescein (5-IAF) may be attached to the peptides for better visualization of interactions. These experiments would need be performed cautiously though, because

the molecular weight of the peptide moieties may be greatly affected by such conjugations and studies using such systems may need to operate under the assumption that peptide-fibrin interactions are not influenced by conjugation of such large moieties to the primary peptide. A setup with fluorescent peptides on microgels can also be subjected to fluorescence recovery after photobleaching (FRAP) experiments, similar to those performed by Chernysh et al.[22] This may provide further insight into the rate of association and dissociation of monomers and oligomers, and the role played by specific spatial organization of microgel-conjugated peptides in the vicinity of these processes.

A large number of flow experiments also remain to be performed for a better understanding of these interactions. An important experiment will involve the utilization of small core/shell (S C/S) microgels in denser clots and examining possible clot degradation. If surface areas of the microgels that present peptides, play a vital role, huge differences may be visible between the types of clots degraded and rates of clot degradation (if observed) acquired when using S C/S microgels vs. the large particles utilized in the experiments in Chapter 4. Furthermore, differences in peptide densities on particles surfaces may also play a crucial role in determining the role of microgel surface area in these phenomena. Lastly, when considering such variations, the importance of microgel deformability through changes in crosslinker contents and the utilization of conventional microgels with functionalities throughout their matrix, may provide important information about microgel movement through clots and the necessity of surface localization of the peptides.

An important factor that has not been investigated in the current experiments is the effect of covalent ligation of fibers with factor XIIIa (activated form of factor XIII).[25]

Experiments that have been conducted by other groups, demonstrating fibrin remodeling have been performed on non-ligated clots. It has been observed that covalent ligation, in essence, causes the clot formation to become irreversible and thus no fiber dissociation or clot dissolution has been observed for such clots. When considering the clots utilized in the experiments presented in Chapter 4, the fibrinogen used contained ~ 8 Loewy units of factor XIII per mg (Enzyme Research Laboratories). In comparison to the physiological concentration of factor XIII in plasma, (~ 100 Loewy units/mL),[26] this is at least an order of magnitude lower. Therefore, an interesting experiment would involve the introduction of factor XIII at physiological concentrations in flow experiments similar to those described in Chapter 4. Since microgels appear to be more efficient than free peptide, in clot disruption, they may be able to disrupt clots that have been covalently ligated. Perhaps their multivalency can take these studies a step further and a system can be developed, that may be capable of dissolving seemingly irreversible fibrin clots. Disruption of such clots has not been demonstrated before and thus, establishing a system that could perform such complex lysis would have abundant applications in developing highly efficient fibrinolytics.

Finally, the utilization of core/shell microgels in this study opens up possibilities to encapsulate additional theranostic agents. For example, supplemental fibrinolytic agents, such as tissue-type plasminogen activator (tPA), for site-specific release and faster clot disruption may be loaded into the microgels. Alternately, agents for simultaneous imaging, such as those that have been used for visualization of fibrin clots before,[27,28] may be released at the site of clots, having been delivered to the site by targeted microgel carriers.

The development of targeted systems for delivery of thrombolytic agents has progressed due to the necessity to diminish their off-target effects. However, the microgel-peptide systems described in Chapter 4 are unique in their ability to target and disrupt clots without the use of additional fibrinolytic agents. A number of future studies need to be conducted in order to understand the complex processes involved in this clot dissolution, in detail. Therefore, several computational and experimental investigations will need to be performed, in order to understand and optimize this system for future utilization.

## 5.3 References


(1) Thaiboonrod, S.; Berkland, C.; Milani, A. H.; Ulijn, R.; Saunders, B. R.: Poly(vinylamine) microgels: pH-responsive particles with high primary amine contents. *Soft Matter* **2013**, *9*, 3920-3930.

(2) Farley, R.; Saunders, B. R.: A general method for functionalisation of microgel particles with primary amines using click chemistry. *Polymer* **2014**, *55*, 471-480.

(3) Dhamgaye, S.; Devaux, F.; Manoharlal, R.; Vandeputte, P.; Shah, A. H.; Singh, A.; Blugeon, C.; Sanglard, D.; Prasad, R.: In Vitro Effect of Malachite Green on Candida albicans Involves Multiple Pathways and Transcriptional Regulators UPC2 and STP2. *Antimicrob. Agents Chemother.* **2012**, *56*, 495-506.

(4) Lambert, C.; Sarna, T.; Truscott, T. G.: Rose-bengal radicals and their reactivity. *J. Chem. Soc.-Faraday Trans.* **1990**, *86*, 3879-3882.

(5) Culp, S. J.; Beland, F. A.: Malachite green: A toxicological review. *J. Am. Coll. Toxicol.* **1996**, *15*, 219-238.

(6) Richards, C. I.; Hsiang, J. C.; Dickson, R. M.: Synchronously Amplified Fluorescence Image Recovery (SAFIRe). *J. Phys. Chem. B* **2010**, *114*, 660-665.

(7) Jo, Y. S.; Gantz, J.; Hubbell, J. A.; Lutolf, M. P.: Tailoring hydrogel degradation and drug release via neighboring amino acid controlled ester hydrolysis. *Soft Matter* **2009**, *5*, 440-446.

(8) Turturro, M. V.; Christenson, M. C.; Larson, J. C.; Young, D. A.; Brey, E. M.; Papavasiliou, G.: MMP-Sensitive PEG Diacrylate Hydrogels with Spatial Variations in Matrix Properties Stimulate Directional Vascular Sprout Formation. *Plos One* **2013**, *8*.

(9) Nayak, S.; Gan, D. J.; Serpe, M. J.; Lyon, L. A.: Hollow thermoresponsive microgels. *Small* **2005**, *1*, 416-421.

(10) South, A. B.; Lyon, L. A.: Direct Observation of Microgel Erosion via in-Liquid Atomic Force Microscopy. *Chemistry of Materials* **2010**, *22*, 3300-3306.

(11) Juliano, R. L.: Factors affecting the clearance kinetics and tissue distribution of liposomes, microspheres and emulsions. *Adv. Drug Delivery Rev.* **1988**, *2*, 31-54.

(12) Zhou, T.; Wu, W. T.; Zhou, S. Q.: Engineering oligo(ethylene glycol)-based thermosensitive microgels for drug delivery applications. *Polymer* **2010**, *51*, 3926-3933.

(13) Lutz, J. F.: Thermo-Switchable Materials Prepared Using the OEGMA-Platform. *Adv. Mater.* **2011**, *23*, 2237-2243.

(14) Chi, C. L.; Cai, T.; Hu, Z. B.: Oligo(ethylene glycol)-Based Thermoresponsive Core-Shell Microgels. *Langmuir* **2009**, *25*, 3814-3819.

(15) Pikabea, A.; Ramos, J.; Forcada, J.: Production of Cationic Nanogels with Potential Use in Controlled Drug Delivery. *Particle & Particle Systems Characterization* **2014**, *31*, 101-109.

(16) Seiffert, S.; Romanowsky, M. B.; Weitz, D. A.: Janus Microgels Produced from Functional Precursor Polymers. *Langmuir* **2010**, *26*, 14842-14847.

(17) Kumar, S.; Richards-Kortum, R.: Optical molecular imaging agents for cancer diagnostics and therapeutics. *Nanomedicine (London, U. K.)* **2006**, *1*, 23-30.

(18) Nayak, S.; Lee, H.; Chmielewski, J.; Lyon, L. A.: Folate-mediated cell targeting and cytotoxicity using thermoresponsive microgels. *J. Am. Chem. Soc.* **2004**, *126*, 10258-10259.

(19) Lu, S.; Neoh, K. G.; Huang, C.; Shi, Z.; Kang, E.-T.: Polyacrylamide hybrid nanogels for targeted cancer chemotherapy via co-delivery of gold nanoparticles and MTX. *J. Colloid Interface Sci.* **2013**, *412*, 46-55.

(20) Das, M.; Mardyani, S.; Chan, W. C. W.; Kumacheva, E.: Biofunctionalized pH-responsive microgels for cancer cell targeting: Rational design. *Adv. Mater. (Weinheim, Ger.)* **2006**, *18*, 80-83.

(21) Lanza, G. M.; Abendschein, D. R.; Hall, C. S.; Marsh, J. N.; Scott, M. J.; Scherrer, D. E.; Wickline, S. A.: Molecular imaging of stretch-induced tissue factor expression in carotid arteries with intravascular ultrasound. *Invest. Radiol.* **2000**, *35*, 227-234.

(22) Chernysh, I. N.; Nagaswami, C.; Purohit, P. K.; Weisel, J. W.: Fibrin Clots Are Equilibrium Polymers That Can Be Remodeled Without Proteolytic Digestion. *Sci Rep* **2012**, *2*.

(23) Bale, M. D.; Muller, M. F.; Ferry, J. D.: Effects of fibrinogen-binding tetrapeptides on mechanical-properties of fine fibrin clots. *Proc. Natl. Acad. Sci. U. S. A.* **1985**, *82*, 1410-1413.

(24) Walker, J. M.; Zaleski, J. M.: Non-Enzymatic Remodeling of Fibrin Biopolymers via Photothermally Triggered Radical-Generating Nanoparticles. *Chemistry of Materials* **2014**, *26*, 5120-5130.

(25) Weisel, J. W.: Fibrinogen and fibrin. *Adv.Protein Chem.* **2005**, *70*, 247-+.

(26) Mosesson, M. W.; Siebenlist, K. R.; Hernandez, I.; Lee, K. N.; Christiansen, V. J.; McKee, P. A.: Evidence that α2-antiplasmin becomes covalently ligated to plasma fibrinogen in the circulation: a new role for plasma factor XIII in fibrinolysis regulation. *Journal of thrombosis and haemostasis : JTH* **2008**, *6*, 1565-1570.

(27) Pan, D.; Pramanik, M.; Senpan, A.; Yang, X.; Song, K. H.; Scott, M. J.; Zhang, H.; Gaffney, P. J.; Wickline, S. A.; Wang, L. V.; Lanza, G. M.: Molecular Photoacoustic Tomography with Colloidal Nanobeacons. *Angew. Chem., Int. Ed.* **2009**, *48*, 4170-4173, S4170/1-S4170/9.

(28) Pan, D.; Senpan, A.; Caruthers, S. D.; Williams, T. A.; Scott, M. J.; Gaffney, P. J.; Wickline, S. A.; Lanza, G. M.: Sensitive and efficient detection of thrombus with fibrin-specific manganese nanocolloids. *Chem. Commun. (Cambridge, U. K.)* **2009**, 3234-3236.

# APPENDIX A

# THE DEVELOPMENT OF ULTRALOW CROSSLINKED MICROGELS: NEUTRAL PARTICLES (NULCs) AND SMALL PARTICLES (SULCs)

*Portions adapted from*

Bachman, H.*; Brown, A. C.*; Clarke, K. C.*; Dhada, K. S.*; Douglas, A.*; Hansen, C. E.*; Herman, E.*; Hyatt, J. S.*; Kodlekere, P.*; Meng, Z. Y.*; Saxena, S.*; Spears, M. W.*; Welsch, N.*; Lyon, L. A.: Ultrasoft, highly deformable microgels. *Soft Matter* **2015**, *11*, 2018-2028.

*Equally contributing authors

## A.1 Introduction

Traditionally, NIPAm (N-isopropylacrylamide) based microgels are synthesized in the presence of a crosslinking agent, such as N,N'-methylenebisacrylamide (BIS). Microgel crosslinking modulates individual microgel mechanical properties. Below their lower critical solution temperature (LCST), pNIPAm microgels crosslinked with 2 mol % BIS were found to have a Young's modulus of approximately 80 kPa, compared to 10 mol % BIS crosslinked particles, which were found to have a Young's modulus of approximately 500 kPa.[1] In 2003, Gao and Frisken demonstrated that ultra-low crosslinked (ULC) pNIPAm microgels could be synthesized under 'crosslinker free' conditions.[2] These particles are self-crosslinked through a chain transfer reaction at the tert-carbon sites which could occur on either the pendent isopropyl group or on the main

chain backbone. These chain transfer reactions are rare, and therefore these particles have extremely low (<0.5%) degrees of crosslinking, which appears to be core localized. Previous studies have demonstrated that size and solid density of self-crosslinked pNIPAm microgels can be finely tuned by controlling reaction temperatures, monomer and initiator concentrations.[3] Because crosslinking affects microgel mechanical properties, we hypothesized that ULC microgels would be softer and more deformable than traditionally crosslinked microgels. Microparticle elastic modulus affects numerous biological responses including in vivo dynamics, cellular uptake and extracellular matrix interactions. For example, soft microparticles resembling red blood cells in size have longer circulation times than rigid microparticles of an identical size.[4] Furthermore, hydrogel nanoparticle elasticity has been shown to influence macrophage uptake. Banquy et al. recently demonstrated that soft nanoparticles with Young's moduli of ~ 18 kPa were internalized through macropinocytosis, nanoparticles with Young's moduli between 35 and 130 kPa were internalized via clathrin and/or caveolae-mediated endocytosis, and stiff nanoparticles with Young's moduli of ~ 200 kPa were internalized through clathrin-mediated endocytosis.[5] The enhanced spreading capability of ULC particles compared to crosslinked particles is presumed to be due to an increased degree of deformability due to the exceedingly low connectivity of ULC microgels. Herein, the deformation of ULC particles is characterized by AFM analysis of spreading on glass surfaces and the ability to translocate through nanopores significantly smaller than the hydrodynamic diameter of the particles. The data presented here particularly deals with neutral ULC particles (NULCs) and small ULC particles (SULCs).

## A.2 Synthesis of NULCs and SULCs

NULCs-1 and NULCs-2 were synthesized under the exact same conditions, in a manner similar to a traditional microgel synthesis (refer to Chapter 2, section 2.2.2), with a total NIPAm concentration of 100 mM. The two syntheses were initiated using different concentrations of the anionic initiator ammonium persulfate (APS): 0.5 mM and 8 mM respectively.

SULCs-1 and SULCs-2 were synthesized in a similar manner, but with 5 mol % acrylic acid (AAc). In both these syntheses, the concentration of APS used was the same (1 mM). The concentration of surfactant sodium dodecyl sulfate (SDS) utilized was varied (0.2 mM for SULC-1 and 1 mM for SULC-2). Microgels were purified by centrifugation.

## A.3 Neutral ULCs (NULCs)

NULCs were synthesized in two different size ranges, denoted as NULCs-1 and NULCs-2, by varying initiator concentration while leaving all other synthesis conditions unaltered. NULC size was characterized via DLS, AFM and qNano analysis. AFM imaging of NULCs-1 deposited under conditions of active and passive deposition indicated that the microgels spread significantly on the glass surface, with the spreading being most pronounced under conditions of active deposition when the microgels were at sub-monolayer conditions (Figure A.1, A–D). While NULCs-2 deposited readily under packed conditions, they could not be deposited as a sub-monolayer, suggesting that microgel–microgel interactions are preferred over microgel–surface interactions. When deposited as a packed monolayer, NULCs-2 were found to have a height of 11 ± 2 nm

when deposited through passive deposition and 6 ± 1 nm when deposited through active deposition.

**Table A.1** Size characterization of NULCs

| | | **NULCs-1** | | **NULCs-2** | |
|---|---|---|---|---|---|
| **Hydrodynamic Radius (nm): DLS** | | 469 ± 29 | | 723 ± 48 | |
| | | Sub-monolayer | Packed monolayer | Sub-monolayer | Packed monolayer |
| **Diameter (μm) : AFM** | Passive deposition | 1.58 ± 0.11 | 1.23 ± 0.07 | N/A | 2.65 ± 0.24 |
| | Active deposition | 1.91 ± 0.29 | 1.06 ± 0.11 | N/A | 2.37 ± 0.13 |
| **Height (nm) : AFM** | Passive deposition | 16 ± 1 | 15 ± 2 | N/A | 11 ± 2 |
| | Active deposition | 13 ± 2 | 14 ± 3 | N/A | 6 ± 1 |

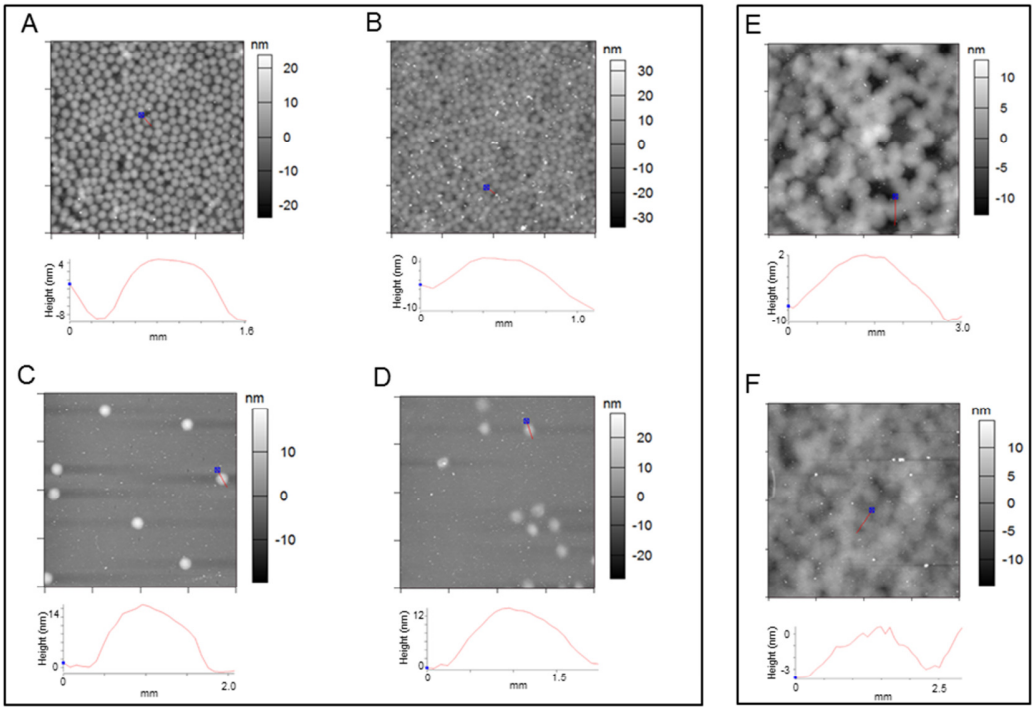


**Figure A.1.** AFM height traces of Neutral ULCs (NULCs) deposited on APTMS-functionalized glass under different conditions. (A) NULCs-1 deposited by passive deposition for 1 h from a 20 mg/mL solution. (B) NULCs-1 deposited by active deposition at 2250 × g for 30 minutes from a 0.1 mg/mL solution. (C) NULCs-1 deposited by passive deposition for 3 h from a 0.1 mg/mL solution. (D) NULCs-1 deposited by active deposition at 2250 × g for 7 minutes from a 0.1 mg/mL solution. (E) NULCs-2 deposited by passive deposition for 1 h from a 10 mg/mL solution. (F) NULCs-2 deposited by active deposition at 2250 × g for 1 minute from a 0.1 mg/mL solution. All images are 20 µm × 20 µm

Hydrodynamic radii of NULCs-1 and NULCs-2 were 469 ± 29 nm and 723 ± 48 nm, respectively, and radii determined through qNano, were 434 ± 91 nm and 348 ±153 nm, respectively. The similarities in radii measurements via DLS and qNano for NULCs-1 suggest behavior characteristic of less deformable particles. NULCs-2, however, appear

to be more deformable, and like anionic ULCs, have physical radii that are considerably smaller than their hydrodynamic radii. While the two types of NULCs behave differently due to differences in their sizes and network structures, they nevertheless demonstrate the deformability that is characteristic of ULCs, albeit to different extents.

### A.4 Small ULCs (SULCs)

In addition to their charge, the size of ULCs can also be modulated. Small ULCs (SULCs) with diameters less than a micron were obtained by performing syntheses in the presence of a surfactant. Modification of the surfactant concentration yielded SULCs of two different sizes: SULCs-1 with a hydrodynamic radius of 409 ± 18 nm and SULCs-2 with a hydrodynamic radius of 211 ± 4 nm. SULCs-1 were found to have a radius of 164 ± 22 nm through qNano analysis, however, SULCs-2 were not detectable with this method, even using the smallest pore size available for the system (~ 100 nm in diameter). We conclude that due to the small size and deformability of these particles, the smallest pore size available does not hinder translocation of SULCs-2, resulting in undetectable translocation events. AFM imaging on SULCs-1 revealed the presence of a second, minor population of particles, slightly larger than the SULCs-1 themselves (Figure A.2 A). The spreading of both SULCs-1 and SULCs-2 on a flat surface was also observed via AFM imaging, and these particles were found to have spread radii of 805 ± 105 nm and 395 ± 55 nm, respectively, and heights of 10 ± 1 nm and 3 ± 1 nm, respectively, which demonstrates the deformability of ULCs even in the size range of the SULCs.

**Table A.2** AFM image analysis of SULCs

| | SULC-1 | SULC-2 |
|---|---|---|
| **Diameter (µm) : AFM** | 1.61 ± 0.21 | 0.79 ± 0.11 |
| **Height (nm) : AFM** | 10 ± 1 | 3 ± 1 |

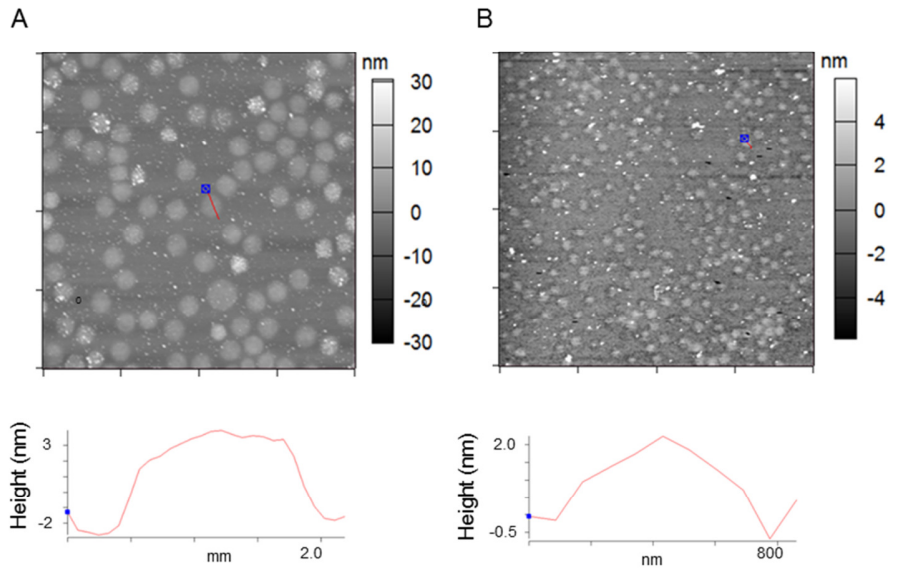


**Figure A.2**. AFM height traces of SULCs deposited on APTMS functionalized glass. (A) SULCs-1 deposited by active deposition at 2250 × g for 10 minutes from a 0.0001 mg/mL solution. (B) SULCs-2 deposited by active deposition at 2250 × g for 10 minutes from a 0.001 mg/mL solution. All images are 20 µm × 20 µm

## A.5 References

(1) Burmistrova, A.; Richter, M.; Uzum, C.; von Klitzing, R.: Effect of cross-linker density of P(NIPAM-co-AAc) microgels at solid surfaces on the swelling/shrinking behaviour and the Young's modulus. *Colloid and Polymer Science* **2011**, *289*, 613-624.

(2) Gao, J.; Frisken, B. J.: Cross-linker-free N-isopropylacrylamide gel nanospheres. *Langmuir* **2003**, *19*, 5212-5216.

(3) Gao, J.; Frisken, B. J.: Influence of reaction conditions on the synthesis of self-cross-linked N-isopropylacrylamide microgels. *Langmuir* **2003**, *19*, 5217-5222.

(4) Merkel, T. J.; Jones, S. W.; Herlihy, K. P.; Kersey, F. R.; Shields, A. R.; Napier, M.; Luft, J. C.; Wu, H. L.; Zamboni, W. C.; Wang, A. Z.; Bear, J. E.; DeSimone, J. M.: Using mechanobiological mimicry of red blood cells to extend circulation times of hydrogel microparticles. *Proc. Natl. Acad. Sci. U. S. A.* **2011**, *108*, 586-591.

(5) Banquy, X.; Suarez, F.; Argaw, A.; Rabanel, J. M.; Grutter, P.; Bouchard, J. F.; Hildgen, P.; Giasson, S.: Effect of mechanical properties of hydrogel nanoparticles on macrophage cell uptake. *Soft Matter* **2009**, *5*, 3984-3991.

# APPENDIX B

# ADDITIONAL CHARACTERIZATION OF CATIONIC MICROGELS AND MICROGEL-DYE CONJUGATES

## B.1 Synthesis and characterization of functional cationic microgel constructs

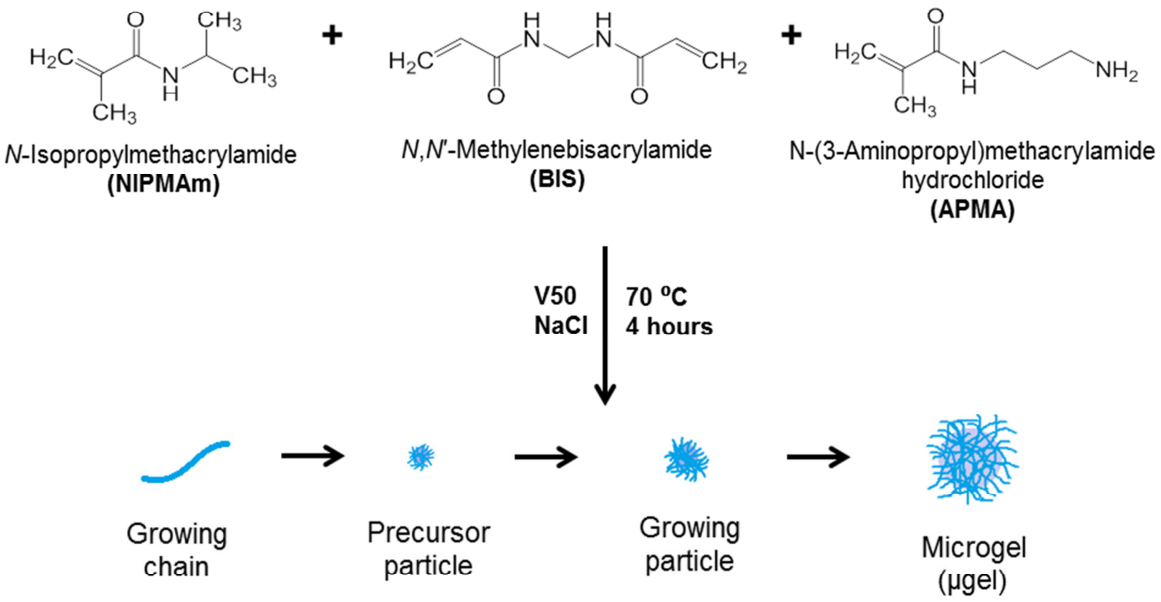


**Scheme B.1.** General representation of a one step synthesis of p(NIPMAm-co-APMA) microgels

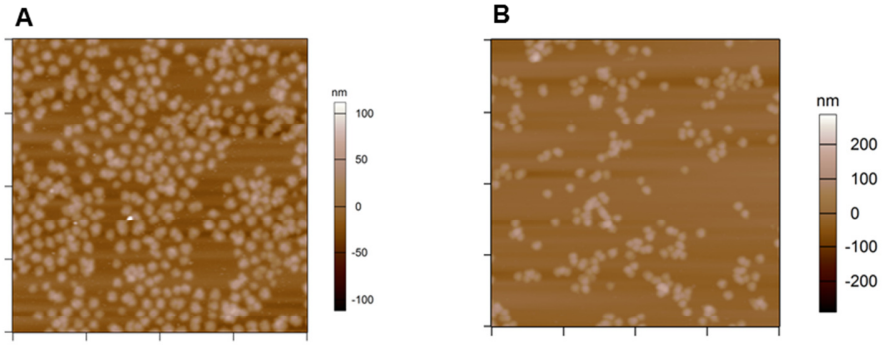


**Figure B.1.** AFM height traces of microgels synthesized with [NaCl] (A) and [APS] (B) above a threshold (specific to the synthesis conditions) leads to the formation of misshapen particles (all images are 20µm × 20µm). Microgels were deposited on APTMS-functionalized glass by centrifugal deposition at 2250 × *g* for 15 minutes at 25 $^{0}$C

## B.2 Cationic microgels crosslinked with PEG-DA

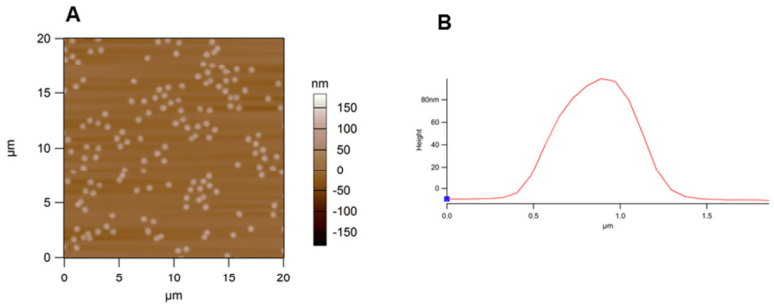


C

| | |
|---|---|
| $R_H$ (nm) at pH 5 | 412 ± 27 |
| $R_H$ (nm) at pH 7 | 404 ± 21 |
| $R_H$ (nm) at pH 9.8 | 412 ± 17 |

**Figure B.2.** AFM height trace of µgelPEG (A), representative height profile (B) and $R_H$ measured in buffers of different pH values (C). Microgels were deposited on APTMS-functionalized glass by centrifugal deposition at 2250 × *g* for 15 minutes at 25 $^{0}$C

Analysis of μgelPEG using the CBQCA assay revealed the number of moles of APMA in the analyzed solution to be $(1.97 \pm 0.04)\times10^{-8}$, with the efficiency of primary amine incorporation being 39 ± 1 %.

### B.3 pH titrations for analysis of primary amine incorporation

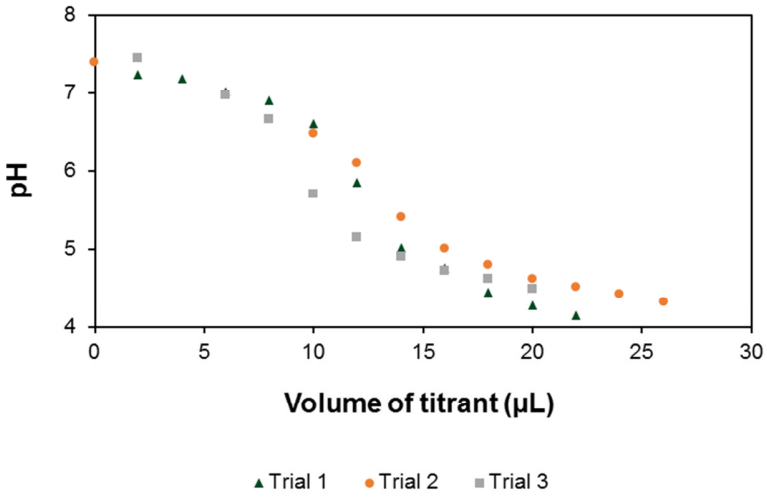


**Figure B.3.** pH titration curves of μgel2 solutions using 0.101 M HCl as a titrant for quantification of primary amine groups

pH titrations were performed using a Vernier pH Electrode and LabQuest Software (Vernier Software and Technology, LLC., Beaverton, OR). Microgels were diluted to a total concentration of 1 mg/mL in 20 mL distilled, deionized water. Titration was performed against 0.101 M HCl (standardized against 0.099 M $Na_2CO_3$) under a $N_2$ purge with stirring, at ambient temperature. Measurements of solution pH were made after 300 s equilibration following each addition of titrant.

## B.4 Conjugation of dyes to amine functionalized microgels

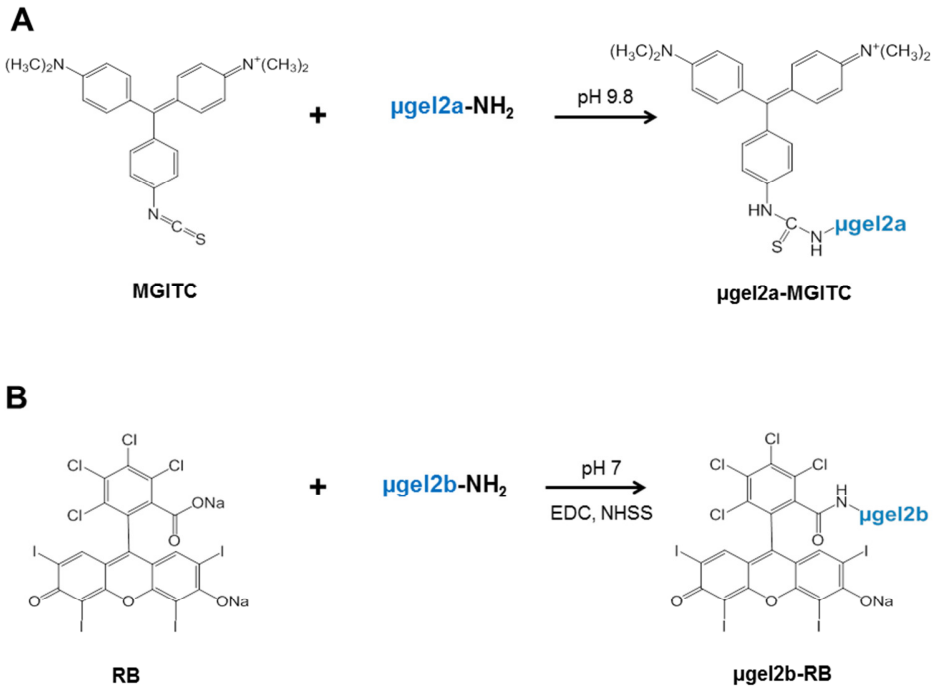


**Scheme B.2.** Conjugation reactions utilized for synthesis of µgel2a-MGITC (A) and µgel1-RB, µgel2-RB, µgel2b-RB and µgel6-RB (B) conjugates

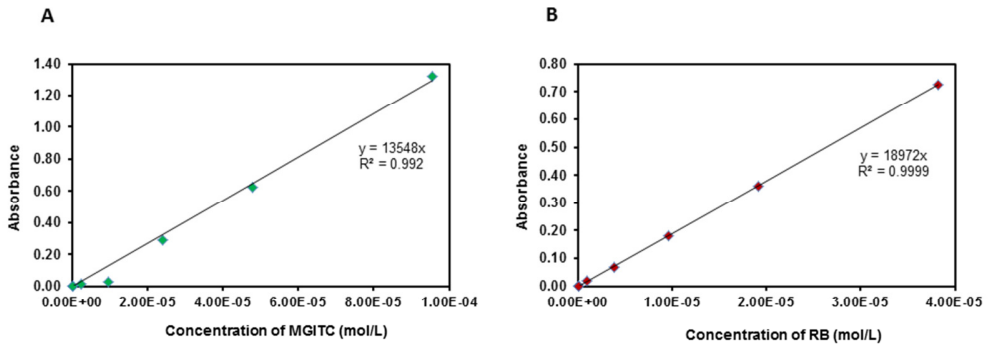


**Figure B.4.** Standard curves for absorbance measurements of malachite green isothiocyanate (A) and Rose Bengal (B) solutions at $\lambda_{max}$ values of 625 nm and 540 nm respectively

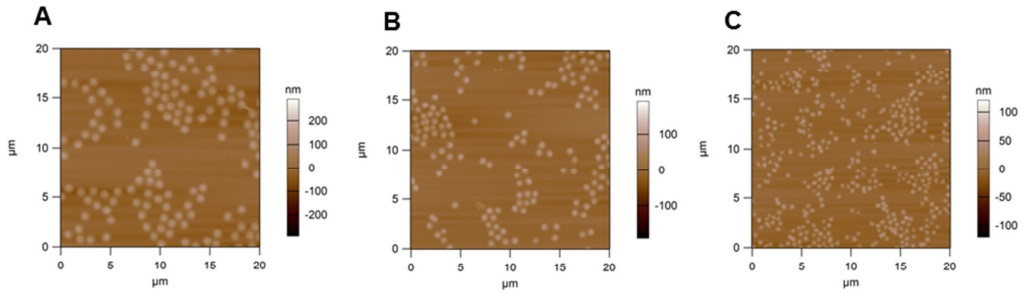


**Figure B.5.** AFM height traces of µgel1-RB (A), µgel2-RB (B) and µgel6-RB (C) represent spherical microgels

**Table B.1** Deswelling data for µgel2b-RB at 37 $^0$C vs. 20 $^0$C

| Temperature ($^0$C) | $R_H$ (nm) |
|---|---|
| **20** | 401 ± 21 |
| **37** | 349 ± 18 |

*Values obtained at pH 7 (Phosphate buffer, 50 mM ionic strength)*

The average percent deswelling of the microgels is 33.33% by volume, demonstrating that as a result of pNIPMAm having an LCST of ~ 44 $^{0}$C, the microgels are not completely deswollen at physiological temperature.

### B.5 Viability studies using NIH3T3 fibroblasts

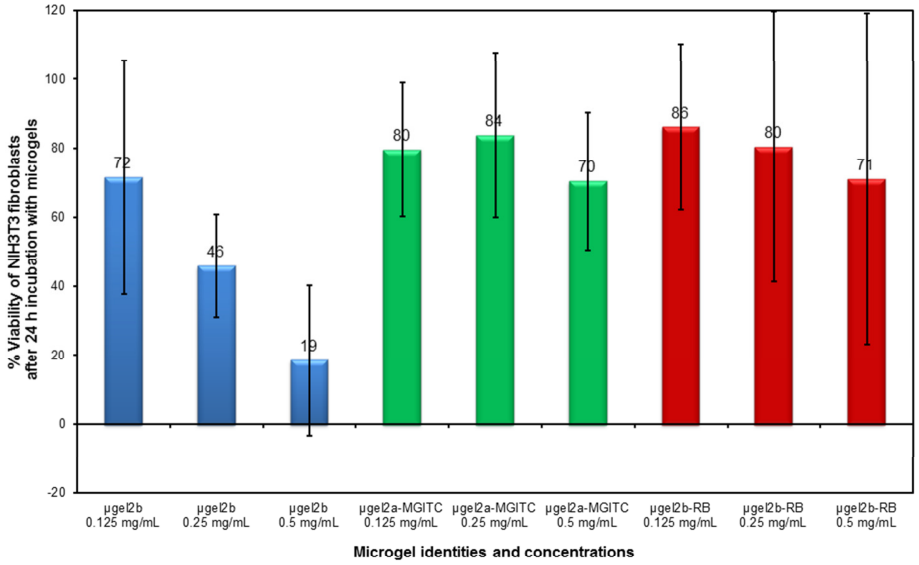


**Figure B.6.** Viability data for NIH3T3 fibroblasts incubated for 24 h with unconjugated microgels (blue bars), microgels conjugated to malachite green (green bars) and microgels conjugated to Rose Bengal (red bars) *(Average of 4 trials presented)*

## B.6 Photoacoustic signals from microgel-dye constructs

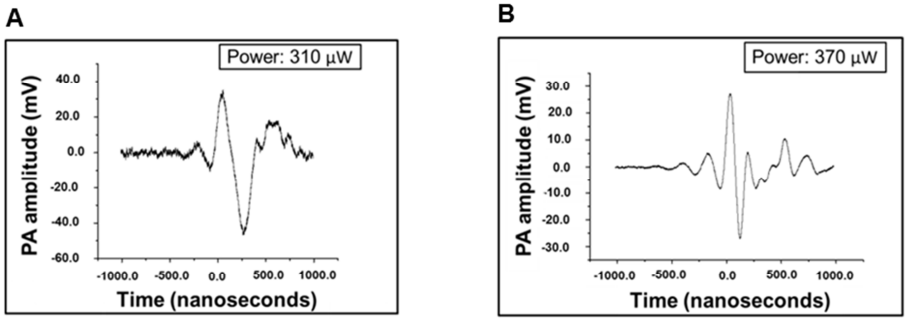


**Figure B.7.** Photoacoustic signals generated from μgel2a-MGITC (A) and μgel2b-RB (B) conjugates incorporated into tissue phantoms *(Aida Demissie, Dickson research group, Georgia Tech)*

# APPENDIX C

# NANOGELS AS VEHICLES FOR TARGETED DELIVERY OF SIRNA TO DRUG RESISTANT OVARIAN CANCER CELLS

## C.1 Core/shell nanogel synthesis and characterization

Core/shell nanogels were synthesized using a previously established procedure.[1,2] The synthesis was performed in a manner similar to that described in Chapter 2, section 2.2, but with the incorporation of Acrylamidofluorescein (AFA) in the cores, to facilitate visualization.

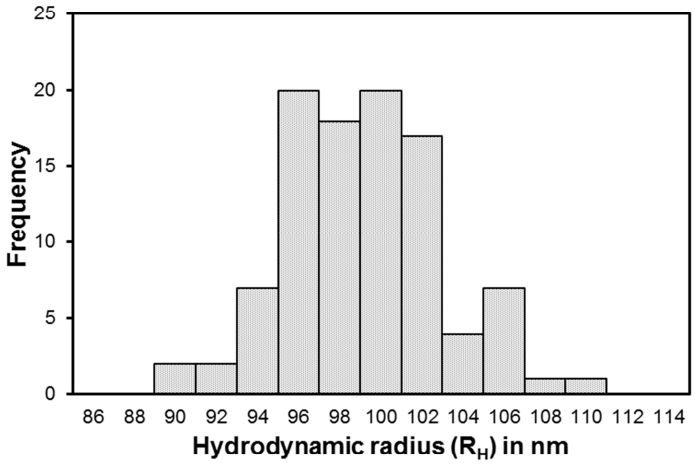


**Figure C.1.** $R_H$ distribution of core/shell nanogels obtained via dynamic light scattering (DLS), in phosphate buffer (pH 7, ~ 50 mM ionic strength)

### C.2 Peptide conjugation to nanogels

Peptides were conjugated to nanogels using a two step approach, similar to that used before.[2] The first step involved covalent conjugation of a heterobifunctional crosslinker, 6-maleimidohexanoic acid (EMCA) by carbodiimide coupling, to the amine functionalized nanogel shells. This was followed by conjugation of the relevant peptide, YSA (YSAYPDSVPMMSC) or its scrambled version SCR (DYPSMAMYSPSVC) through thiol-maleimide coupling.

### C.3 *In vitro and in vivo* studies

*(experiments performed by Dr. Erin Dickerson, University of Minnesota)*

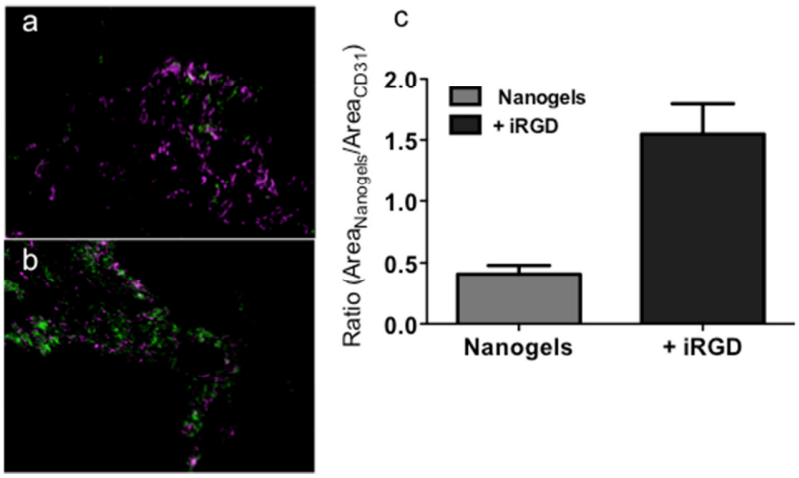


**Figure C.2.** Delivery of siRNA into HeyA8 tumors. YSA-nanogels were co-injected with or without iRGD via the tail vein into mice, and the tumors harvested and sectioned. YSA-nanogels (green) and blood vessels stained with CD31 (magenta) (a) YSA-nanogels +iRGD (b) and analysis of YSA-nanogel to CD31 pixel area (Image J) demonstrating increased the increased distribution of YSA-nanogels in the presence of iRGD (c)

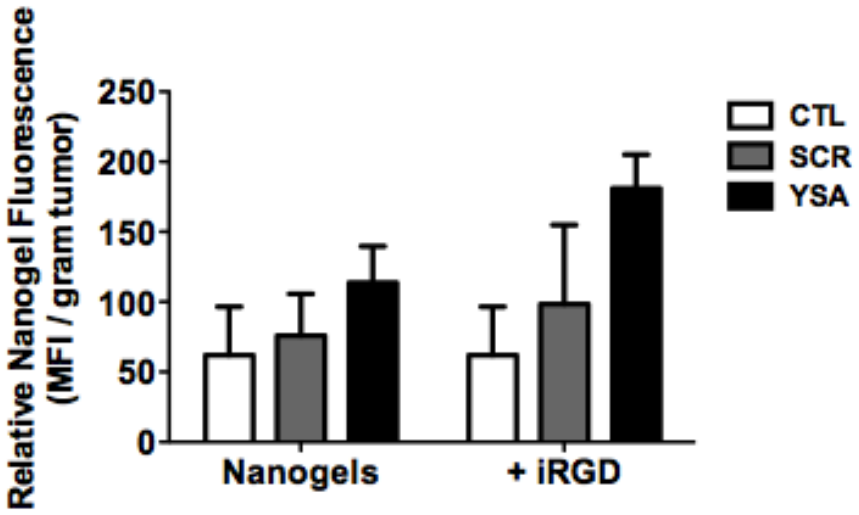


**Figure C.3.** Uptake of YSA-nanogels by individual tumor cells, determined by flow cytometry. The relative nanogel fluorescence values for all groups (N=3, 2 mg/mouse injected) were normalized by using the Mean Fluorescent Intensity (MFI) from each sample and dividing it by the tumor weight (grams). Values were determined in the absence (nanogels) and presence of iRGD. CTL=Control cells, no nanogels present; SCR=nanogels linked to the SCR peptide, used as a control for non-specific uptake of nanogels; YSA=nanogels linked to the YSA peptide to direct the nanogel payload to tumor cells expressing EphA2 receptors

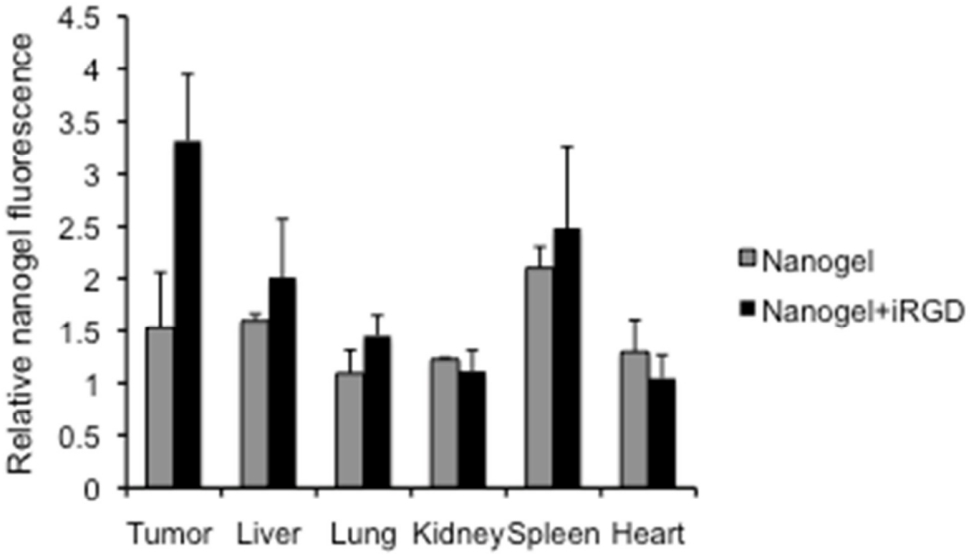


**Figure C.4.** Distribution of YSA-nanogels in HeyA8 tumors and mouse tissues after injection of YSA-nanogels alone or in the presence of iRGD. Three mice were used for each treatment group, and the relative nanogel fluorescence in tumor and tissue lysates compared to untreated controls is presented

The data presented in figures C.2, C.3 and C.4 indicated that co-administration of YSA-conjugated nanogels with iRGD, a tumor penetrating peptide, increased nanogel uptake in tumor cells and tumors. This can be leveraged towards efficient delivery of EGFR-siRNA, encapsulated within the nanogels.

## C.4 References

(1) Dickerson, E. B.; Blackburn, W. H.; Smith, M. H.; Kapa, L. B.; Lyon, L. A.; McDonald, J. F.: Chemosensitization of cancer cells by siRNA using targeted nanogel delivery. *BMC Cancer* **2010**, *10*.

(2) Blackburn, W. H.; Dickerson, E. B.; Smith, M. H.; McDonald, J. F.; Lyon, L. A.: Peptide-Functionalized Nanogels for Targeted siRNA Delivery. *Bioconjugate Chem.* **2009**, *20*, 960-968.

# VITA

## PURVA GANESH KODLEKERE

Purva Ganesh Kodlekere was born in Mumbai, India and attended school in Muscat, Oman. Following this, she earned her B.Sc. in Chemistry in 2008 and M.Sc. in Analytical Chemistry in 2010 from Ramnarain Ruia College, University of Mumbai. She came to Georgia Tech to pursue a Ph.D. in Chemistry, in 2011.